NASA CR 54997

CESIUM PLASMA SPECTROSCOPY

ELECTRON NUMBER DENSITY MEASURED
BY STARK SHIFT OF SPECTRAL LINES

by

R. F. Majkowski and R. J. Donohue

prepared for

NATIONAL AERONAUTICS AND SPACE ADMINISTRATION

CONTRACT NAS 3-6470

RESEARCH LABORATORIES

GENERAL MOTORS CORPORATION

FINAL REPORT

CESIUM PLASMA SPECTROSCOPY

ELECTRON NUMBER DENSITY MEASURED
BY STARK SHIFT OF SPECTRAL LINES

by

R. F. Majkowski and R. J. Donohue

Frank E. Jamerson
Project Supervisor

prepared for

NATIONAL AERONAUTICS AND SPACE ADMINISTRATION

January 14, 1966

CONTRACT NAS 3-6470

Technical Management
NASA Lewis Research Center
Cleveland, Ohio
Space Electric Power Office
Harold Nastelin

Research Laboratories, General Motors Corporation
Twelve Mile and Mound Roads
Warren, Michigan
48090

CESIUM PLASMA SPECTROSCOPY
ELECTRON NUMBER DENSITY MEASURED
BY STARK SHIFT OF SPECTRAL LINES

ABSTRACT

N 66-21655

The widths and shifts of atomic spectral lines were measured
for an rf (8 Mc) electrodeless cesium discharge in which the elec-
tron density was varied from 0.5 to 3×10^{14} cm^{-3} with a temperature
range from 2500 to 3100°K. The measured shifts were from 0.008 to
1.4 Å and shift to width ratios were from 0.33 to 1.40. These
measurements were compared to theoretical predictions in order to
evaluate the shift measurement as a diagnostic method to measure
electron density.

Author

TABLE OF CONTENTS

CESIUM PLASMA SPECTROSCOPY

ELECTRON NUMBER DENSITY MEASURED
BY STARK SHIFT OF SPECTRAL LINES

SUMMARY

The objective of this program (conducted under cost sharing contract No. NAS 3-6470) was to develop a diagnostic method to obtain the electron density by measuring the shift of spectral lines from a radiating cesium plasma. The validity of the theory of line shifts was to be tested. Two plasma sources were developed in order to make accurate measurements. A stable electrodeless discharge provided a high density $(0.5$ to $3x10^{14} cm^{-3})$ plasma source and a low power microwave discharge provided a low density $(10^{12} cm^{-3})$ reference source for the unshifted spectral line position.

The local electric fields due to ions and electrons in a dense plasma greatly affect the distribution of energies within the spectral lines of atoms and ions in the plasma. These Stark profiles are characterized primarily by two parameters; the width (at half the intensity maximum) and the line position (at the intensity maximum). Theory predicts that the magnitude of these parameters varies almost linearly with the electron density and exhibits an additional contribution due to the ions which is significant for broad lines in a high density plasma.

It has been established by others that the width of cesium lines can predict electron density. However the use of line shifts to determine electron density has not been established. A shift measurement does not require knowledge of the entire line profile as for the width measurement. Moreover, the most intense lines in the cesium spectra are highly broadened because of absorption effects which make the width determinations especially difficult.

The widths of optically thin lines determined electron density. The shifts of all the measured lines were then compared to theory for electron densities of 0.5 to $3x10^{14} cm^{-3}$. The results of these observations and analyses are:
1. The measured direction of the shift (i.e. to higher or to lower wavelengths) agrees with theory.

2. Theory overestimates the shift when the ion contribution to the shift is significant. For the highest members of two of the three series studied, the difference between theory and experiment is greatest: 70% for 13D-6P, 40% for 9F-5D.

3. Shift measurements agree with theory for the following lines: 6F-5D, 7F-5D, 9D-6P, 10D-6P, 11S-6P, 12S-6P. Their shift magnitude was from 0.05 to 0.5 Å.

4. The profiles of four optically thin lines compared well with theory. A value of the ion broadening coefficient computed from the wings of one of these lines was less than the theoretical value. This could possibly account for the discrepancy noted in 2.

5. For lines where bulk and self-absorption are present, the width overestimates electron density by a large factor (>2) whereas the shift for these lines gives reliable values of electron density.

6. The experimental shift values larger than 0.05 Å tabulated in this report are sufficiently accurate to serve as a calibration for electron density vs line shift.

7. The continuum intensity is a sensitive monitor of plasma electron density stability. In addition, temperature stability is simultaneously indicated.

8. A rf electrodeless discharge in cesium provides a stable high density plasma.

9. A low power microwave discharge provides a stable low density source for the unperturbed (unshifted) spectra.

10. The spectrometer resolution required for accurate width measurements can be specified for each line. Minimum resolution is found for the highest series members, e.g. at 10^{14} cm^{-3}, 6000 for 14D-6P, 3000 for 10F-5D and 9000 for 14S-6P. For any given line, spectrometer resolution has to be better (up to a factor of 3) for width measurements than for shift measurements.

I. INTRODUCTION

In general, physical measurements made on devices, such as cesium therm-
ionic energy converters, provide parameters necessary to develop a valid theo-
retical analysis of the operation of the device. Theoretical I-V characteris-
tics of cesium diodes have been developed which require knowledge of ion, elec-
tron and neutral particle densities and temperatures in the plasma.[1] Measure-
ments of these quantities may be made independently by means of optical spec-
troscopy, probes, or microwave spectroscopy.

Optical spectroscopy is mainly used to determine particle temperatures and
densities in dense (electron density greater than $10^{13} cm^{-3}$) plasmas because it
is one of the diagnostic methods which do not perturb the plasma. Thus, it is
well suited for analysis of plasma in cesium diodes. The various methods of
plasma spectroscopy are reviewed in Appendix A. Of these several methods, the
one of primary interest is the determination of electron number densities from
the profile of the emitted spectral lines.

The profile, or energy distribution, of a spectral line may be character-
ized by two parameters. The first is the width; its numerical value is given
as the half width of the line taken at half the maximum intensity. The second
is the position of the line maximum (either in frequency or wavelength units);
its numerical value is given as a shift, a frequency or wavelength difference
from some fixed initial value.[*] Both the spectral line width and shift are
functions of the electron density, and thus they both can be used to measure
this electron density. The line width which is based on sound theory[2] has
been successfully used to measure electron density in cesium diodes.[3] The
line shift theory has not been tested fully by experiment.[4] However, the
line shift method should be more precise since it is largely unaffected by
absorptions in the plasma (see Appendix B). It should be experimentally sim-
pler since it is easier to measure a change in the position at the maximum of
a line profile than to measure the shape of the profile.

(*) The initial position of the line maximum is that obtained when the shift
    mechanism in the plasma is very small. For practical purposes in our
    cesium plasma this condition exists for an electron density of approxi-
    mately $10^{12} cm^{-3}$ or less.

The purpose of this program was to measure the line shift for many lines from a cesium plasma source and to correlate shift data with line width data and the theory of line shifts. The successful development of the line shift method as a diagnostic technique will provide a method that has the following desirable characteristics.

1. The plasma is unperturbed by the measurement.
2. Shift measurements are not greatly influenced by absorption effects.
3. The method is based on verified theory.
4. Other correlative parameters, such as electron temperature, need not be known precisely to evaluate shift data.
5. Line shifts can often be measured more accurately than line widths.

This report discusses the applicable theory of spectral line profile analysis, the experimental arrangement used and analysis of the line profile data. A cesium plasma generated by rf excitation and contained in a glass envelope provided a source in which the electron number density was varied from 0.5 to $3 \times 10^{14} cm^{-3}$ which corresponds to densities typically found in a thermionic converter.[3] A reference cesium plasma source, produced by using microwave excitation, was used to determine the unperturbed position of the spectral lines. The density of this source was typically $10^{12} cm^{-3}$ and provided a narrow, unshifted reference line.

II. THEORY

The profile of a spectral line is determined by a variety of broadening mechanisms which are reviewed in Appendix A. The importance of any given one of these mechanisms in an observed spectral profile depends on the plasma electron density and temperature. For conditions in our cesium plasma, namely electron temperature, $T_e \approx 3000°K$ and electron density $N_e \approx 10^{13}\text{-}10^{14} cm^{-3}$, the full line widths that correspond to these broadening mechanisms are:

Width	$\overset{\circ}{A}$	Reference
Natural	10^{-4}	Appendix A
Doppler	$\sim 1 \times 10^{-2}$	Appendix A
Resonance	3×10^{-3}	Appendix A for $N_1 = 10^{15} cm^{-3}$
Stark	10^{-2} to 0.8 Most lines are $> 5 \times 10^{-2}$	Reference 5

Thus, for all but the low level sharp series lines the largest broadening mechanism is Stark broadening and Stark broadening theory will be applied to our measured line profiles.

Stark Broadening

The theory of Stark broadening of spectral lines has been described in a number of recent papers.[2] In general the broadening is treated by perturbation theory. The wave functions of the emitting atoms are perturbed by the plasma ion and electron fields. For hydrogenic atoms, such as cesium, the transitions are assumed to be a change of state of the single valence electron, and therefore only a one-electron wave function is required. Furthermore the perturbers are assumed to be sufficiently distant so that their interaction with the atom can be approximated by the first term of a multipole expansion. That is, the interaction potential of the ith perturber is equal to the electric field of that perturber at the radiating atom times the dipole moment of the atom.

Within this framework there are two approximations which describe the interactions of radiating atoms and charged particles.[*] Electron interactions are treated by the impact approximation. Ion interactions are treated by the quasi-static (or Holtsmark) approximation. These two approximations arise from the difference of the thermal velocities of the ions and electrons.

In the quasi-static description, the perturbers (ions) move relatively slowly. Thus the perturbation is practically constant over the times of interest, i.e. of the order of the inverse line width. This time is inversely proportional to the line width in units of angular frequency. The validity criterion for the quasi-static approximation can thus be stated as

$$w > \frac{1}{\tau_{coll}} \simeq \left| \frac{v_i}{\rho} \right| \quad \text{(quasi-static approximation)} \qquad (1)$$

where τ_{coll} is the average ion collision time and w is the line half width (at half maximum intensity) ρ is the impact parameter, and v_i is the ion velocity.

In the impact approximation we deal with relatively fast moving perturbers (electrons). Thus for all but long range (strong) impact interactions,

---

(*) The formalism to be used here follows closely that of Stone and Agnew[2] and Griem.[5]

the emitting system is considered to exist in an unperturbed state for most of the time, being perturbed only when it interacts with the field of the fast moving electron. The resultant broadening is described in terms of impacts that are well separated in time. The validity criterion for the impact approximation can thus be stated as

$$\tau_e \ll 1/w \quad (\text{impact approximation}) \qquad (2)$$

where τ_e is the average electron collision time. Impact broadening has been calculated both by a semi-classical and quantum mechanical treatment. The results of the two have been shown to be equivalent. For the strong impacts, i.e. those in which the interaction may exist even at long range and thus over a long time, the electron collisions are not actually separated in time. However, it has been shown that the impact approximation is still valid provided the average interaction over these times is weak.

The Stark broadening can be computed for a heavy element such as cesium but an error must be expected due to uncertainties in the atomic matrix elements required to compute the above perturbation. However, there is also a simplification in these computations due to the fact that the broadened lines can be considered to be isolated. That is, practically all the broadening is caused by interactions between the upper state of the line in question and neighboring levels but lower state interactions can be neglected. In other words the excited levels do not overlap.

After detailed calculation using the above assumptions, limitations and simplifications, the profile of a Stark broadened line can be written as

$$I(\omega) = \frac{w}{\pi} \int_0^\infty \frac{W(\mathcal{E}) \, d\mathcal{E}}{w^2 + \left[(\omega - \omega_0) - d - \alpha_i \mathcal{E}^2\right]^2} \qquad (3)$$

Here $I(\omega)$ is the intensity at angular frequency ω, $\omega_0 = \hbar^{-1}(E_i - E_f)$ is the frequency at the maximum intensity for the unperturbed line and is equal to the difference between the unperturbed initial (E_i) and final (E_f) energy levels, $W(\mathcal{E})$ is the ion electric field distribution, $W(\mathcal{E}) \, d\mathcal{E}$ is the probability of the ion producing an electric field between $\mathcal{E}$ and $\mathcal{E} + d\mathcal{E}$ at the radiating atom, α_i is the second order Stark coefficient (discussed in detail later) and d and w are the line shifts and half widths due to electron impacts alone.

The electron impact widths and shifts are given by Eqs. 4 and 5.

$$w = N_e \int f(v)\, dv \times \left[\pi\, v\rho_{min}^2 + \frac{4\pi}{3}\left(\frac{e^4}{\hbar v}\right) \sum_k \left|r_{ik}\right|^2 a(z_{ik_{min}}) \right] \qquad (4)$$

$$d = N_e\, \frac{4\pi}{3}\left(\frac{e^4}{\hbar^2}\right) \times \int f(v)\, dv\, \frac{1}{v} \sum_k \left|r_{ik}\right|^2 S_n(z_{ik_{min}})\, b(\tfrac{3}{4} z_{ik_{min}}) \qquad (5)$$

with $z_{ik\,min} = \omega_{ik}\rho_{min}/v$

N_e is the electron density, and $f(v)$ is the electron velocity distribution. r_{ik} is the unperturbed matrix element between the levels i and k of the position operator r. ω_{ik} is the frequency difference between the levels i and k. ρ_{min} is the minimum impact distance below which the impact perturbation theory is invalid, and a and b are functions of $z_{ik_{min}}$, the perturbation due to electron impact. S_n is a notation meaning "sign of" and allows the shifts to be towards higher or lower frequency. For plasma diagnostics the above expression can be simply written as

$$w = \text{Const. } N_e \qquad (4a)$$

$$d = \text{Const. } N_e \qquad (5a)$$

The constants are actually weak functions of plasma temperature (introduced by the velocity distribution $f(v)$). Values of these "constants" have been computed and theoretical widths and shifts for various cesium spectral lines have been tabulated.[5] A plot of the theoretical line widths and shifts as a function of electron number density for two lines each of the diffuse and fundamental series of cesium for an electron temperature of 2500°K are shown in Figs. 1 and 2.

Quasi-static ion broadening effects enter through the quadratic Stark coefficient α_i which can be computed from

$$\alpha_i = e^2 \sum_k \frac{\left|z_{ik}\right|^2 (\omega_i - \omega_k)}{\hbar\, \omega_{ik}} \qquad (6)$$

where e is the electronic charge and the other terms have been defined above. The ion broadening introduces additional terms in the final form of the width and shift equations.

7
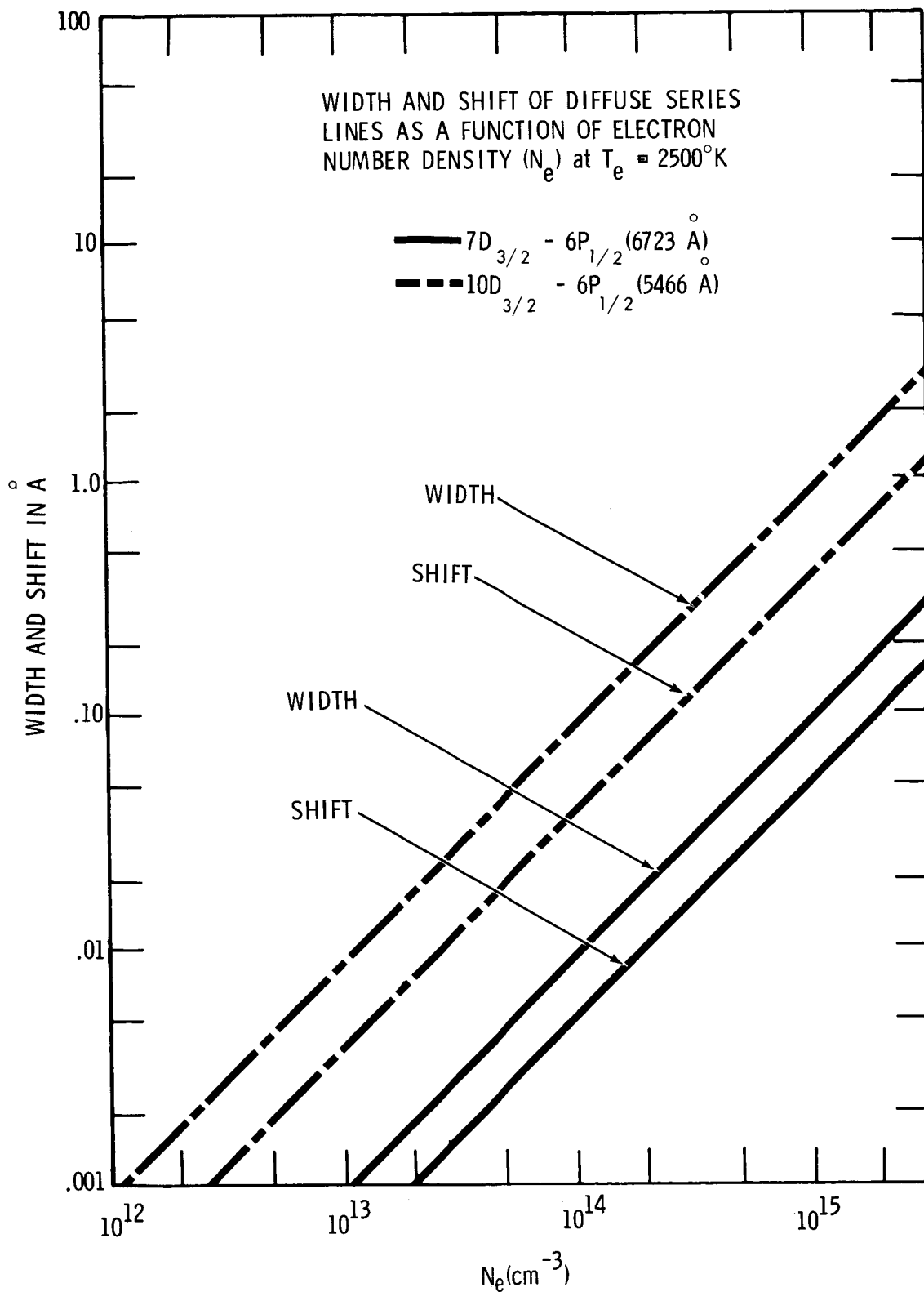
Fig. 1. Width and shift of diffuse series lines as a function of electron number density (N_e) at $T_e = 2500°K$.

WIDTH AND SHIFT OF FUNDAMENTAL SERIES LINES
AS A FUNCTION OF ELECTRON NUMBER DENSITY (N_e)
AT T_e = 2500°K

———— $7F_{5/2} - 5D_{3/2}$ (6825 Å)

— — — $10F_{5/2} - 5D_{3/2}$ (6326 Å)
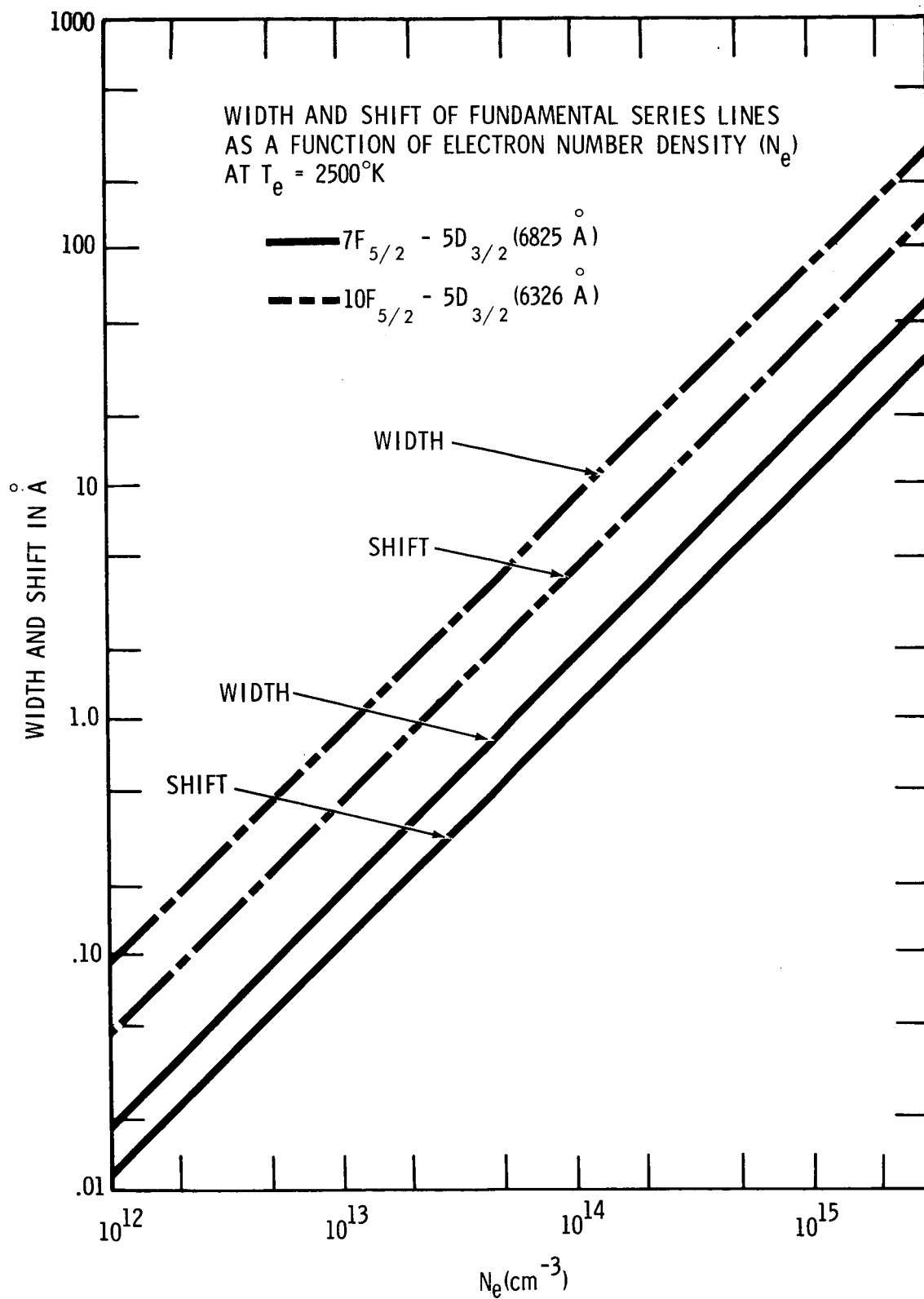
Fig. 2. Width and shift of fundamental series lines as a function
of electron number density (N_e) at T_e = 2500°K.

9

For numerical evaluation, however, it is more convenient to use a reduced line profile $J(x) \equiv I(\omega)w^{-1}$. This reduced profile has been tabulated by Griem[5] and for $-2.0 < x < 5.0$.

$$J(x) = \frac{1}{\pi} \int_0^\infty \frac{W_r(\beta)\, d\beta}{1 + (x - \alpha^{4/3}\beta^2)^2} \qquad (7)$$

where $\quad x = \dfrac{\omega - \omega_0 - d}{w}$

$\omega_0 \quad = \quad$ frequency of unperturbed line

d and $w \quad = \quad$ shift and width due to electron impact

$\beta \quad = \quad$ reduced electric field, $\mathcal{E}/$Holtsmark field

$\alpha \equiv (\alpha_i/w)^{3/4} N_e =$ ion broadening factor.

The total widths and shifts of these profiles can be approximated by Eq.8 when $\alpha \le 0.5$ and $r \le 0.8$.

$$w_{total} = w_t \cong (1 + 1.75\,\alpha\,(1 - 0.75\,r))\ w$$

$$d_{total} = d_t \cong (\tfrac{d}{w} + 2.0\,\alpha\,(1 - 0.75\,r))\ w$$

$$(8)$$

Line shifts can occur to either longer or shorter wavelengths which depend on details of the perturbation calculation.[5] The sign of d is positive for red shifts and negative for blue shifts. The second term (α contribution) always carries the sign of the low temperature d.*

The ion broadening factor α is proportional to $N_e^{1/4}$ since w is proportional to N_e and is < 0.5 for the electron densities considered here.[5] The quantity r is equal to the ratio of the mean ion-ion separation ρ_m and the Debye radius ρ_D

$$r = \rho_m/\rho_D = 0.1\ N_e^{1/6}\ T^{-1/2} \qquad (9)$$

---

* For example, the CsI nD-6P lines change their shift from blue to red at high (over 20,000 °K) electron temperature. Here, the α term maintains the negative sign for all temperatures.

For $N_e = 10^{14} cm^{-3}$ and $T = 3000°K$, $r = 0.3$, so that Eq.8 is valid for our range of plasma density and temperature. The parameter r is important in dense plasmas where the perturbing ions cannot be considered statistically independent. When this arises the ion distribution function $W(\mathcal{E})d\mathcal{E}$ (Eq.3) is replaced by one which takes into account Debye shielding of the electrons.

The total width and total shift (Eq.8) are equal to width and shift due to electron impact plus terms due to quasi-static (ion) broadening. Since α is proportional to $N_e^{1/4}$, the ion contribution increases relatively slowly with N_e. For the cesium S series, $d/w \sim 1.5$, and for the D and F series, $d/w \sim 0.5$. Thus the shift of the sharp series should be less affected by ion broadening than the D and F series.

To evaluate w_t and d_t for a given line the electron impact values w, d/w and α listed by Griem[5] for $N_e = 10^{16}$ and each cesium line is scaled by the appropriate dependence on N_e. The quantity r is determined from Eq.9.

III. EXPERIMENTAL ARRANGEMENT

The basic arrangement of the spectroscopic instrumentation which measures the shape of a spectral line is straightforward. Light from the stable cesium plasma is focused on the slit of a high resolution grating spectrometer with a photoelectric read-out, and recording system. The spectrometer has sufficient resolution to define the true shape of most of the spectral lines. For the narrow lines correction for the apparatus broadening was made. For the shift measurements we were required to measure either the absolute position (in frequency or wavelength units) or the change in position from some initial unshifted position. The final arrangement involved a low plasma density reference source that determined the unshifted line position. The ability to measure quickly and accurately the spectral shift differentiates this system from the more conventional spectroscopic setups.

Optical System

Figure 3 schematically shows the overall arrangement of the experimental apparatus. This system consists of: 1) two cesium light sources, 2) the optical system, 3) the high resolution spectrometer and 4) the monochromator.
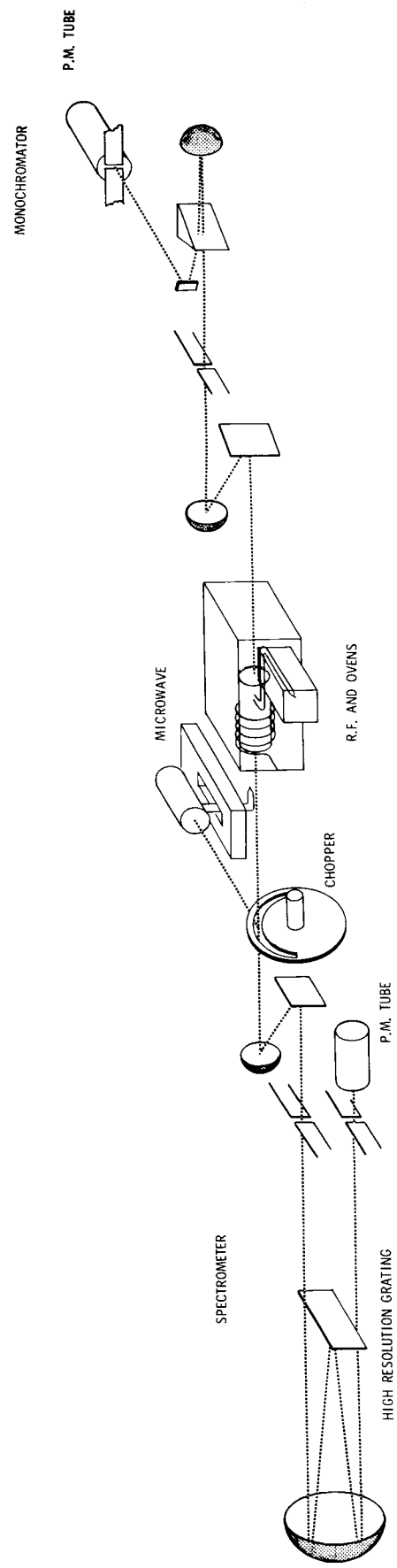
Fig. 3. Schematic view of overall experimental arrangement.

12

The primary measurements were the profiles of the spectral lines emitted by the radio frequency excited cesium plasma (rf plasma) source. The electron number density of the rf plasma was varied from approximately 0.5 to $3 \times 10^{14} cm^{-3}$. The very narrow lines emitted by the microwave excited cesium plasma gave the fiduciary position (unperturbed line) from which the shifts of the rf plasma line are measured. These two sources are focused sequentially by the same spherical mirror-plane mirror system onto the entrance slit of the high resolution spectrometer. A rotating chopper is put in the optical path of both the rf and microwave source. The chopper first allows the light from the rf source to pass to the focusing system through the slotted segment of the chopper while the light of the microwave source passes through and out of this focusing system. In the next half cycle light from the rf source is blocked while light from the microwave source is reflected into the focusing system by a mirror on the non-slotted segment of the chopper. Light focused on the entrance slit of the spectrometer is dispersed by its grating and the spectrum of this light is focused at the exit plane of the spectrometer. An exit slit lies in this exit plane directly below the entrance slit. The spectrum is scanned across the exit slit by rotation of the grating. A photomultiplier directly behind the exit slit measures the light intensity which is recorded on a strip chart.

The resolution and dispersion of the spectrometer determines the scan speed which provides the most accurate line profile. At the same time the fiduciary position (the corresponding microwave plasma line) is displayed on the same chart. The photomultiplier signals from the rf and microwave light sources are read on a dual pen recorder synchronized with the optical chopper. Each pen is active only when light from the corresponding source appears at the entrance slit. The photomultiplier signal is kept on the inactive pen while the other one is active. This results in a "stepped" appearance on the signal tracing. However by keeping the chopper speed large with respect to the scan speed the effect of these "steps" are kept small. An example of a line recording of both sources is shown in Fig. 4. The synchronization of the dual pen recorder and chopper was necessary because one amplifier was used for both signals. The preferred system would be individual amplifiers for each signal.

While the high resolution spectrometer measures profiles of spectral lines from the rf plasma, a scanning monochromator measures the intensity of the continuum from the plasma. The electron temperature of the rf plasma is determined
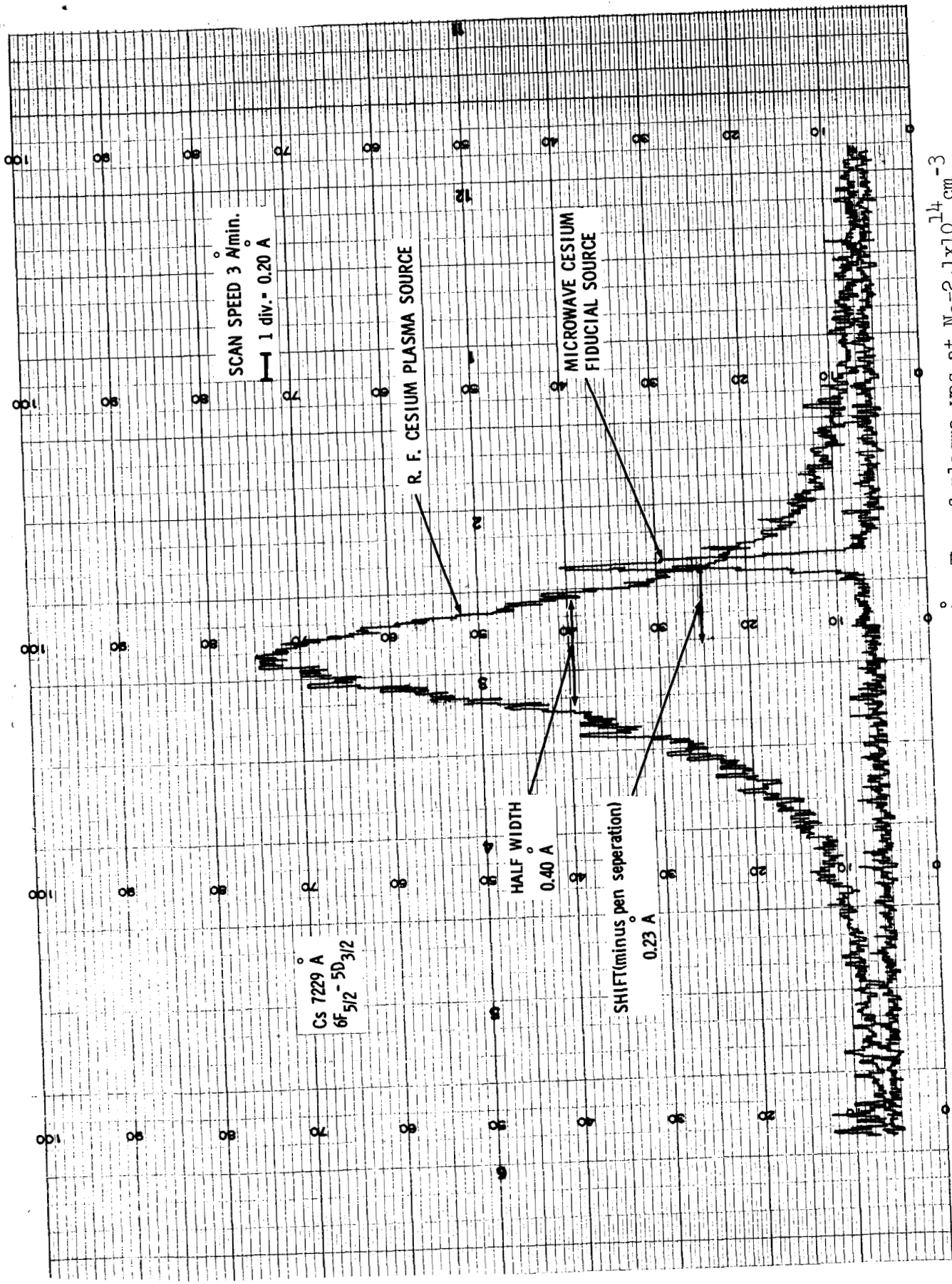
13

Fig. 4. Photomultiplier tracing for CsI 7229 Å. The rf plasma was at $N_e = 2.1 \times 10^{14} cm^{-3}$, and the microwave plasma at $N_e \leqslant 10^{12} cm^{-3}$. Rate of rotation of optical chopper was 54 rpm while the wavelength scan speed was 1.2 Å per minute.

14

from these continuum measurements (see Appendix A). Radiation from the rear of the rf source is focused on a slit of the monochromator by a plane mirror-spherical mirror system. A NBS tungsten ribbon filament standard lamp is used to calibrate the monochromator. The continuum intensity was also used to monitor the stability of the rf source for the duration of each run.

The relevant parameters of the spectroscopic apparatus are summarized in Table I.

<div align="center">TABLE I. Spectroscopic apparatus.</div>

High Resolution Spectrometer

Make: Jarrell-Ash 3.4 meter Ebert mount

Grating: M.I.T. 300 grooves per mm

Resolution (minimum measured value): 145,000 in 6th order at 6000Å using
                                        15 micron entrance and exit slits

Slit Width: 15 micron entrance and exit slits

Photomultiplier: E.M.I. 9558C (non-cooled)

Monochromator

Make: Perkin-Elmer Model 98 prism monochromator

Prism: Quartz

Photomultiplier: E.M.I. 9558C (non-cooled)

<div align="center">R. F. Plasma Source</div>

Figure 5 is an exploded view of the rf cesium source and ovens. The cesium plasma is generated in an alkaline resistant (Corning 1720) glass tube. This tube consists of a cylinder 10 cm long, 2.6 cm diameter with flat (Corning 1723) faces at either end. An arm protrudes from the middle of the tube and is parallel to the cylinder for 2 cm beyond the end; at that point it is perpendicular to the tube for 17 cm. The cold spot of the tube is maintained at the tip of this arm. After bakeout at 450°C the tube pressure is 6×10^{-9} torr. Cesium is introduced by "firing" cesium chromate pellets in an arm which is detached after cesium transfer.

The cylindrical portion of the tube is located in an open ended quartz jacket 3.9 cm diameter. This jacket, in turn, is located in an insulated box which is the main oven. Double walled quartz windows are positioned at the front and rear of the main oven in line with the plasma tube. Also a double

<div align="center">15</div>
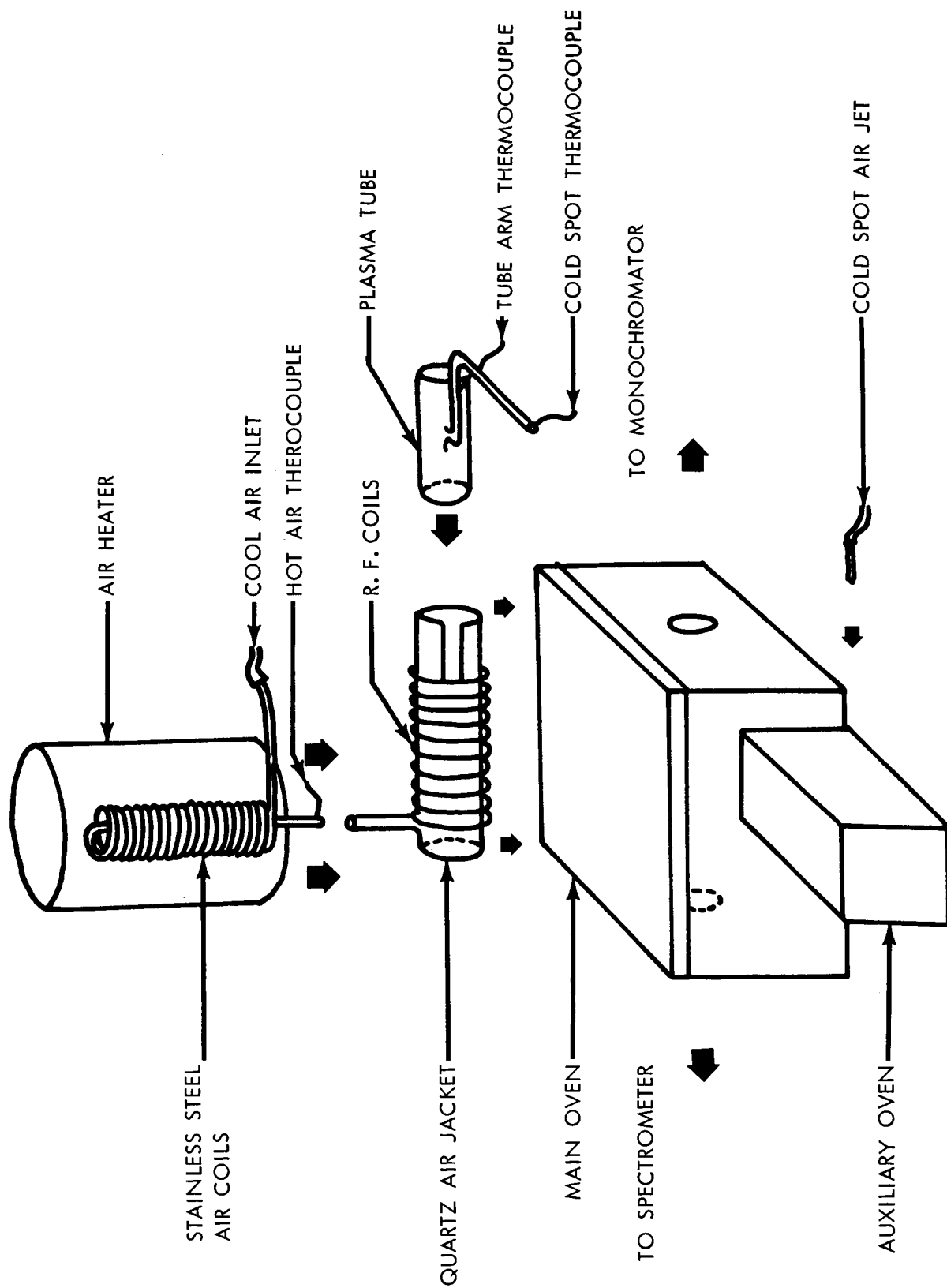
Fig. 5. Exploded view of cesium rf source.

AIR HEATER

COOL AIR INLET

HOT AIR THEROCOUPLE

PLASMA TUBE

TUBE ARM THERMOCOUPLE

COLD SPOT THERMOCOUPLE

R.F. COILS

TO MONOCHROMATOR

COLD SPOT AIR JET

STAINLESS STEEL
AIR COILS

QUARTZ AIR JACKET

MAIN OVEN

TO SPECTROMETER

AUXILIARY OVEN

16

wall quartz window is located in the side of the main oven opposite the plasma tube for viewing. Hot dry air is fed into this quartz jacket to control the main bulb temperature over the range 130°C to 450°C. The small arm tube is located in an auxiliary oven which consists of a nichrome heater and small air jet for fine temperature control.

Chromel-alumel thermocouples monitor the temperature of the cold spot (tip of the arm at the point it is cooled), a point on the arm close to the main bulb and in the main oven which was hotter than the auxiliary oven. Plasma stability was measured by the intensity of a given segment of the cesium continuum. Experience with the source dictated the appropriate cold spot temperature and thermal gradients to obtain the desired plasma conditions.

A cesium plasma was established in this tube by an electrodeless rf discharge. An rf coil was wrapped around the outer quartz jacket. This coil was a single 14 turn layer of 0.48 cm copper tubing approximately 30 cm long with coil inside diameter of 4.2 cm. The coil extended about one turn beyond each end of the plasma tube.

A Lepel 2.5 kW variable frequency (2-16 Mc) generator supplied the rf power. The frequency for these experiments was 8 Mc (measured at the rf coil). By adjusting the pressure (given by the cold spot temperature) an atomic or ionic spectra stable up to eight hours was obtained. In that time, the electron density varied $\pm$ 10%..

Microwave Plasma Source

The shift measurements required a stable cesium plasma of relatively low electron density ($\leq 10^{12} cm^{-3}$) for the source of unperturbed cesium lines. For this purpose a microwave excited source was developed (see Fig. 3). The construction and processing of the microwave plasma tube was almost identical to that of the rf plasma tube with the exception that the arm of the tube extended directly perpendicularly from the cylindrical portion of the tube. This however does not seem to be essential and the rf tube could actually be used in the microwave source. The arm of the microwave tube was positioned in a turntable waveguide section of a 2.7 Gc Raytheon Microtherm microwave generator. The cylindrical part of the plasma tube was wrapped with a heater tape. The temperatures at the tip of the arm and the rear flat face of the tube were

monitored. The spectra was observed through the front face of the tube. A
fine jet of cool air was blown at the rear face of the tube which served as
the cold spot.

A stable low density plasma could be maintained at a cold spot temperature
of 100°C. The other parts of the tube were kept at 180°C or greater. The
plasma was initially ignited in the tube arm in the waveguide and then diffused
into the entire tube as sufficient cesium vapor pressure built up. The meas-
ured half widths of almost all of the spectral lines from this source were
equal to the instrument half width which was 0.04 Å. However the best approxi-
mation of the true width of these lines gave an upper limit to the plasma
density of $10^{12} cm^{-3}$. A microwave source similar to this was used by Kleiman[6]
to make interferometric measurements of the spectrum of atomic cesium. He
observed no shift in the cesium lines from this source and claims a wavelength
position uncertainty (with respect to unshifted values) of ± 0.001 Å. The
tubes in the Kleiman experiment were filled with a low pressure of argon or
neon to start the discharge before enough cesium could be vaporized to carry
the discharge.

IV. DATA AND ANALYSIS

The electron density, N_e, in the bulk of the plasma was determined by com-
paring the measured width of all of the optically thin lines with the theory
of Griem.[5] The line shifts are measured for the optically thick as well as
the thin lines and these shifts are compared to theory. The entire profile of
one line from each of the S, D and F series is compared with the theoretically
predicted profile (Eq.7) and shown to compare favorably with the theory. The
reliability of the shift measurement over the width to determine N_e is demon-
strated for lines which are partially volume absorbed and self-absorbed.

The electron temperature was measured from the relative intensity of the
free-bound continuum to the 6P doublet using the empirical equation developed
by Agnew[2] which is based on Mohler's[7] experiments. An unsatisfactory
absolute calibration of the monochromator did not allow the use of the con-
tinuum intensity data to determine N_e independently.

Width and Shift Measurements

The widths and shifts of several doublets from each of the S, D and F series were measured for N_e from 0.5 to $3 \times 10^{14} \text{cm}^{-3}$, corrected for instrument broadening, and are listed in Table II. In addition Table II lists the electron density computed from the widths and the theoretical values of shift.

The electron density is calculated as follows. Griem[5] lists w (which scales linearly with N_e) at $N_e = 10^{16} \text{cm}^{-3}$. The measured width w_m is first set equal to the electron impact width w and an initial value of the electron density N_e^w is computed (Table II). This value N_e^w is then used to evaluate r from Eq.(9) and α from Griem.[5] Now the measured width w_m is set equal to the total width w_t which with these values of α and r are used in Eqs.(8) to evaluate a new electron impact width w'. Finally this new value w' is used with the tabulated values of Griem[5] to give an electron density $N_e^{w'}$. This now represents our best value of electron density which is henceforth plotted as N_e. Since these two values of N_e differ by less than 20% for any given line and α and r are weak functions of N_e ($N_e^{1/4}$ and $N_e^{1/6}$ respectively), additional iterations were not considered necessary.

The electron impact shift value d is computed using $N_e^{w'}$ and the electron impact width w in Griem's table.[5] The total shift d_t is subsequently computed from Eq.8 where d, w, α and r are now known. This theoretical total shift value d_t is thus to be compared to the measured value d_m listed in Table II.

Figures 6, 7 and 8 display the measured shift vs N_e for the S, D and F series lines where the solid line represents the theoretical value d_t. The shifts of the sharp series lines are the average of the shift of the doublets, $nS_{1/2}-6P_{1/2}$ and $nS_{1/2}-6P_{3/2}$ for n=9,10,11 and 12. The shift of each member differs only slightly and the values can be easily averaged.

The D series shift values are those of the $nD_{5/2}-6P_{3/2}$ lines for n=8,9,10, 11, 12 and 13. Another branch of the nD-6P series, $nD_{3/2}-6P_{1/2}$, was measured and the shifts are lower by the predicted theoretical ratio but are not plotted since no additional information is to be gained by this display. The $nD_{3/2}-6P_{3/2}$ lines were not measured since the intensity of these lines is much weaker than the other members of the series. Likewise with the nF-5D series lines, only the strongest member of the series $nF_{5/2,7/2}-5D_{5/2}$ is plotted for n=5,6,7,8 and 9. The shifts of the $nF_{5/2}-5D_{3/2}$ are almost identical but some of the lines of this series were interfered with thus precluding their use.

19

TABLE II. Measured and computed values for cesium line widths and shifts.

Plasma conditions: Electron number density $(N_e) = .48 \times 10^{14} cm^{-3}$
Electron temperature $(T_e) = 2800°K$
(Ion shielding parameter $r = .36$)

Cs I Line Transition	Wavelength (Å)	w_m Å	$N_e w$ x10^{14}cm^{-3}	α	$N_e w'$ x10^{14}cm^{-3}	d_m Å	d Å	d' Å
$nS_{1/2}-6P_{1/2}$								
$nS_{1/2}-6P_{3/2}$								
9	6586†	.031	.68	.04		.008	.006	.006
10	5839†	.01	.73	.06		.015	.012	.013
10	6034†	.011	.60	.06		.014	.012	.013
11	5568†	.031	.97	.07		.025	.022	.023
11	5746†	.03	.85	.07		.025	.024	.025
12	5407	.031	.52	.09	.48	.045	.041	.044
12	5573	.031	.49	.09	.45	.047	.044	.047
$nD_{3/2}-6P_{1/2}$								
$nD_{5/2}-6P_{3/2}$								
8	6010†	.036	1.5	.04		-.019	-.007	-.007
8	6213†	.037	1.2	.04		-.011	-.007	-.007
9	5664†	.034	.68	.05		-.018	-.013	-.015
9	5845†	.037	.60	.06		-.019	-.016	-.018
10	5466	.084	.51	.06	.48	-.023	-.023	-.025
10	5635	.062	.50	.07	.47	-.031	-.029	-.031
11	5340	.085	.50	.07	.47	-.038	-.037	-.046
11	5503	.11	.50	.09	.45	-.045	-.047	-.056
12	5414	.186	.54	.11	.48	-.064	-.073	-.097
13	5197	.33	.61	.11	.54	-.095	-.09	-.115
13	5349	.32	.58	.13	.50	-.10	-.107	-.125
$nF_{5/2}-5D_{3/2}$								
$nF_{5/2,7/2}-5D_{5/2}$								
5	8018	.048	.84	.07	.49	.019	.017	.020
5	8081	.045	.83	.07	.49	.020	.018	.020
6	7229	.09	.57	.12	.49	.054	.042	.056
6	7280	.09	.57	.12	.49	.054	.043	.056
7	6825	.16	.53	.15	.45	.094	.083	.11
7	6871	.17	.54	.15	.46	.094	.083	.11
8	6586	.26	.51	.19	.42	.18	.14	.20
8	6629	.30	.58	.19	.48	.17	.14	.20
9	6473	.46	.53	.24	.42	.25	.21	.36

* Bulk-absorbed and self-absorbed lines.

† Bulk-absorbed lines.

Plasma conditions: Electron number density $(N_e) \cong 0.7 \times 10^{14}$ cm^{-3}
Electron temperature $(T_e) = 3100°K$
(Ion shielding parameter $r = 0.38$)

Cs I Transition	Line Wavelength(Å)	w_m Å	N_e^w ×10^{14}cm^{-3}	α	N_e^w ×10^{14}cm^{-3}	d_m Å	d Å	d' Å
$nS_{1/2}-6P_{1/2}$								
$nS_{1/2}-6P_{3/2}$								
9	6586	.010	1.13	.05	1.07	.013	.09	.10
12	5407	.06	.99	.10	.87	.056	.053	.057
$nD_{3/2}-6P_{1/2}$								
$nD_{5/2}-6P_{3/2}$								
10	5466	.074	.79	.07	.70	-.036	-.030	-.036
11	5340	.150	.86	.08	.76	-.056	-.051	-.064
11	5503	.167	.87	.10	.75	-.072	-.062	-.078
12	5414	.30	.88	.12	.77	-.111	-.097	-.140
13	5349	.50	.92	.15	.74	-.15	-.14	-.23
$nF_{5/2}-5D_{3/2}$								
$nF_{5/2,7/2}-5D_{5/2}$								
5	8018	.069	1.21	.08		.033	.0247	.029
5	8081	.074	1.36	.08		.036	.0247	.029
8	6586	.46	.89	.20	.65	.27	.20	.30
8	6629			.20	.65	.30	.20	.30
9	6432	.71	.85	.25	.62	.43	.33	.54
9	6473	.73	.83	.25	.60	.40	.33	.54

Plasma conditions: Electron number density $(N_e) \sim 0.9$ cm^{-3}
Electron temperature $(T_e) = 2800°K$
(Ion shielding parameter $r = 0.40$)

Cs I Transition	Line Wavelength(Å)	w_m Å	N_e^w ×10^{14}cm^{-3}	α	N_e^w ×10^{14}cm^{-3}	d_m Å	d Å	d' Å
$nS_{1/2}-6P_{1/2}$								
$nS_{1/2}-6P_{3/2}$								
9	6586	.04	4.9	.05		.02	.012	.013
10	5839	.025	1.43	.06		.025	.022	.024
10	6034	.028	1.62	.06		.030	.022	.024
11	5568	.033	1.04	.08	0.95	.043	.042	.045
12	5573	.073	1.20	.11	1.06	.086	.078	.086
$nD_{3/2}-6P_{1/2}$								
$nD_{5/2}-6P_{3/2}$								
7	6723*	.08	7.9	.03		-.0056	-.008	-.008
8	6010*	.091	3.9	.04		-.017	-.012	-.013
8	6213*	.11	3.9	.05		-.023	-.016	-.017
9	5664	.071	1.46	.06		-.028	-.025	-.03
9	5845	.097	1.55	.07		-.039	-.031	-.041
10	5635	.12	1.00	.08	0.90	-.055	-.056	-.067
$nF_{5/2}-5D_{3/2}$								
$nF_{5/2,7/2}-5D_{5/2}$								
6	7229	.18	1.04	.14	.88	.11	.08	.11
6	7280	.20	1.28	.14	1.09	.09	.08	.11
7	6825	.31	1.07	.18	.87	.18	.16	.22
7	6871	.31	1.04	.18	.85	.18	.16	.22
8	6629	.57	1.08	.22	0.84	.31	.27	.41

Plasma conditions: Electron number density $(N_e) \approx 0.95 \times 10^{14} cm^{-3}$
Electron temperature $(T_e) = 2630°K$
(Ion shielding parameter $r = 0.43$)

Cs I Transition	Line Wavelength(Å)	W_m Å	$N_e W$ x10^{14}cm^{-3}	α	$N_e W'$ x10^{14}cm^{-3}	d_m Å	d Å	d' Å
$nS_{1/2}-6P_{1/2}$								
$nS_{1/2}-6P_{3/2}$								
9	6586	.045	5.0	.05		.02	.013	.014
10	5839	.030	1.89	.07		.033	.022	.027
10	6034	.031	1.91	.07		.036	.022	.027
11	5568	.049	1.48	.08		.055	.042	.05
11	5746	.037	1.12	.08		.055	.043	.05
12	5407	.082	1.19	.11	1.06	.10	.074	.082
12	5573	.069	1.19	.11	1.06	.095	.079	.087
$nD_{3/2}-6P_{1/2}$								
$nD_{5/2}-6P_{3/2}$								
7	6723*	.13	12.5	.03		-.007	-.008	-.008
8	6010	.094	1.98	.04		-.017	-.012	-.014
8	6213	.12	4.2	.05		-.022	-.016	-.018
9	5664	.091	1.84	.06		-.037	-.025	-.03
9	5845	.12	1.85	.07		-.055	-.031	-.043
10	5466	.14	1.46	.07		-.055	-.045	-.055
10	5635	.13	1.10	.08	1.02	-.072	-.056	-.067
11	5340	.19	1.12	.09	1.02	-.083	-.074	-.093
11	5503	.23	1.11	.11	1.00	-.10	-.090	-.120
12	5414	.47	1.36	.13	1.19	-.17	-.14	-.19
$nF_{5/2}-5D_{3/2}$								
$nF_{5/2,7/2}-5D_{5/2}$								
5	8018	.13	2.3	.08		.053	.033	.038
5	8081	.21	3.86	.08		.053	.033	.038
6	7229	.21	1.36	.14		.12	.08	0.12
6	7280	.23	1.46	.14		.12	.08	0.12
7	6825	.37	1.27	.18	1.05	.23	.156	.24
7	6871	.36	1.23	.18	.98	.23	.156	.24
8	6629	.60	1.15	.22	.90	.38	.30	.44
9	6473	1.1	1.23	.28	.90	.58	.43	.73

Cs I Line Transition	Wavelength(Å)	$\frac{W_m}{A}$	$\frac{N_e W}{\times 10^{14} \text{cm}^{-3}}$	α	$\frac{N_e W'}{\times 10^{14} \text{cm}^{-3}}$	$\frac{d_m}{A}$	$\frac{d}{A}$	$\frac{d'}{A}$
$nS_{1/2}-6P_{1/2}$								
$nS_{1/2}-6P_{3/2}$								
9	6355	.036	4.4	.06		.023	.0135	.0145
9	6586	.054	6.1	.06		.024	.0145	.0155
10	5839	.034	2.1	.07		.036	.025	.027
10	6034	.036	2.1	.07		.039	.026	.028
11	5568	.054	1.6	.09	1.45	.056	.041	.052
12	5407	.083	1.4	.12	1.15	.075	.082	.090
12	5573	.10	1.6	.12	1.30	.084	.088	.095
$nD_{3/2}-6P_{1/2}$								
$nD_{5/2}-6P_{3/2}$								
7	6973*	.120	9.0	.03		-.005	-.008	-.009
8	6010*	.13	5.4	.04		-.022	-.014	-.016
8	6213*	.16	5.0	.04		-.030	-.018	-.020
9	5664*	.12	2.3	.06		-.047	-.030	-.033
9	5845	.15	2.3	.07		-.055	-.039	-.045
10	5466	.15	1.5	.08	1.4	-.067	-.053	-.065
10	5635	.18	1.5	.09	1.3	-.083	-.066	-.083
11	5340	.21	1.2	.1	1.1	-.10	-.088	-.115
11	5503	.25	1.2	.11	1.1	-.13	-.103	-.140
12	5414	.38	1.1	.14	0.97	-.18	-.165	-.24
13	5349	.66	1.2	.17	1.03			
$nF_{5/2}-5D_{3/2}$								
$nF_{5/2,7/2}-5D_{5/2}$								
5	8018*	.175	2.8	.09		.067	.039	.045
5	8081*	.170	3.0	.09		.060	.039	.046
6	7229	.25	1.6	.15	1.40	.13	.093	.14
6	7280	.25	1.6	.15	1.40	.13	.095	.14
7	6825	.45	1.5	.19	1.24	.24	.185	.026
7	6871	.45	1.5	.19	1.24	.26	.187	.25
8	6629	.75	1.4	.24	1.1	.35	.32	.48
9	6473	1.10	1.3	.30	1.0	.63	.52	.88

Plasma conditions: Electron number density (N_e) = 2.8×10^{14} cm^{-3}
Electron temperature (T_e) = 2900°K
(Ion shielding parameter r = 0.48)

| Cs I Line Transition	Wavelength (Å)	W_{om} A	$N_e W$ x10^{14}cm^{-3}	α	$N_e W'$ x10^{14}cm^{-3}	d_{om} A	d_o A	d' A
$nS_{1/2}$-$6P_{1/2}$								
$nS_{1/2}$-$6P_{3/2}$								
9	6586	.084	9.45	.07		.04	.055	.046
10	5839	.069	4.30	.09		.063	.078	.070
10	6034	.075	4.80	.09		.0675	.092	.076
11	5568	.11	3.40	.11	3.0	.12	.17	.132
11	5746	.12	3.63	.11	3.25	.125	.16	.140
12	5407	.20	3.26	.15	2.8	.22	.23	.25
12	5573	.22	3.40	.15	2.92	.234	.28	.272
$nD_{3/2}$-$6P_{1/2}$								
$nD_{5/2}$-$6P_{3/2}$								
7	6723*	.36	36.0	.03		-.014	-.022	-.15
8	6010*	.26	11.0	.05		-.035	-.045	-.038
8	6213*	.66	20.3	.06		-.045	-.066	-.053
9	5664	.25	5.10	.08	.	-.072	-.10	-.088
9	5845	.33	5.38	.09		-.092	-.11	-.11
10	5466	.32	3.37	.10	3.0	-.13	-.14	-.166
10	5635	.38	3.14	.11	2.8	-.16	-.17	-.21
11	5340	.56	3.28	.12	2.9	-.22	-.22	-.29
11	5503	.67	3.22	.14	2.8	-.27	-.28	-.37
12	5414	1.14	3.32	.17	2.8	-.40	-.40	-.62
13	5349	1.94	3.58	.21	2.96	-.59	-.61	-1.0
$nF_{5/2}$-$5D_{3/2}$								
$nF_{5/2,7/2}$-$5D_{5/2}$								
5	8018*	.37	6.49	.11		.13	.10	.12
5	8081*	.47	8.55	.11		.13	.10	.12
6	7229	.59	3.68	.18	3.1	.32	.24	.34
6	7280	.53	3.40	.18	2.8	.31	.24	.34
7	6825	.91	3.10	.22	2.5	.56	.47	.70
7	6871	1.03	3.46	.22	2.8	.64	.47	.70
8	6629	1.97	3.76	.28	2.82	.98	.84	1.35
9	6473	2.6	2.97	.35	2.1	1.68	1.33	2.40
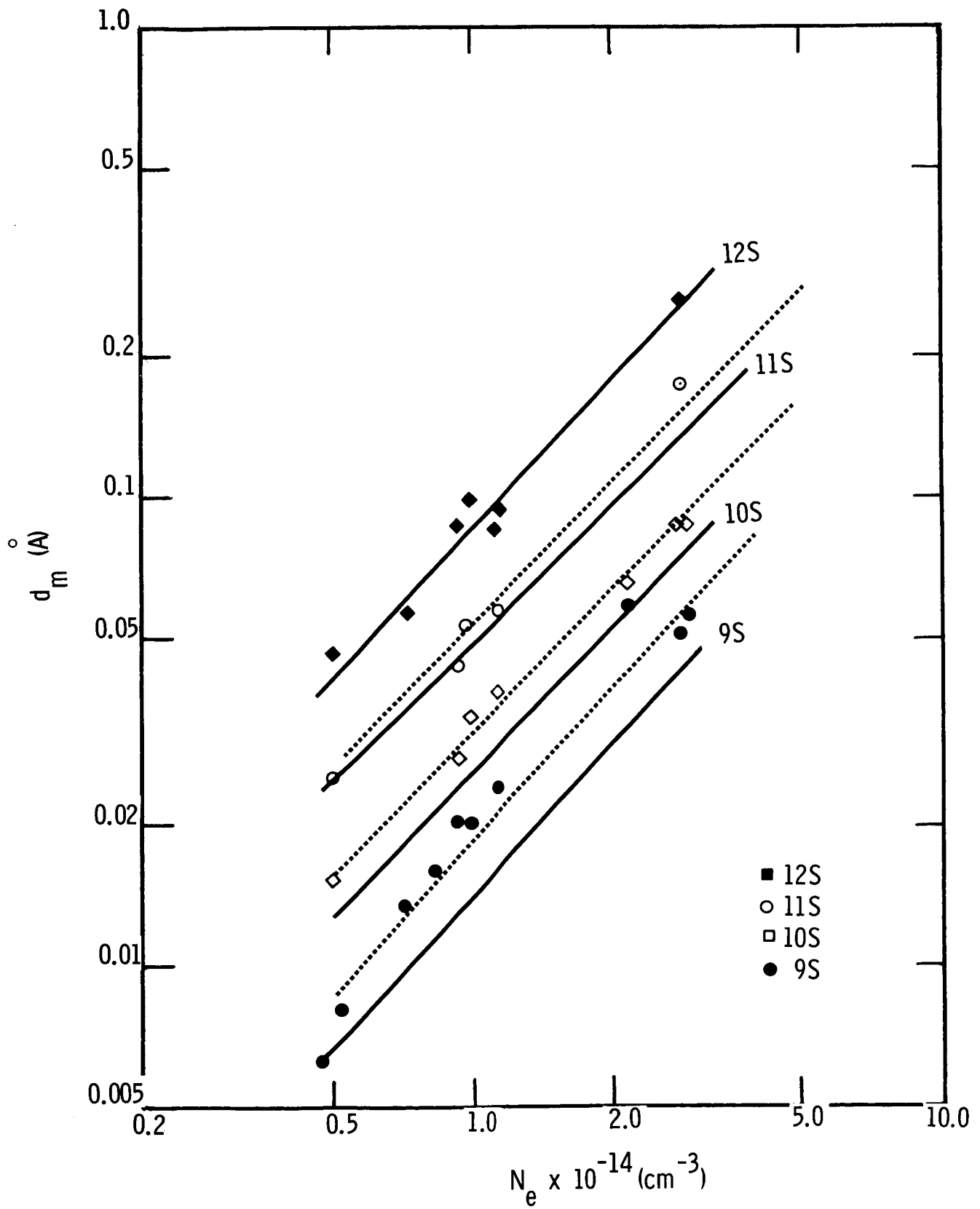
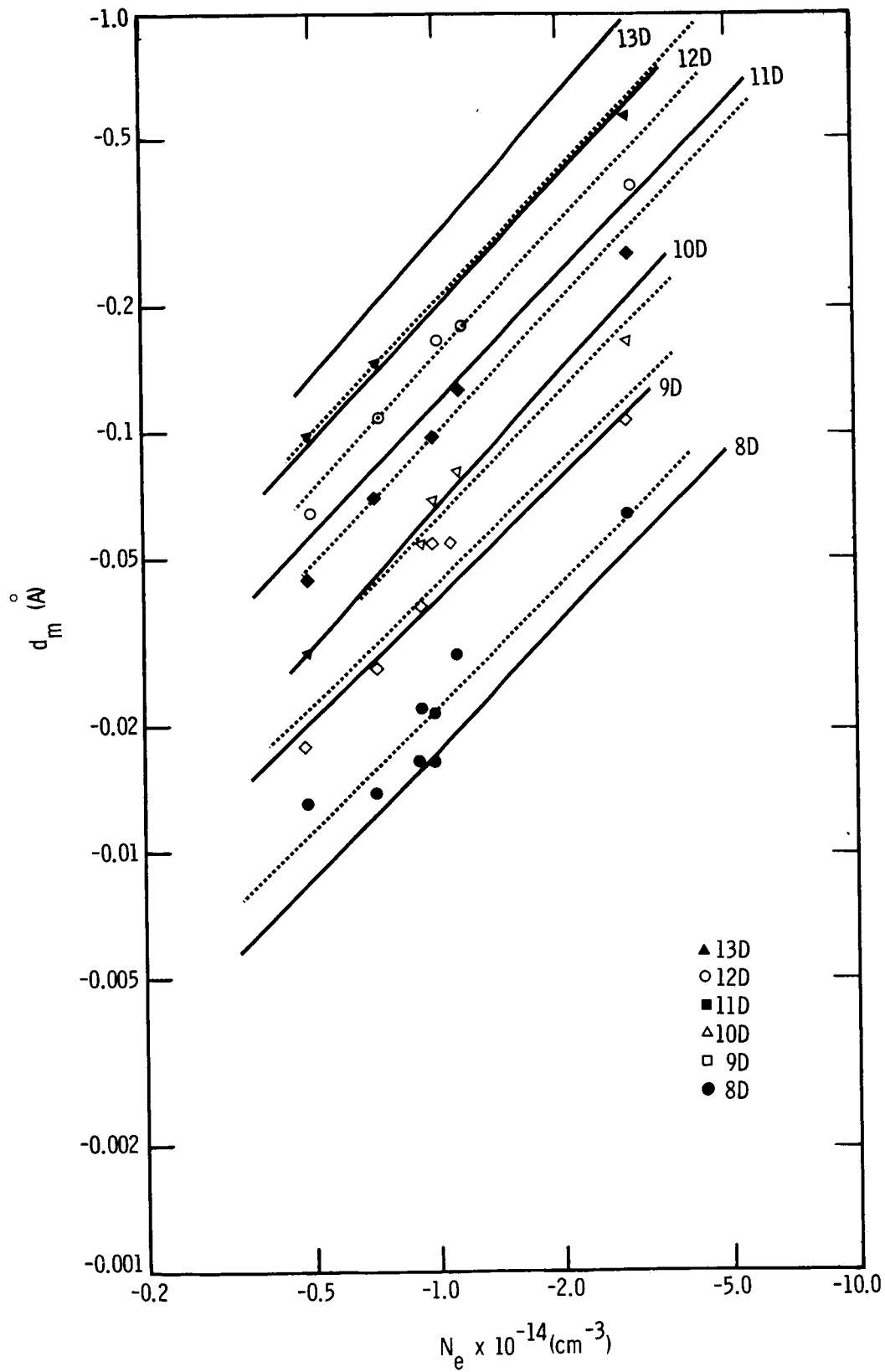Fig. 6. Measured shift (d_m) vs N_e for S series lines.

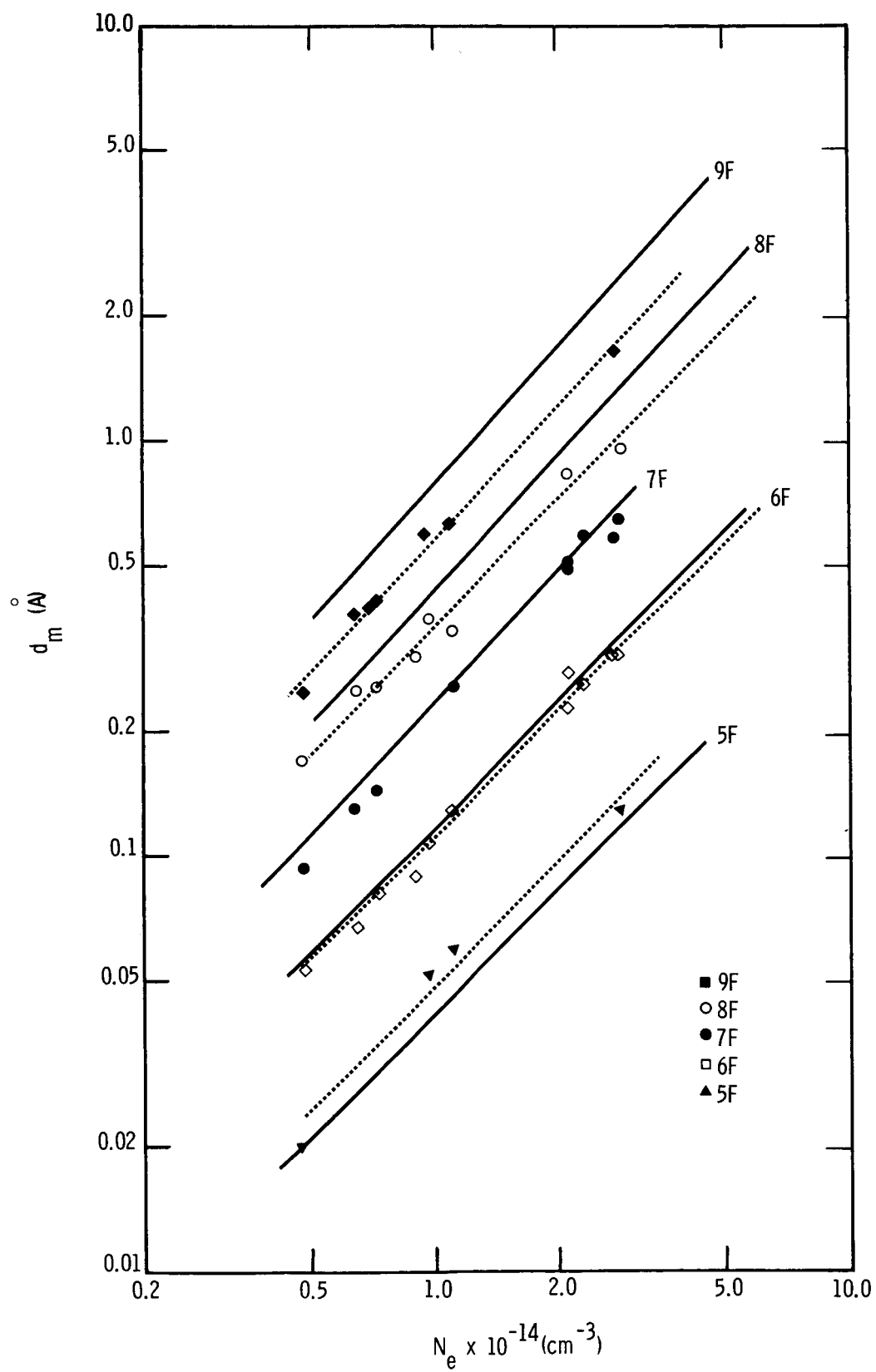Fig. 7. Measured shift (d_m) vs N_e for D series lines.

Fig. 8. Measured shift (d_m) vs N_e for F series lines.

For all series, the experimental shift values are higher than the theoretical values for the lower series members, match theory for the middle series members and are lower than theory for the higher series members. The nS-6P and the nF-5D series shifts are to longer wavelengths and the nD-6P series lines are to shorter wavelengths, as predicted. A line drawn through the data points is roughly parallel to the theoretical curve. The slopes of the experimental curves are at 45° for the low series members of the F and D series and for all the S series where the α correction is small indicating a linear relationship between N_e and d_m.

However, the slopes for d_m and d_t for the higher series lines are larger than 45° although both are parallel. This indicates that the contribution of the ion broadening term which involves α and r increases as N_e increases. These data were taken at electron temperatures ranging from 2630°K to 3100°K so that some degree of scatter is expected, although scatter due to this temperature variation should not exceed 10%. For this reason no attempt was made to reduce the data to a common temperature.

The cause of the change of position of the experimental lines from above the theoretical line to below it with increasing shift values was first thought to be a systematic experimental error. However this seems to be precluded by the fact that the displacement of the data from the theory remains constant (i.e. parallel) over a factor 7 in N_e. If a systematic error in the experiment caused the displacement of the experimental points above the theory for small shifts and below for large shifts one would expect the data for a range of shift values between these two limits to have curvature, i.e. at the small shift limit data would be above theory and at the high shift limit data would be below theory. This does not occur.

Another display of the data which will allow a good comparison of the data with theory is a plot of the width vs shift for each series (Figs. 9 and 10). Theory predicts that the d/w ratio is constant with N_e and for the α values in the range of N_e investigated, d_t/w_t is essentially constant and equal to d/w. The slope of a line drawn through the data points is shown with the theoretical value of d/w. Most of the lines are at a 45° angle which means that the d/w ratio is constant. The d_m/w_m ratio for the S and F series are essentially constant with total quantum number, n, and agree well with the theoretical values. The d/w ratio for the D lines plotted is negative and decreases with n. The values for n=10 and 11 agree with theory whereas the value at n=13 is 50% lower.
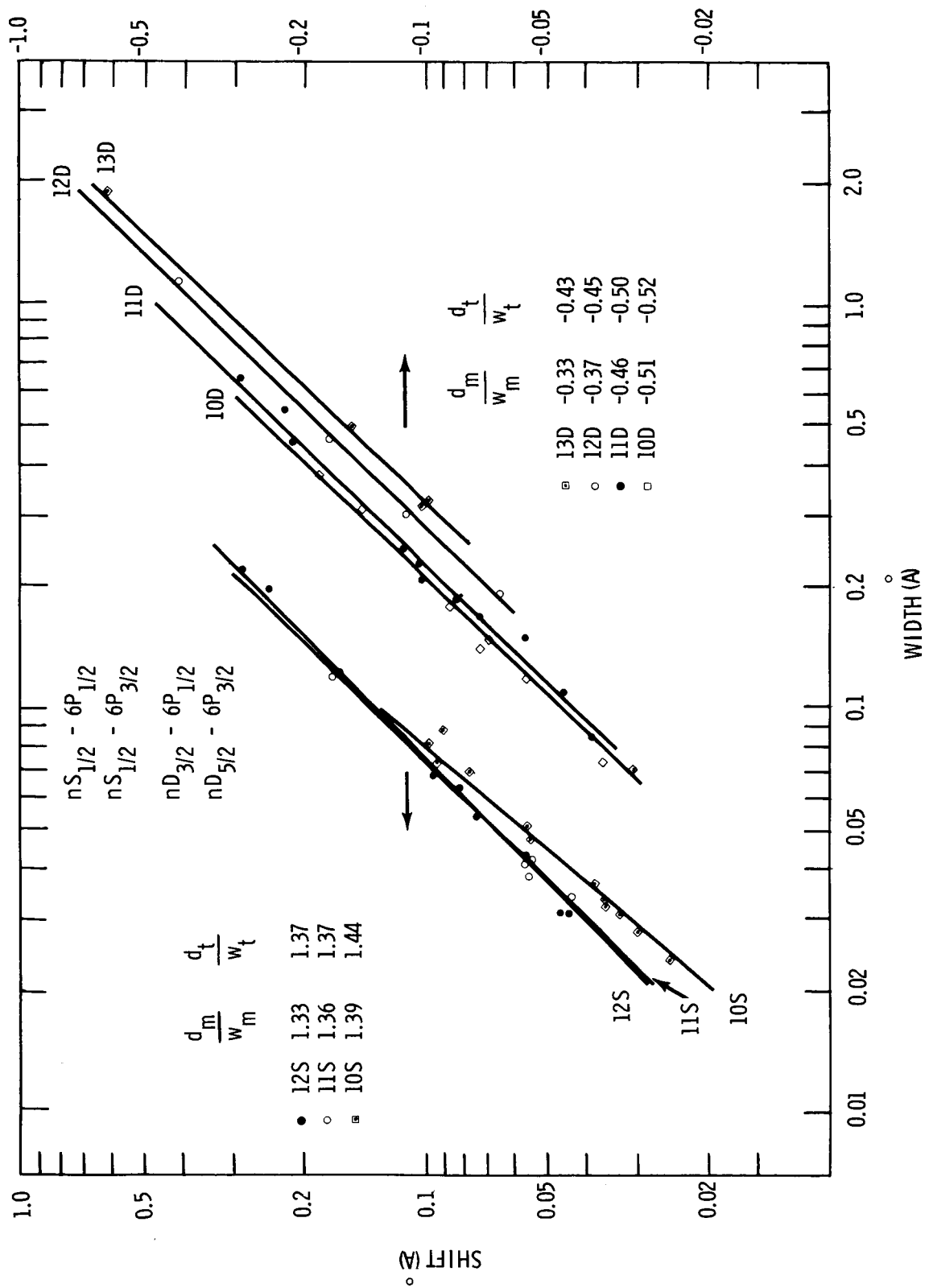
Fig. 9. Measured shift (d_m) vs measured width (w_m) for S and D series lines.
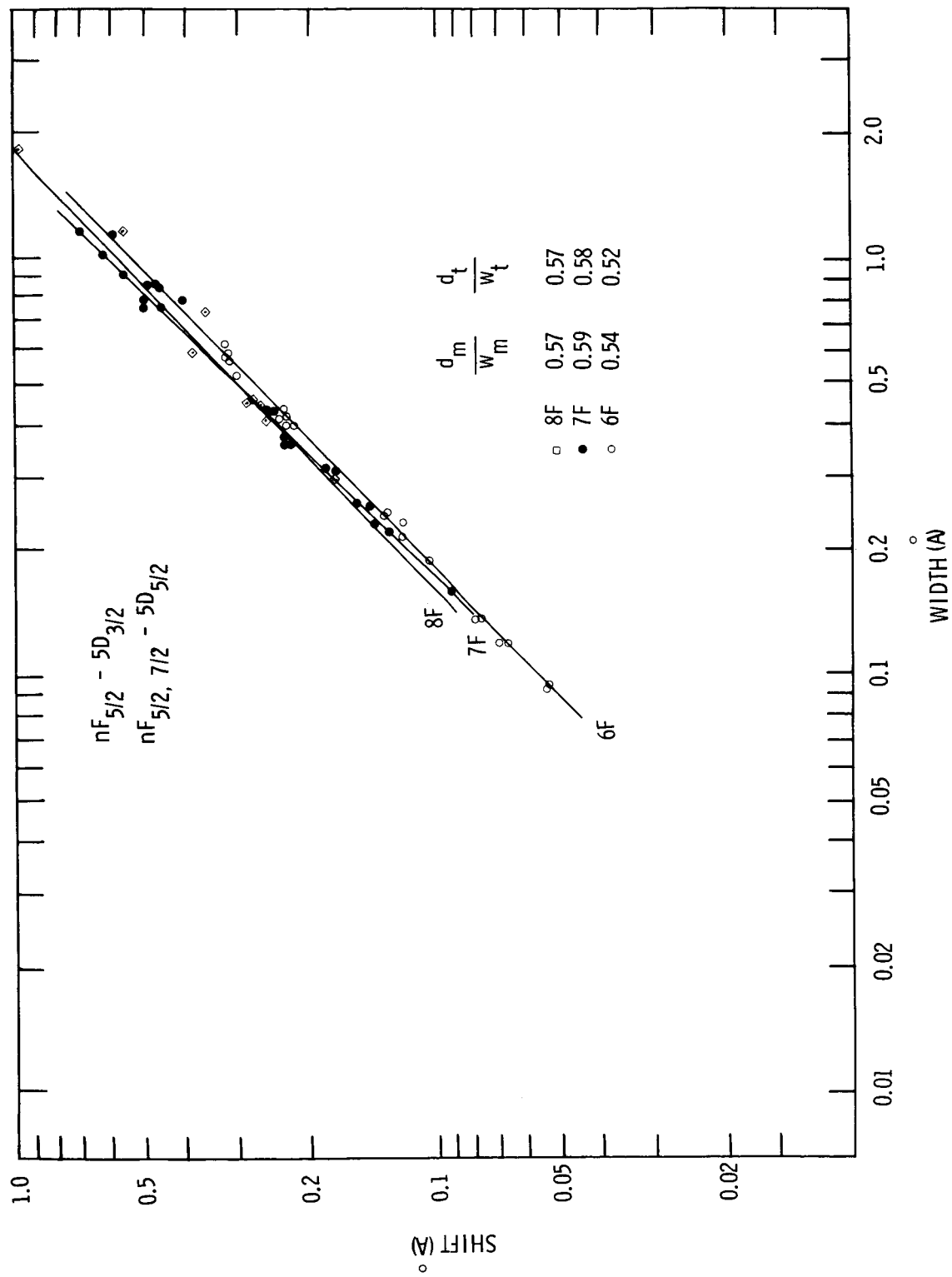
29

Fig. 10. Measured shift (d_m) vs measured width (w_m) for F series lines.

30

Line Profiles

We will analyze in detail four line profiles to compare the experimental line shapes with the profiles predicted by Griem. The profiles of the $7F_{5/2,7/2}$-$5D_{5/2}$, $7F_{5/2}$-$5D_{3/2}$, $10D_{5/2}$-$6P_{3/2}$, and the $11S_{1/2}$-$6P_{3/2}$ lines are displayed in Figs. 11, 12, 13 and 14. The theoretical profiles were compiled from Eq.(7) where the areas under the experimental and theoretical profiles have been normalized. These particular lines were chosen because the wings could be measured without interference from other lines and they showed good signal to noise characteristics. All of the experimental shapes agree well with theory and show the predicted asymmetry towards the shifted position.

The d_m vs N_e data showed that the theoretical shift d_t overestimates the shift for all values of d_m where α makes a substantial contribution to the shift. In fact Table II shows that the value of d_m appears between the theoretical values for d and d_t. This effect might be caused by an overestimate of the ion contribution to the width, assuming, of course, that the electron impact shift, d, is accurate. Therefore an experimental value of α was computed from the wings of the experimental profile from the relations for the reduced intensity in the wings.

$$J_a = \frac{1}{\pi x^2} + \frac{0.75\,\alpha}{x^{7/4}} \quad \text{(asymmetric side)}$$

$$(10)$$

$$J_s = \frac{1}{\pi x^2} \quad \text{(symmetric side)}$$

$$\text{for} \quad x \geq 4 \text{ where } x = \frac{\lambda - \lambda_o - d}{w}$$

The difference between the intensity in the wings at $\pm\, x$ is a function of α,

$$\text{or,} \quad J_a - J_s = \frac{0.75\,\alpha}{x^{7/4}}. \quad (11)$$

The line profile was then replotted for this new α along with a) the measured profile and b) the profile with α given by theory[5] in Fig. 14.
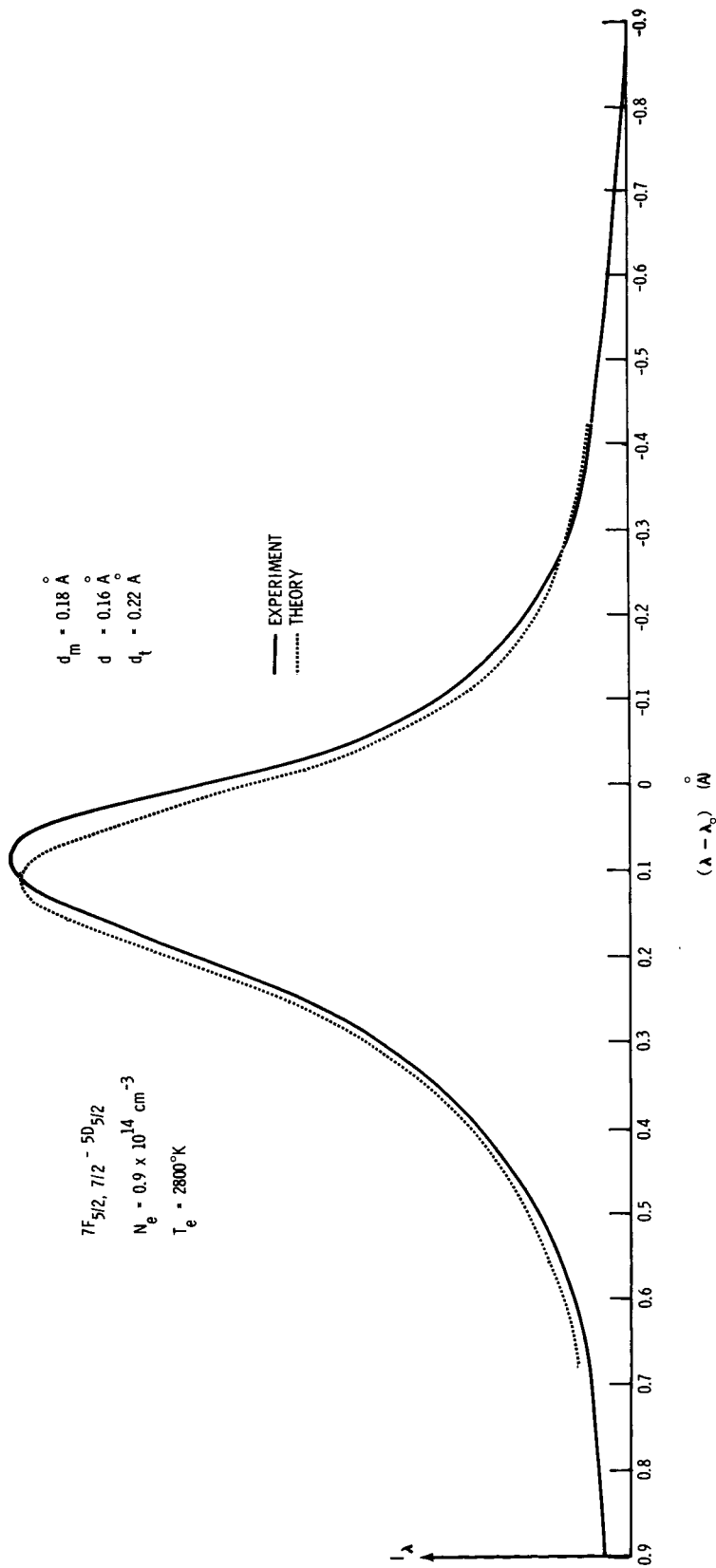
31

Fig. 11. Experimental and theoretical line profile of $7F_{7/2,5/2} - 5D_{5/2}$ line.

$d_m = 0.18$ Å
$d = 0.16$ Å
$d_t = 0.22$ Å

— EXPERIMENT
······ THEORY

$7F_{5/2, 7/2} - 5D_{5/2}$
$N_e = 0.9 \times 10^{14}$ cm^{-3}
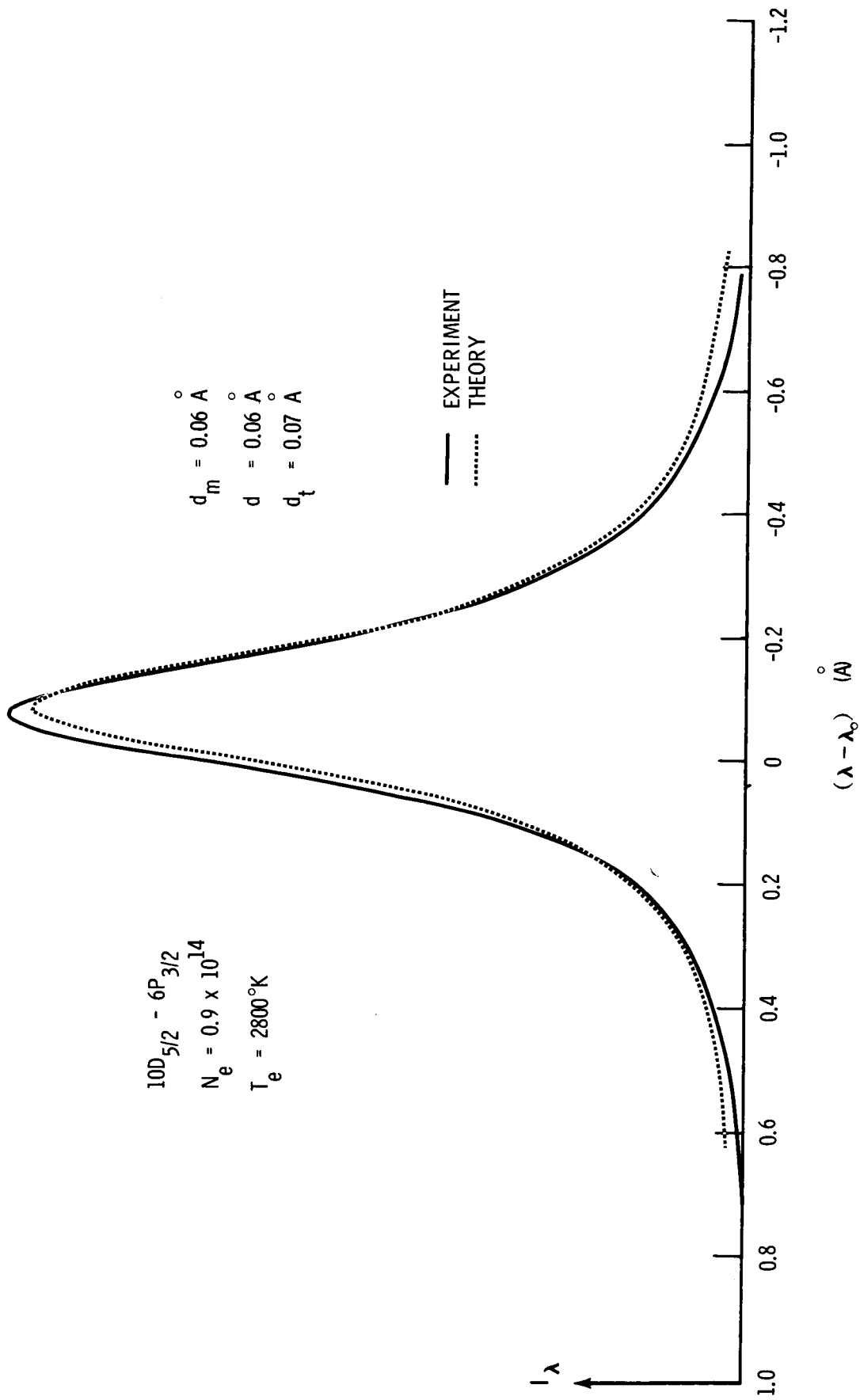$T_e = 2800°K$

$(\lambda - \lambda_0)$ (Å)

32

Fig. 12. Experimental and theoretical line profile of $10D_{5/2} - 6P_{3/2}$.

33

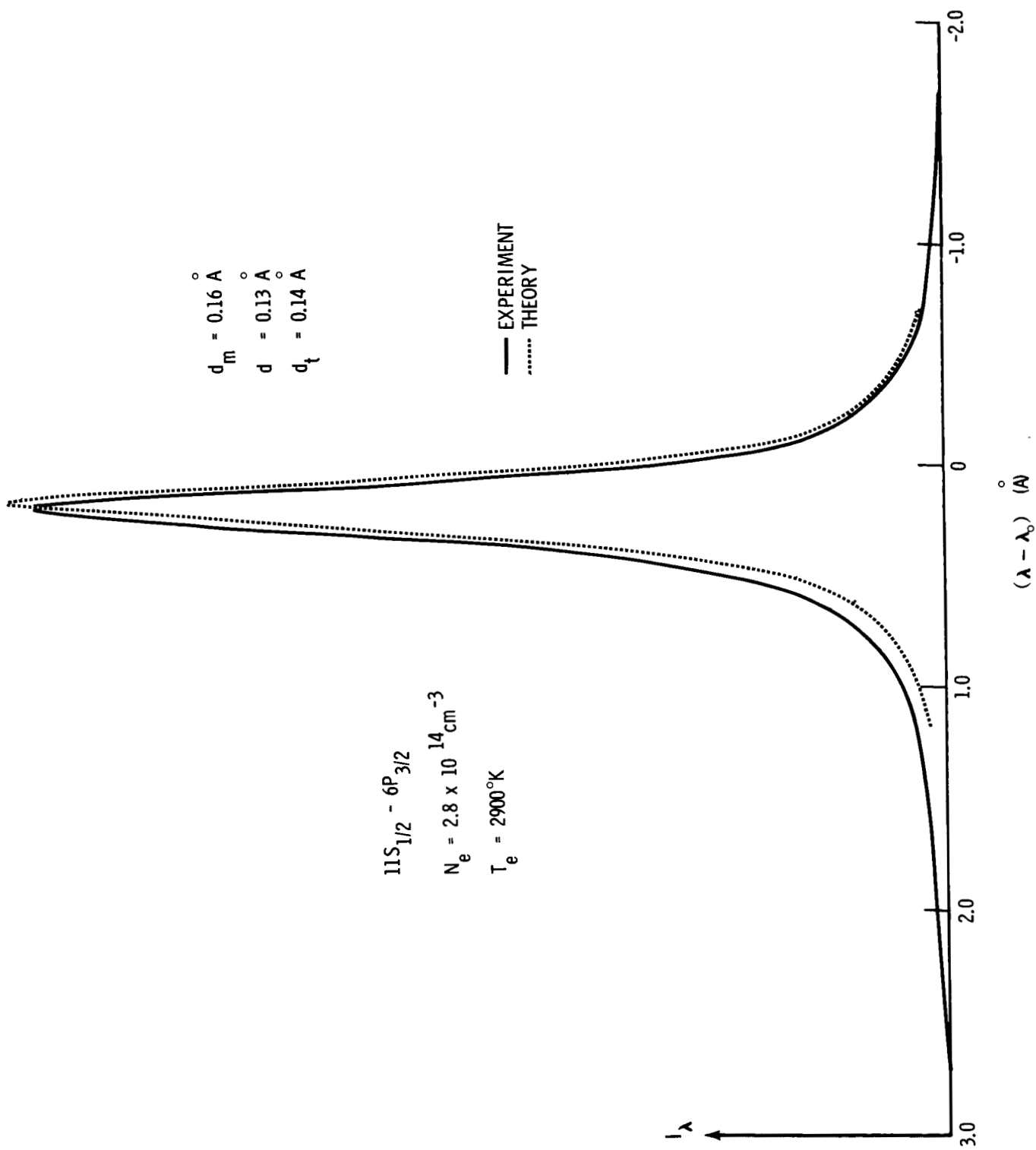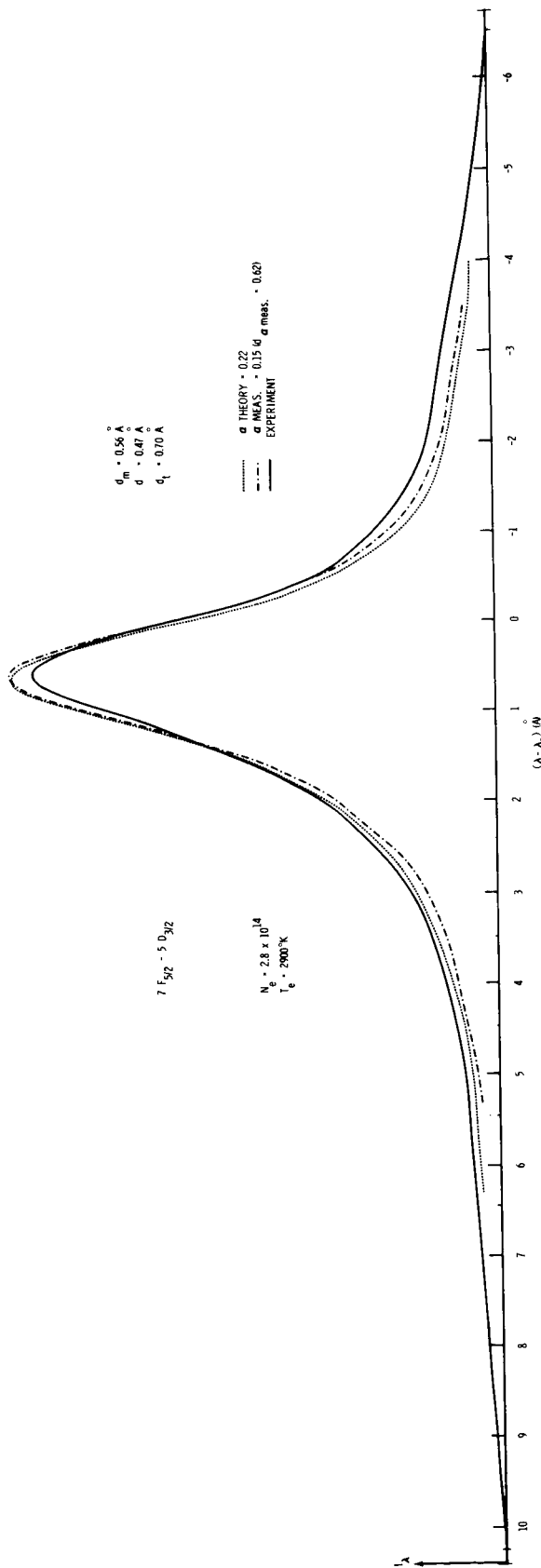Fig. 13. Experimental and theoretical line profile of $11S_{1/2} - 6P_{3/2}$.

$11S_{1/2} - 6P_{3/2}$

$N_e = 2.8 \times 10^{14} cm^{-3}$

$T_e = 2900°K$

$d_m = 0.16 \text{ Å}$

$d = 0.13 \text{ Å}$

$d_t = 0.14 \text{ Å}$

——— EXPERIMENT
········ THEORY

$(\lambda - \lambda_o) \ (\text{Å})$

Fig. 14. Experimental and theoretical line profiles $7F_{5/2} - 5D_{3/2}$.

For this purpose the $7F_{5/2}-6P_{3/2}$ line was chosen because it displayed the best signal to noise ratio in the wings of a line at the highest density $(N_e=2.8\times10^{14}cm^{-3})$. The α computed from the profile is 0.15 whereas the predicted value is 0.22. This α of 0.15 value yielded a smaller d_t which agrees better with the measured value.

Viz.

$$d_m = 0.56 \text{ Å for } 7F_{5/2}-5D_{3/2}$$
$$d = 0.47 \text{ Å}$$
$$d_t = 0.70 \text{ Å for } \alpha = 0.22$$
$$d_t = 0.62 \text{ Å for } \alpha = 0.15$$

Of course all of these values for d are relatively close to each other so that the reevaluation of d_t by computing α from the experimental curve is not as dramatic as it would be if it could be made on the lines with larger α's. However these lines (8F and 9F lines 11D, etc.) have very large widths which means that wing intensities must be measured at $\Delta\lambda$'s which are the order of 10 Å in order to use the asymptotic form for $J(x)$. It was difficult to find lines which have no interfering lines over this spectral distance.

This F series line is representative of all the broad lines. In fact, the measured shift appears to be closer to the predicted electron impact shift, d, where $\alpha=0$ than to the value for d_t obtained by using the predicted α.[4] The difficulty in measuring the wings at greater distances from the line peak hampers a more accurate measurement of α, which might yield values of α which predict the measured shift more accurately.

A similar situation exists for the broad D lines where the predicted shift is larger than the measured one and $d_m \cong d$. Finally the shifts for the broadest S series lines agree more closely with prediction but here the value of d/w is large and the contribution due to the term containing α is much smaller than those of the D and F lines.

We did not determine the influence of α determined from the wing data on the total width w_t. The contribution of α to the width is generally a factor of two less than its contribution to the shift and therefore less important. Also the results of Gridneva and Kaslov[4] showed good agreement between experimental and theoretical widths for lines with α as large as 0.31.

Absorption Effects

Three absorption mechanisms which affect the line profiles have been considered in the analysis of these data. A line will be broadened because of repeated absorption and re-emission throughout the volume of the plasma. This bulk absorption is described in Appendix B. In addition the absorption of a line in the cold layer near the boundary of the plasma, where the ratio of absorbers to emitters is much larger than in the bulk of the plasma, will cause a dip in the central region of a line. This self-absorption can be described in terms of the absorption coefficients for a non-radiating gas derived in Appendix A (see Fig. 3 and its discussion).

Finally, the resonance lines, already widened by bulk absorption and self reversed, may further exhibit an emission peak within the self-absorbed portion of the line. This effect has been observed in our plasma, and will be described later.

Only optically thin spectral lines were used to determine the widths. However the shift values of all the lines could be used because the center of the line is unaffected by bulk absorption. Also, the shift of the center of a self-absorbed line can be used to give an approximate value for the electron number density. The center of the line is approximately determined by bisecting equal intensity position of the wings on either side of the center where absorption effects are negligible. Also, since the strongly absorbed lines are the lower members of a particular series, the asymmetry is small so that the center can be determined accurately.

Lines which are optically thin for a given series, should lead to a reasonably constant electron density evaluated from the width. The influence of absorption effects are shown in Fig. 15 which is a composite of five $nD_{5/2}$-$6P_{3/2}$ lines with their centers matched at the center of the first line in the series ($7D_{5/2}$-$6P_{3/2}$). These data show the progression (as n increases) of the shape of a series of lines from a self-and bulk-absorbed condition to the optically thin condition.

Table III shows the measured widths and shifts from the D series lines which include the data of Fig. 15. The values of N_e^d and $N_e^{d'}$ in Table III were obtained in the same way as those of N_e^w and $N_e^{w'}$ in Table II except the iteration on N_e was performed using the line shift data and electron impact width w from the plasma parameters of Table III. In addition $N_e^{w'}$ was computed as before.
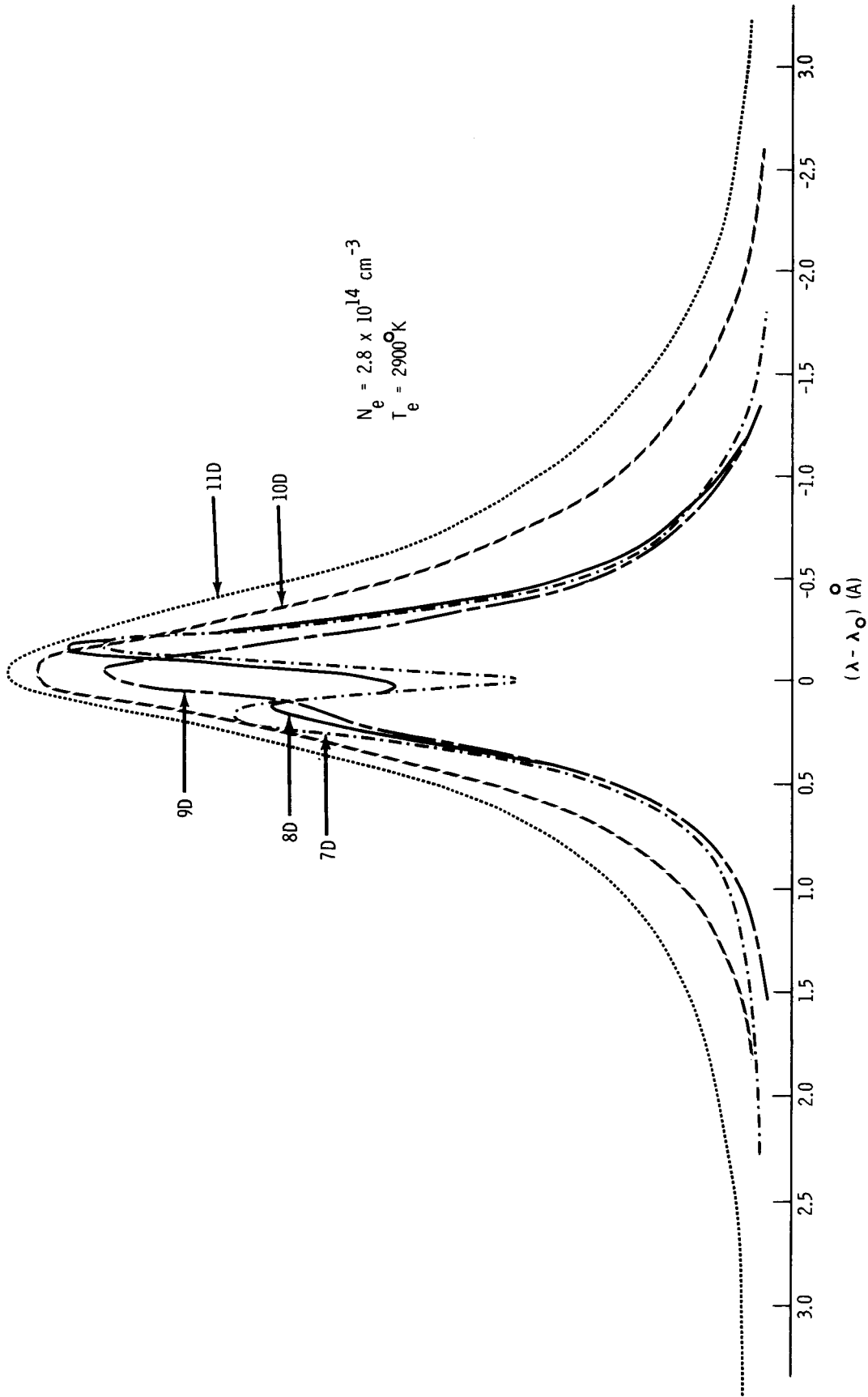
Fig. 15. Composite of 5D series lines showing progression from bulk and self-absorbed condition to optically thin condition.

$N_e = 2.8 \times 10^{14} \text{ cm}^{-3}$

$T_e = 2900^{\circ}\text{K}$

$(\lambda - \lambda_o) \ (\overset{o}{\text{A}})$

11D

10D

9D

8D

7D

TABLE III. Shift and width data for D series lines at
$N_e = 2.8 \times 10^{14} \text{cm}^{-3}$, $T_e = 2900°\text{K}$.

Line	λ_0 A	w_m A	d_m A	$N_e^{w'}$ 10^{14}cm^{-3}	N_e^d 10^{14}cm^{-3}	$N_e^{d'}$ 10^{14}cm^{-3}
$7D_{3/2} - 6P_{1/2}$	6723*	0.36	0.022	36	4.2	4.0
$8D_{3/2} - 6P_{1/2}$	6010*	0.26	0.045	11.0	3.36	3.0
$8D_{5/2} - 6P_{3/2}$	6213*	0.66	0.066	20.3	3.60	3.0
$9D_{3/2} - 6P_{1/2}$	5664†	0.25	0.10	5.1	3.65	3.2
$9D_{5/2} - 6P_{3/2}$	5845†	0.33	0.11	5.38	3.2	2.7
$10D_{3/2} - 6P_{1/2}$	5466	0.32	0.14	3.0	3.50	2.7
$10D_{5/2} - 6P_{3/2}$	5635	0.38	0.17	2.8	3.34	2.5
$11D_{3/2} - 6P_{1/2}$	5340	0.56	0.22	2.9	3.60	2.7
$11D_{5/2} - 6P_{3/2}$	5503	0.67	0.28	2.8	3.45	2.5
$12D_{5/2} - 6P_{3/2}$	5414	1.14	0.40	2.8	3.34	2.2
$13D_{5/2} - 6P_{3/2}$	5349	1.94	0.59	3.0	3.40	2.0

* Self-absorbed and bulk absorbed lines.
† Bulk absorbed.

These data show that bulk absorption, combined with self-absorption (which can cause an inaccurate estimate of the intensity maximum) causes an overestimate of $N_e^{w'}$ by an order of magnitude for the lower series members (7D and 8D) and pure bulk absorption causes an overestimate by a factor of two for the 9D lines. On the other hand, the widths of the 10D, 11D, 12D and 13D lines predict the same N_e value and thus fulfill optically thin criteria.

If we ignore the 7D value, then $N_e^{d'}$ is seen to vary by only a factor of 1.5 over all the series members. The 7D line is bulk absorbed to such an extent that it is very difficult to determine its center. The value of $N_e^{d'}$ decreases from 8D to 13D because of the increasing effect of the α term as indicated in the section on widths and shifts.

From these data we conclude that the values of $N_e^{w'}$ and $N_e^{d'}$ substantiate the concept that the N_e measurement from shift data is independent of absorption effects and hence more reliable.
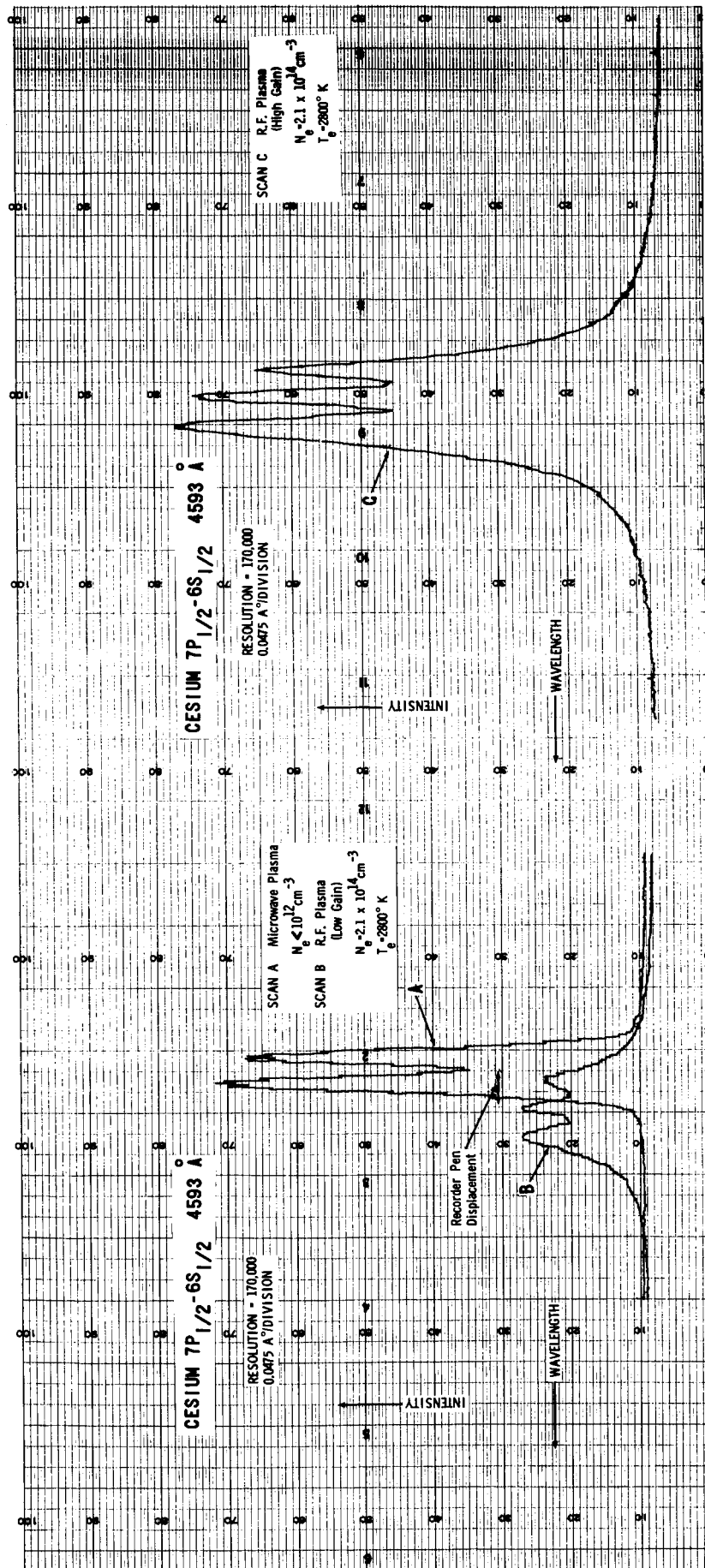
Fig. 16. Emission peak in self-absorption minimum of $7P_{1/2} - 6S_{1/2}$ line. Profiles B and A are the simultaneous tracing of $7P_{1/2} - 6S_{1/2}$ line from the rf (hot) plasma and from the microwave (cold) plasma (fiduciary line). Note that the position of the central peak of profile B coincides with the pen displacement. Profile C is a re-scan of B at high gain to show the details.

The shift of a self-absorbed line can also be measured by determining the position of the center of the line with respect to the absorption dip. Since the absorption occurs in a relatively cool region of the plasma, where the electron density is low, this dip corresponds closely to the unperturbed line position. This measurement allows an estimate of electron density without the use of a fiduciary.

Bulk and self-absorption are common to lines in all spectral series. An additional effect has been observed in lines of the principal (resonance) series which is the appearance of an emission peak within the self-absorbed portion of the lines. This resonance fluorescence is displayed in Fig. 16 which is a tracing of $7P_{1/2} - 6P_{1/2}$. The emission peak in the absorption dip is believed to be caused by a right angle scattering of the radiation in the region near the viewing window where the optical depth is less than unity. If this hypothesis is correct, the center of this emission peak should be very close to the unshifted position of the line, a fact substantiated by measurement. The resonance line emission peak in Fig. 16 lies at the position of the self-absorption minimum of the fiduciary line which corresponds to the unshifted line position. Additional studies beyond the scope of this program would be required to completely explain this phenomenon.

Continuum Measurements

The radiation intensity emitted by the recombination of free electrons into the 6P bound states (henceforth called the continuum intensity) in a region free of interferences was monitored during the time over which the profile data were obtained. Since this intensity, I_λ , is proportional to N_e^2, its fluctuation provided a good indication of the fluctuation of N_e. The rf power and oven conditions were adjusted so that N_e was held to within $\pm$ 10%.

At appropriate time intervals a scan was made over the wavelength region from the 6P series limit ($\sim$ 4900 Å) to 4000 Å. The expression which relates the 6P continuum intensity to N_e was derived by Agnew[2,8] from the experimental results of Mohler.[7]
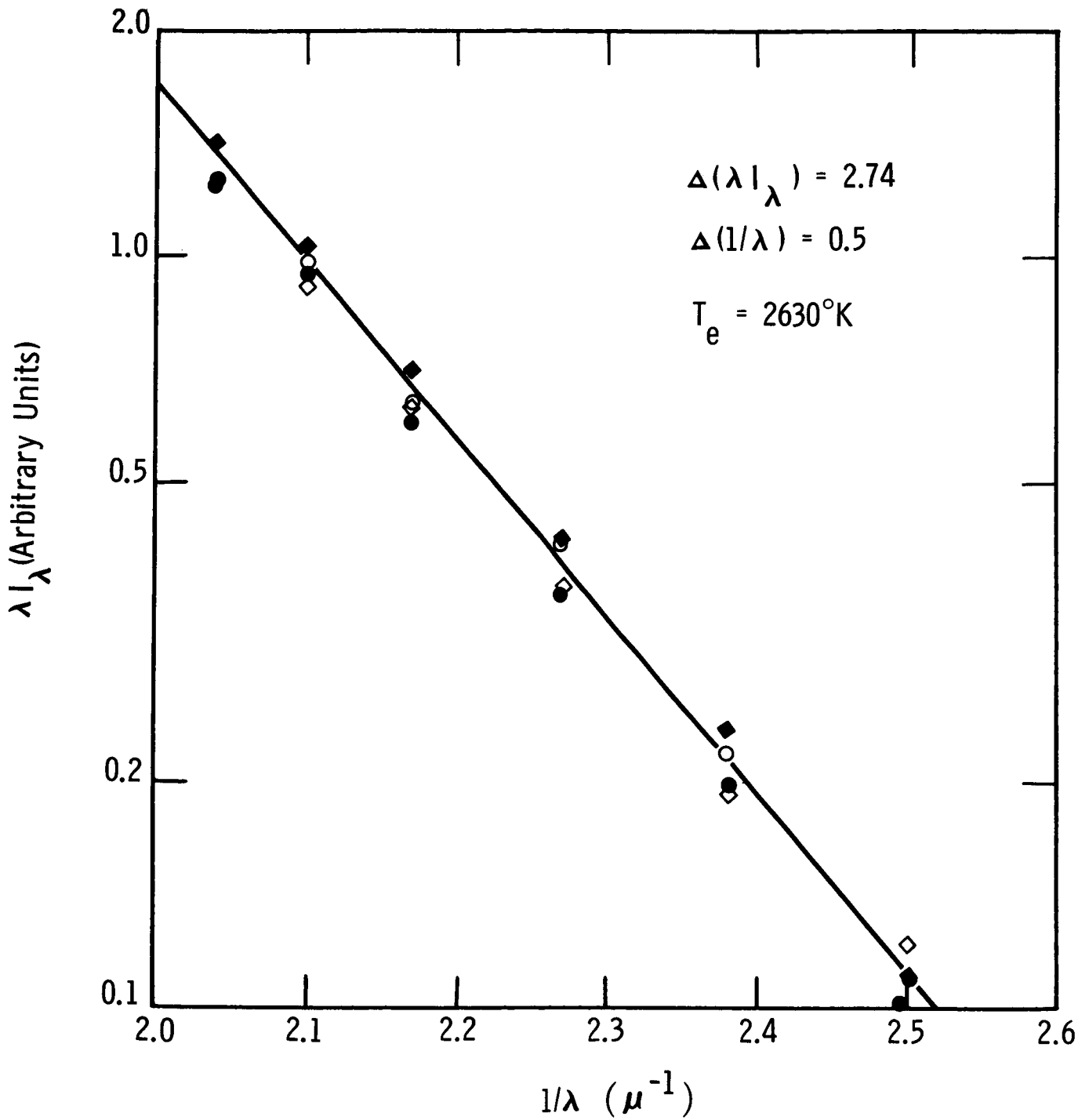
Fig. 17. Representation of continuum for temperature measurement; λI_λ versus $1/\lambda$.

$$I_{\nu} = \frac{4 \, N_e^{\,2} \left[1.56 \times 10^{-56}\right] (k \, T_e)^{-3/2}}{\nu \left[2 \, \pi m_e\right]^{1/2}} \, e^{-\frac{hc}{kT_e}\left[\frac{1}{\lambda_{6P}} - \frac{1}{\lambda}\right]}$$

or,

$$I_{\lambda} = \frac{0.49 \times 10^{-18}}{\lambda} \, \frac{N_e^{\,2}}{T_e^{\,3/2}} \, e^{\frac{hc}{kT_e}\left[\frac{1}{\lambda_{6P}} - \frac{1}{\lambda}\right]} \qquad \frac{\text{ergs}}{\text{cm}^3\text{-sec-ster}}$$

$$\left.\rule{0pt}{6.5em}\right\} \quad (12)$$

where λ_{6P} is the wavelength at the 6P series limit

λ is the wavelength at the measured position

T_e is the electron temperature

Equation (12) can be rewritten in a simplified form to show the wavelength dependence of I_{λ}.

$$\ell n \left(\lambda I_{\lambda}\right) = \text{const} - \frac{hc}{k \, T_e} \left(\frac{1}{\lambda}\right) \qquad (13)$$

Therefore, a plot of λI_{λ} vs λ^{-1} will yield the electron temperature, T_e. Figure 17 is a typical plot of these data.

The wavelength dependence of the continuum intensity $(I(\lambda))$, obtained from a hydrogenic approximation (Eq.10 Appendix B) is λ^{-2} instead of λ^{-1} derived by Agnew. We choose to use Eq.(12) since it has been experimentally verified by Agnew[2] and by Gridneva and Kasalov.[4]

We plotted the hydrogenic continuum dependence with our data, and obtained temperatures 10% lower than those quoted in the text. (Table II). These differences were not significant as far as our primary determinations of shifts and widths were concerned. But if the absolute continuum intensity were used to determine the electron density, the differences between values obtained from the two expressions would be significant. This would require a very accurate absolute calibration of the monochromator. However we did not take into account such factors as a change in the transmission of the glass of the plasma tube with time and variations in photomultiplier sensitivity, which placed doubt on the constancy of our initial calibration. Thus we were unable to obtain a value of N_e from continuum intensity or test the validity of continuum expressions with these data.

Error Analysis

The accuracy with which the Stark broadening theory of Griem predicts the electron density at $9 \times 10^{13} \text{cm}^{-3}$ in a cesium plasma (for the optically thin lines which we use) has been ascertained to be $\pm 10\%$.[4] This uncertainty combined with our reproducibility of these line shapes of $\pm 5\%$ gives a maximum uncertainty of $\pm 15\%$ in the determination of N_e. The shift measurements are reproducible to ± 0.01 A. This limitation is caused by the uncertainty in the position of the peak of the line combined with the variation of the recorder pen displacement. To attribute the large d_m values (compared with theory) to this uncertainty we believe is precluded by the data of the 9 and 10S series lines. The peaks of these lines were the sharpest and most accurately determined. Yet the displacement of the shift from theory is constant over the range of shift values from 0.008 A to 0.1 A.

The electron temperature measurement from the continuum slope, appears to be well within $\pm 10\%$ and is probably more like $\pm 5\%$. The width and shift values are insensitive to this temperature which therefore does not influence the quoted accuracy above on this shift measurement.

An experimental error of 0.01 A in shift would correspond to an uncertainty in N_e of $\pm 2\%$ at N_e equal to 10^{14}cm^{-3} for the 9F lines, $\pm 15\%$ for the 9D lines and $\pm 45\%$ for the 9S lines. The quoted experimental uncertainty in the width predictions of N_e is $\pm 5\%$. However the line required for meaningful width measurements must be optically thin. This restriction limits us to broader lines which automatically lead to the low $\pm 5\%$ uncertainty. Shifts for these same lines (for example 9F) are at least this accurate. Furthermore accuracy of this magnitude or better may be also obtained in the shifts of lines entirely unsuitable for width measurements but highly desirable for other reasons. An example is the accuracy in the shift of the S series lines which have large shifts, high intensity but small widths.

For any practical diagnostic application, lines can be selected which have less stringent resolution requirements than many of the lines measured here. The resolving power of a spectrometer is defined as $\lambda/\Delta\lambda$ where λ is the wavelength of the spectral region of interest and $\Delta\lambda$ is the separation of the peaks of two narrow lines which merge at half maximum. The resolving power of our spectrometer is 145,000 at 6000 Å in the 6th order (where most of the

data were obtained) with 15µ entrance and exit slit widths. This allows lines with separation of 0.04 Å or greater to be resolved and it also means that the width of the slit function at half maximum (called the apparatus width) is 0.04 Å. Since the profile of every line is modified by this function, those lines whose true widths are less than the apparatus widths require large corrections. Our experiments show that lines with true widths equal to and larger than the apparatus width can be suitably corrected and their true widths obtained. Therefore we consider the minimum resolving power required for a line width measurement to be that number obtained when $\Delta \lambda$ is set equal to the true line width.

Since the slit function is symmetric, the resolution requirement is not as stringent for the shift measurement. For example, our shift data are accurate for shifts of 0.015 Å or greater. Thus if the line width and shift were equal, approximately 3 times the resolution would be required to measure the width with the same accuracy as the shift. For the diffuse and fundamental series the widths will be a factor of about 2 or more greater than the shifts and thus the requirements on the instrument are only slightly more severe for the widths than the shifts. For the sharp series where the shift is 1.2 to 1.5 times greater than the widths, the resolution of the instrument required for shift measurements is about 1/4 that required for the widths, as evident by the fact that only the widths of the 11S or 12S lines gave accurate values of N_e. Thus the resolution of the spectrometer depends on the method to be used (i.e. shifts or widths) and the spectral series. The lowest number in any series requires the highest resolution.

Table IV gives the resolution required for measurements at an electron density of 10^{14} cm^{-3} with an accuracy of 20% for selected cesium lines by the shift and width methods. The resolution tabulated scales inversely with the electron density.

TABLE IV. Spectrometer resolution requirements for width and shift measurements.

Cesium Line Series Designation	Resolution Shift	Resolution Width
8 D - 6 P	68,000	210,000
10 D - 6 P	30,000	48,000
12 D - 6 P	12,000	16,000
14 D - 6 P	6,000	7,000
6 F - 5 D	28,000	46,000
8 F - 5 D	8,000	13,000
10 F - 5 D	3,000	5,000
10 S - 6 P	84,000	350,000
12 S - 6 P	22,000	87,000
14 S - 6P	9,000	31,000

REFERENCES

1. Thermionic Conversion Specialist Conference, Oct. 25-27, 1965, San Diego, Calif., Session I, Transport Theories.
2. H. Griem, M. Baranger, A. C. Kolb and G. Oertel, Phys. Rev. 125, 177 (1962).
    H. Griem, Phys. Rev. 128, 515 (1962).
    P. Stone and L. Agnew, Phys. Rev. 127, 1157 (1962).
    M. Baranger, Phys. Rev. 112, 855 (1958).
3. R. Donohue, R. Majkowski, J. Appl. Phys., 33, 3, (1962).
    W. Reichelt, W. Kruer, Thermionic Conversion Specialist Conference, San Diego, Calif., October 25-27, 1965, p.129.

4. S. Gridneva, G. Kasalov, "Oscillator strengths and profiles of spectral lines in cesium plasma" presented at VII International Conference on Phenomena on Ionized Gases, Belgrade, (1965).

A preprint of this article was obtained from Dr. L. Agnew of Los Alamos Scientific Laboratory. The original Russian was translated and can be summarized as follows. The widths and shifts of a large number of cesium S, D and F series lines were measured for a single set of plasma parameters - electron number density $9 \times 10^{13} \text{cm}^{-3}$ and electron temperature 2380°K. The plasma source was the positive column of a dc discharge in a mixture of cesium and argon. The partial pressure of argon was 80 mm and the cesium cold spot was 250°C. The electron density of this source was measured independent of width and shifts from the continuum intensity. This value was confirmed by using the Saha equation. It appears that the spectral measurements were made with photographic techniques, but few details are given other than the Russian designation of the apparatus. The shifts were measured relative to lines of a dc iron arc displayed on the same photographic plate as the cesium lines but no reference is made to the accuracy of the absolute wavelength calibration of the iron spectrum or stability of iron arc source.

Their measured cesium spectral widths are within 10% of the predicted total width (w_t of Eq.(8)) given by the Griem theory for this plasma condition. Because of limitations in their photographic method, shifts measurement could be made only on lines whose shifts were between 0.05 A and 0.7 A. They measured each value along with a corresponding theoretical value, taken from Griem. However, the theoretical values listed are those of the electron impact shift d, whereas the measured shifts (d_m) should be compared to the predicted total shift (d_t of Eq.(8)).

With these qualifications in mind, their data show these trends: All the measured shifts are larger than theory for the S lines, 9S-6P to 13S-6P with the measured shifts approaching d as n increases. Shifts of the D series lines match theory (d) fairly well from 9D-6P to 14D-6P with the 15D-6P shift larger than theory. Finally, the 9F and 10F-5D shifts matched d.

5. H. Griem, "Plasma Spectroscopy", McGraw-Hill, New York (1965).
6. H. Kleiman, J. Opt. Soc. Am., 52, 441 (1962).
7. F. Mohler, J. Research Natl. Bur. Standards, 849 (1937) Revs. Modern Phys. 1, 216 (1929).
8. Personal communication with Dr. L. Agnew of LASL.

APPENDIX A - Plasma Spectroscopy

INTRODUCTION

There are various ways to investigate plasma parameters. Electrical probes are widely used. They have the disadvantage of perturbing the plasma due to the physical size of the probe. Probes give data relative to ion density, electron temperature and energy distribution. Microwave attenuation is used to measure plasma densities in the range of 10^7 to 10^{12} electrons per cc. Very far infrared attenuation is now being studied for use in the 10^{12} to 10^{14} range. These methods only yield number densities. Perhaps the most powerful tool for investigating plasma temperatures and densities for densities greater than 10^{13} electrons per cm^3 is optical spectroscopy.

Ideally, spectroscopic methods yield the most information for those plasmas in which local thermal equilibrium (L.T.E.) exists. Complete L.T.E. prevails when the kinetic temperatures of the electrons, ions and atoms and those characterizing the distribution over the bound states (Boltzmann factors) and the free states (Saha equation) of the excited particles are alike. This is true when the electron densities are greater than 10^{16} cm^{-3} and temperatures are less than 10 ev. However in plasmas which are collision dominated i.e. in which excitation and de-excitation, ionization and recombination are mainly caused by electron collisions, the L.T.E. criteria only require the equality of the electron temperature with the distributional temperatures of the upper bound states. Then, one can tentatively extend the spectroscopic methods to electron densities of 10^{13} cm^{-3} and temperatures of the order of a tenth ev. The validity of this extension can and should be tested since the spectroscopic methods contain various self consistence tests which show the limits of their applicability.

SPECTROSCOPIC THEORY

Intensity Measurements

The various methods of spectral plasma diagnostics will be discussed in terms of the phenomena observed. In all cases, unless stated otherwise L.T.E. is assumed. The diagnostic method will then be derived from these phenomena. Various checks for the assumption of L.T.E. will also be given. The first phenomena is that of spectral line emission and the intensity of such lines.

Line Intensity:

Figure 1 shows the electronic energy level diagram of an isolated atom. Six excited energy levels are shown. The energy of E_∞ corresponds to the usual ionization potential χ for an isolated atom. Ionization corresponds to exciting the electron beyond E_∞ and into the continuum. The atom normally exists in its ground, or unexcited, state and its outermost electron occupies the ground state level E_0. When the atom is excited, the electron moves to one of the bound excited levels, E_1, E_2, E_3, etc. or if given enough energy (χ or greater) it becomes free of the atom and exists in the continuum (with kinetic energy $E-\chi$). A free electron and ion can recombine and give rise to an excited atom in one of the bound states. Regardless of the manner in which the atom is produced in one of these bound states, it will in time decay to the ground state. Enroute to the ground state the electron may fall momentarily into a number of intermediate lying excited states. For each such

transition, the atom will emit a photon of energy.

$$h\nu_{ul} = E_u - E_l \tag{1}$$

where u and l denote the upper and lower energy levels and ν the frequency of the photon. The emission of this photon gives rise to a discrete spectral line of frequency ν_{ul}. The intensity of this line is

$$I_{ul} = A_{ul} \; N_u \; h\nu_{ul}$$

where A_{ul} is the probability of the rate of the transition occurring from the upper u^{th} state to the lower l^{th} state, N_u is the number of excited atoms in the upper state which can participate in such a transition and $h\nu_{ul}$ the emitted photon energy.

For systems in L.T.E., the population of the various excited states can be expressed by the Boltzmann relation

$$N_u = \frac{g_u}{g_0} \; N_0 e^{-E_u/kT} \tag{2}$$

where N_0 is the population of the ground state, T the temperature characteristic of the manner in which the excited states are populated and g_u and g_0 are the statistical weights of the upper excited and ground state respectively. Since excitation and de-excitation are by electron collision this is the electron temperature. Thus the line intensity becomes

$$I_{ul} = A_{ul} \; N_0 e^{-E_u/kT} \; h\nu_{ul} \; \frac{g_u}{g_0} \tag{3}$$

The degree of ionization in the plasma can be written in terms of a statistical relation, the Saha equation. The Saha equation is obtained by extending the Boltzmann distribution for the bound states (Eq.2) so as to include the electron distribution (considered Maxwellian) for the continuum. As a consequence of this treatment the temperature T in the equation, for a collision dominated plasma, is the electron temperature (given by the Maxwellian distribution). Written in a form relating the electron density, N_e, to the ground state density, N_0, the Saha equation is

$$\frac{N_e^2}{N_0} = S(T) = \text{Const}(kT)^{3/2} e^{X'/kT} \tag{4}$$

where

$$X' = X - \Delta X .$$

X' is the observed ionization potential. X is the usual ionization potential for an isolated atom and ΔX is the amount the ionization potential is lowered due to the presence of fields from neighboring ions.

Continuum Intensities:

The emission of continuous radiation results from two dominant causes: (1) transitions of free electrons within the continuum while in the field of an ion, the free-free radiation or Bremsstrahlung, and (2) the radiative recombination of an electron into one of the bound electronic levels to form an atom in an excited state from an ion-electron pair, the free-bound radiation or recombination continuum.

Bremsstrahlung results from the slowing of a fast electron in the field of the ion. If the electron originally has a kinetic energy $mv^2/2$, the largest frequency that can be radiated in the stopping process is:

$$\nu_{max} = \frac{mv^2}{2h} \qquad (6)$$

From this limit the continuum of frequencies can extend towards lower values since arbitrarily small energy changes may occur in the retardation process. The intensity of the free-free continuum then depends on the velocity distribution (Maxwell-Boltzmann) of the free electrons i.e. on the number of electrons whose velocities permit them to contribute to the radiation at a given frequency in accordance with Eq.(6). Consequently, the free-free intensity can be written

$$I_{(F-F)} = Const\ (kT)^{-1/2}\ N_e^2\ exp(\Delta\chi/kT)\ exp(-h\nu/kT) \qquad (7)$$

The free-free continuum intensity will decrease as the frequency increases.

Superimposed on this free-free continuum is the recombination continuum. This results from a radiative recombination of an electron and ion to form an excited atom. Recombination into each of the bound levels will give rise to a component of the total free-bound continuum. Each of these components will have a lower limit at the frequency equal to the difference between the observed ionization potential, χ' and the lower bound state,l, corresponding to the recombination of an ion with an electron that has zero velocity.

$$\nu_{min} = \frac{\chi' - E_l}{h} \qquad (8)$$

This frequency is called the series limit. There will be a definite series limit for each of the bound states E_l. For upon the recombination of an electron with velocity v, the energy of the emitted photon will be

$$h\nu = 1/2mv^2 + (\chi' - E_l) \qquad (9)$$

The intensity of the recombination continuum for a given bound state is derived by considering transitions between a set of pseudo-hydrogen levels in the continuum and that bound state with the limitation that the first of these pseudo-hydrogen level be at χ'Eq.(8). The intensity of that total free-bound continuum is then found by summing over the various bound states. This free-bound

intensity is

$$I_{(F-B)_\nu} = \frac{Const}{(kT)^{3/2}} \sum \frac{1}{n^3} e^{\Delta E_n/kT} N_e^2 e^{-h\nu/kT} \tag{10}$$

where the n's are the effective quantum numbers. The sum is taken from n_{min} defined by the energy difference between the series limit and the photon energy (see Eq.(9)) and n_{max} defined by the series limit (see Eq.(8)).

Figure 2 shows the total continuum emitted by the six level atom shown in Fig.1. The intensity of this continuum is the sum of the free-free and free-bound contributions as given in Eq. (11).

$$I_{cont\,\nu} = \frac{Const}{(kT)^{1/2}} \left[e^{\Delta \chi/kT} + \frac{Const}{(kT)} \sum \frac{1}{n^3} e^{\Delta E_n/kT} \right] N_e^2 \, e^{-h\nu/kT} \tag{11}$$

Superimposed on the continuum of Fig. 2 is the set of discrete lines (series) resulting from transitions ending in the first excited level, E_1. At the high frequency end this series approaches the series limit Eq. (8) for the recombination continuum into E_1. The frequency difference between the series limit and any given observable series line is equal to the difference between the observed ionization potential χ' and the upper state involved in the transition corresponding to that line. For example, for the series shown in Fig. 2, the lines have frequencies $(E_u - E_1)/h$ and the series limit is $(\chi' - E_1)/h$. The difference between these is then

$$\Delta\nu = \frac{\chi' - E_u}{h} \tag{12}$$

As the observed ionization potential is reduced, $\Delta\nu$ is reduced and the series limit advances towards lower frequencies. If the reduction in ionization potential due to electric fields from neighboring ions is great enough the higher series members will merge into the series limit. The number of observable higher series members are thus a function of the reduction of the ionization potential χ.

Line Profiles

In general spectral lines do not result from the emission of photons of a single frequency, rather they result from the emission of photons having a distribution of frequencies around a value similar to that given in Eq.(1). This results in the line having a defining shape or profile. The limiting line profile is that given by the Heisenberg uncertainty principle

$$\Delta E_u \, \Delta t_u \sim \hbar \tag{13}$$

where ΔE is the uncertainty in the upper energy level from which the transition occurs and Δt_u is the uncertainty in the time for which that level is occupied.

This limiting profile results in the so-called natural line width. The natural line width in wavelength units as given by classical electrodynamics is constant

and is

$$\Delta \lambda_{classical} = \frac{4\pi}{3} \frac{e^2}{mc^2} = 1.17 \times 10^{-4} \, A \qquad (14)$$

The derivation of the natural line width from the uncertainty principle leads to similar results but not to a constant $\Delta \lambda$. A typical value of the quantum mechanical natural width in the optical region ($\nu \cong 10^{15}$ sec^{-1}) is $\Delta \nu \cong 10^7$ sec^{-1} ($\Delta \lambda \cong 1 \times 10^{-4}$Å).

Doppler Broadening:

Since radiating plasma particles are not at rest, the emitted photons can undergo a Doppler shift. The Doppler effect increases the line width because of the motion of the emitting particles relative to a stationary detector. In wavelength units the Doppler width (half width at $1/e$ peak intensity) is

$$\Delta \lambda_D = \left[\frac{2 \, kT_M}{Mc^2} \lambda_o^2 \right]^{1/2} \qquad (15)$$

where T_M is the temperature of the particle of mass M with λ_o the wavelength of the line at maximum intensity. Typical values of the Doppler width for the cesium resonance line at 8521 A are 0.006Å and 0.008Å for atom temperatures of 130°C and 330°C respectively.

Resonance Broadening:

Another broadening phenomenon which influences line profile is called Resonance Broadening (sometimes referred to as Pressure Broadening). This effect is due to collisions between excited and ground state atoms which may be likened to an interaction between oscillators. The oscillator strengths of the resonance lines are usually very high, and the coupling of these oscillators will therefore be correspondingly great. This coupling can result in a distribution in the emitted frequency, and thus in a broadening of the line. The width (in wavelength units) for resonance broadening is given by[1] (full width at half intensity)

$$\Delta \lambda_R = \frac{2}{3\pi} \frac{e^2}{m} \frac{\lambda_o^3}{c^2} f_{lu} \, N_1 \qquad (16)$$

where f_{lu} is the absorption oscillator strength, N_1 is the number density of absorbers (particles in the lower state) and the other quantities are as previously defined. For the cesium resonance line CsI 8521 $\Delta \lambda_R$ in A is

$$\Delta \lambda_R = .3 \times 10^{-17} \, N_1 \quad \text{Angstroms} \qquad (16a)$$

Stark Broadening and Shift:

In dense plasmas at moderate temperatures (plasma in L.T.E.) the Doppler and resonance broadening mechanisms are small compared to those caused by the interaction of the radiating particle with the fields of the ions and electrons in the plasma. Because of their dependence on electric field, the effect of these

52

interactions on line profile is called Stark broadening. The phenomena of Stark broadening may be considered in terms of the following two mechanisms. The radiating atoms find themselves in a static electric field caused by neighboring ions. An electron in an excited level can interact with these fields; this interaction displaces the level from its original (unperturbed) value, and results in a shift in frequency of the emitted photon. The higher frequency lines for a given series will exhibit a greater shift in frequency. There will also be an uncertainty in the position of the shift because of small differences in the fields at each radiator. This will cause the emitted radiation to be broadened about the average shift value.

In addition to these static ionic fields, the radiator is in a rapidly changing field of the fast moving electrons. The actions of these fields may be considered as a collision of the electron and the radiator. After a collision, the radiation process is rapidly quenched. This quenching (cutting off of the emitted wave train) results in an uncertainty in the lifetime of the states involved in the transition, with a corresponding uncertainty in the energy of the emitter photon. This results in a broadening of the spectral line coupled with a shift in its center frequency (the frequency at maximum line intensity). The profile of such a broadened and shifted line can be written as

$$I(\Delta w) = \frac{W}{\pi} \int_0^\infty \frac{F(E) \, dE}{W^2 + (\Delta w - d - \frac{2\pi\alpha}{e^2} E^2)^2} \tag{17}$$

where the frequency Δw (expressed in angular units) is measured relative to the line center w_0. $F(E)dE$ expresses the probability that the radiator is in a field of magnitude between E and $E + \Delta E$, α is a coefficient related to the perturbation of the total energy of the radiator by the field and W and d are the values of the line width (half width at half intensity) and shift. The width and shift are respectively the imaginary and real part of the Hamiltonian of such a perturbed radiator.

$$W = -\operatorname{Im}\left(\frac{H}{h}\right) \tag{18}$$

$$d = \operatorname{Re}\left(\frac{H}{h}\right) \tag{19}$$

The above theoretical consideration results in a spectral line profile identical to that actually observed. The observed line contour is given by a Lorentz distribution

$$I(w) = \operatorname{Const} \, I_{max} \left[\frac{W}{(\Delta w - d)^2 + W^2}\right] \tag{19}$$

where the line width and shift are equal to a constant (weak function of the electron temperature) times the number density

$$W = \operatorname{Const} Ne \tag{20}$$

$$d = \operatorname{Const} Ne \tag{21}$$

References (2,3) have a tabulation of these constants for cesium.

The analysis of the line profile is independent of the limiting assumption of thermal equilibrium and so affords a particularly useful method for plasma diagnostics.

Absorption

Before compiling the various diagnostic techniques which these spectral data afford, it is important to determine the manner in which the emitted line radiation is altered before leaving the plasma. Emitted plasma radiation will in some part be absorbed by the plasma and neutral gas atoms. The derivation of Eq.(3) for spectral radiation requires a simplifying (and necessary) condition that the plasma is optically thin — the emitted radiation is transmitted without absorption. Near the core (w_o) of strong (resonance) lines this is not generally true. Neither are most plasmas truly thick so that the emerging radiation does not approach that of a black body. In analyzing the spectral data some adjustments must therefore be made for this partially thin-partially thick nature.

Absorption is less a factor when transitions between highly excited states are considered. This is due to the lack of a large number of absorbers in these states. Transitions to the ground state, i.e. resonance lines, do exhibit absorption under most conditions and are not selected for line profile analysis. Continuum radiation, especially that on the high frequency side of a series limit, can be considered thin for most laboratory plasmas.

Two types of absorption can play an important role in the observed line profile. First is absorption in a cold layer which may constitute the boundary of an otherwise uniform plasma. This is shown in Fig. 3A. The broadened emission line whose profile is centered around some shifted frequency w' passes into the cold layer which has a thinner absorption profile that is centered about a frequency which is closer to the unshifted frequency w_o. This results in a so-called self-reversed line. The frequency difference between the self-reversal minimum and the emission maximum is a measure of the shift of the line. The intensity at the core of the line will be cut down strongly by the absorption, while the intensity in the wings of the line will be relatively unaffected.

The second type of absorption is volume absorption. This is shown in Fig. 3B. Both the absorption and emission line contours are the same. Both are centered about the shifted frequency w'. The absorption is again greatest at the core of the line, where the absorption coefficient approaches a maximum, but there may still be a non-negligible absorption in the line wings. This results in an observed line which appears quite a bit flatter than the emission line in contour but which is still centered about the shifted frequency w'. A contour similar to self-reversal in a cold layer may result from the volume absorption of a very intense, very broad emission line. True self-reversal will appear in the resonance lines of the lower series members.

Diagnostic Techniques

The spectral phenomena discussed indicate several methods of determining the parameters of temperature and number density in a radiating plasma. Since the plasmas in question are considered dominated by electron collisions the excitation (Boltzmann) and ionization (Saha) temperatures are those of the

electron. Only in the case of the Doppler contour is the temperature that of
the atom. All methods except that of the Doppler contour have been applied at
this laboratory. In the plasmas investigated thus far the Doppler profile of
the line has been overshadowed by its Stark profile. These diagnostic methods
are listed in Table I.

Of the various methods of determining electron density all but the Stark pro-
file and Series Limit methods are sensitive to the condition of L.T.E. The
validity of L.T.E. can be checked by comparing the values obtained from these
measurements with those obtained from measurements which required the assump-
tion of L.T.E. (Saha Equation). The validity of the assumption of a collision
dominated plasma can similarly be checked by comparing the values of excitation,
ionization and kinetic temperatures. And finally if the temperature of the
various particles are known (the ion temperature can be determined from the
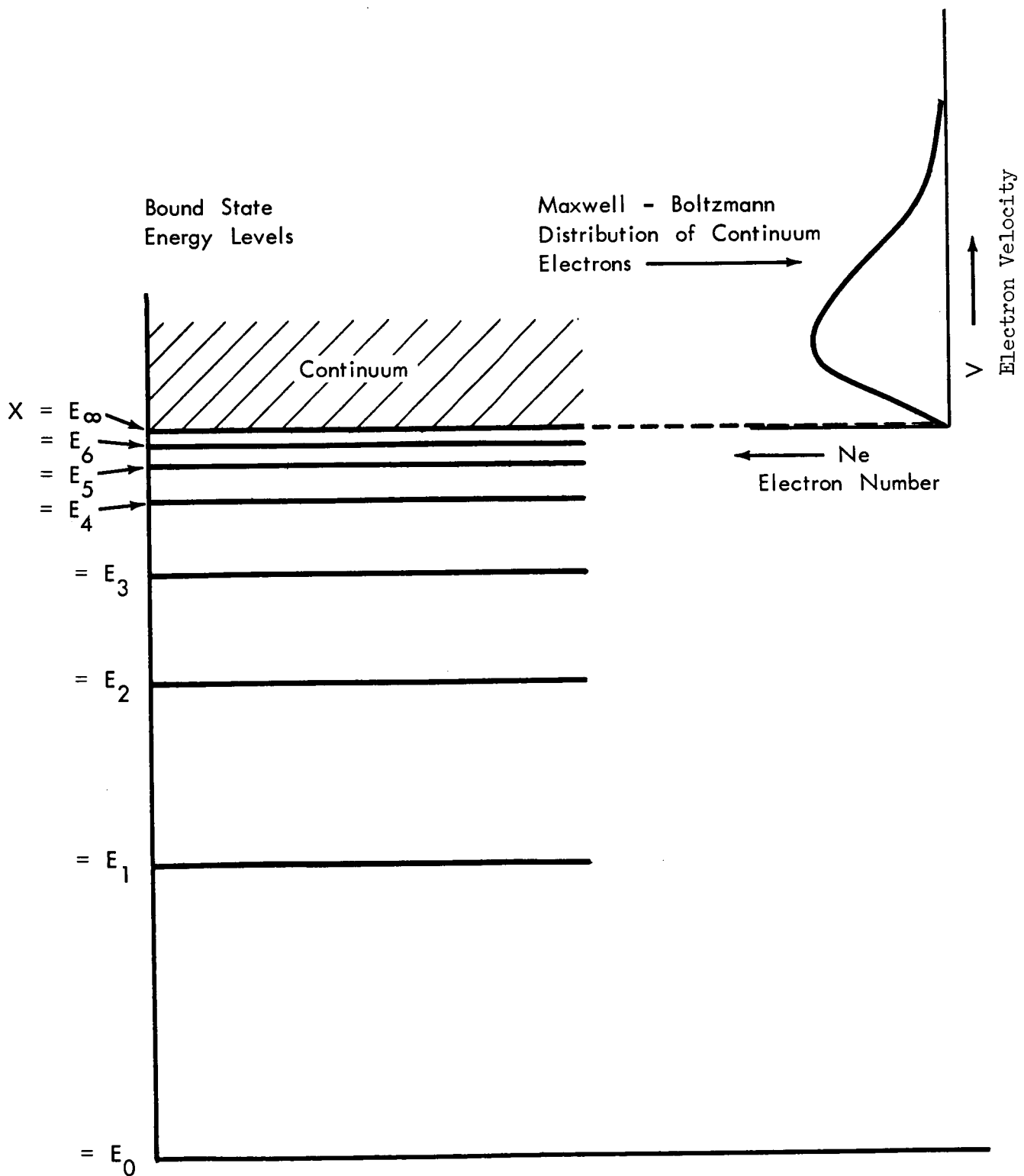Doppler width of an ion line) the completeness of L.T.E. can be checked.

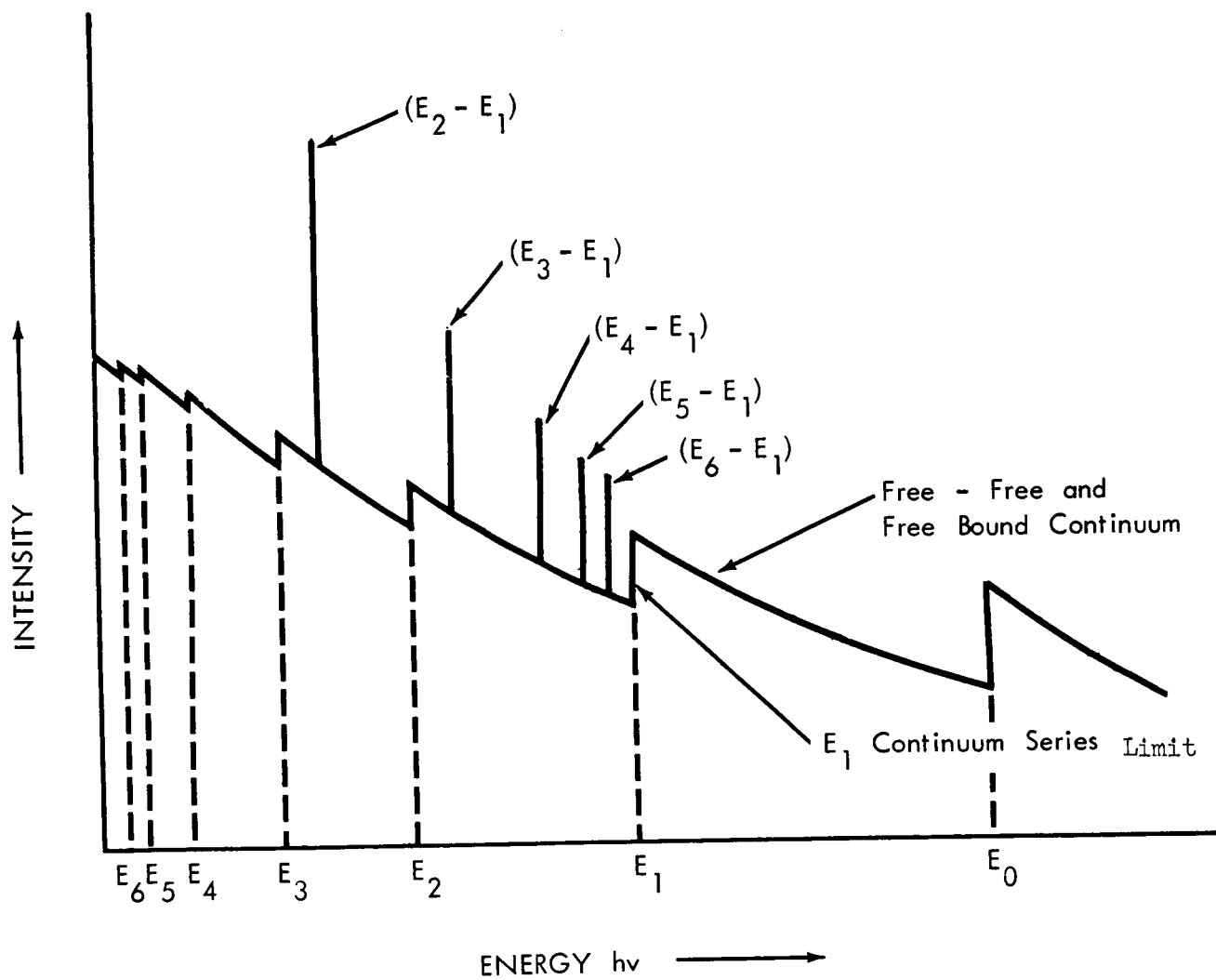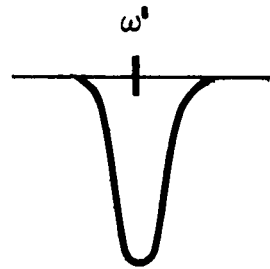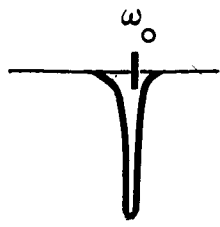Figure 1 - Energy level diagram for pseudo-plasma atom.

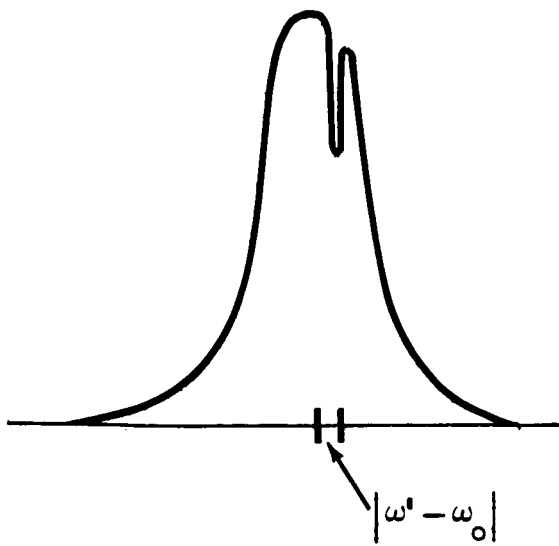Figure 2 - Plasma spectrum showing the full continuum and the E_1 series of spectral lines.

A. COLD LAYER   B. VOLUME
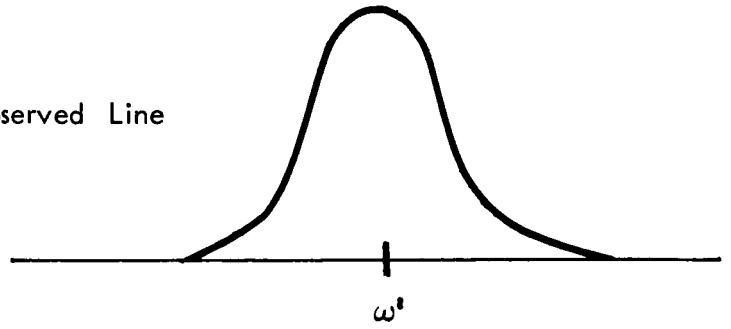
Absorption Line

Emission Line

Observed Line

$|\omega' - \omega_o|$
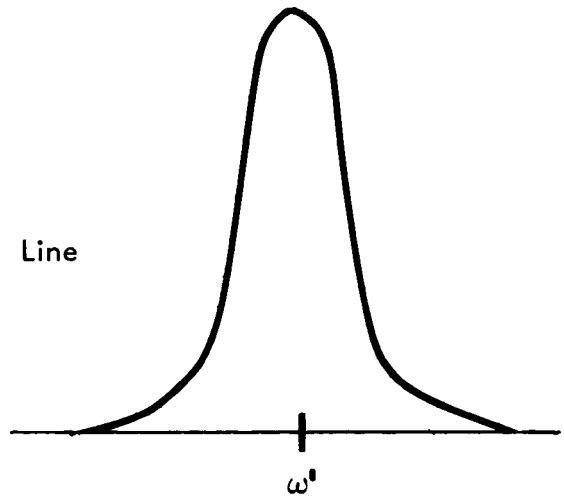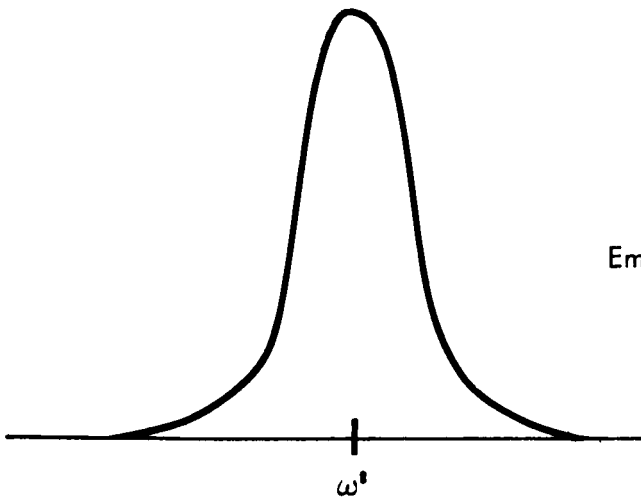
Figure 3 - Discrete line absorption.

TABLE I

Parameter	Diagnostic Technique	Formulation
Electron Temperature		
(a) Excitation Temperature*	Ratio of 2 optically thin lines	$T = \dfrac{E'_u - E_u}{k}\left[\ln\left(\dfrac{I\,\nu'^3 f'}{I'\,\nu^3 f}\right)\right]^{-1}$
(b) Ionization Temperature*	Absolute intensity of optically thin line (plus electron number density)	$T = \dfrac{X - \Delta X - E_u}{k}\left[\ln\left(\dfrac{I_{ul}g_{io}T^{3/2}N_e}{8\times10^{-65}g_1\nu_{ul}^3 f_{lu}L}\right)\right]^{-1}$
(c) Kinetic Temperature*	Ratio of continuum intensity at two frequencies	$T = \dfrac{h}{k}(\nu' - \nu)\left[\ln\dfrac{I}{I'}\right]^{-1}$
Atom Temperature	Doppler width of line	$T_M = \dfrac{(Mc^2\Delta\lambda_D^2)}{2k\,\lambda_o^2}$
Atom Number Density		
(a) Excited State	Absolute line intensity	$N_u = \dfrac{I_{ul}}{Ah\nu L}$
(b) Ground State	Absolute line intensity (plus Boltzmann factor)	$N_o = \left(\dfrac{g_o}{g_u}\right)\dfrac{I\,e^{E_u/kT}}{Ah\nu L}$
(c) Total	Absolute line intensity (plus partition sum)	$N_t = \dfrac{I\,e^{E_u/kT}}{g_u\,Ah\nu}\left[g_o + \sum_i g_i e^{-E_i/kT}\right]$
Electron Number Density		
(a)	Absolute line intensity in Saha Equation (plus electron temperature)	$N_e^2 = N_o\dfrac{2g_{io}}{g_o}\left[\dfrac{2\pi mkT}{h^2}\right]^{3/2} e^{-(X-\Delta X)/kT}$
(b)	Continuum intensity (plus electron temperature)	$N_e^2 = I_\nu\left[\dfrac{(27\pi)^{1/2}}{8}\dfrac{m^2c^3}{e^4hZ^2E_H}\left(\dfrac{kT}{2E_H}\right)^{1/2}\left[e^{\Delta X/kT}+2\left(\dfrac{z^2E_H}{kT}\right)\sum_{n_{min}}^{n_{max}}\dfrac{1}{n^3}\exp\left(\dfrac{\Delta E_n}{kT}\right)\right]\times\dfrac{e^{-h\nu/kT}}{L}\right]^{-1}$

59

TABLE I (cont'd)

Parameter	Diagnostic Technique	Formulation
Electron Number Density		
(c)	Stark width[4]	N_e = Const W
(d)	Stark shift[4]	N_e = Const d
(e)	Advance of Series Limit Inglis-Teller Method	Line counting

* The Excitation, Ionization and Kinetic Temperatures are equal in collision dominated plasmas.

Definitions:

M - mass of atom

λ_D - width of the line shape at 1/e its max. value

λ_o - wavelength at the line peak

c - speed of light

g_{io} - statistical weight of ion ground state

m - electron mass

k - Boltzmann constant

T - electron temperature

E_H - ionization potential of hydrogen

Z - degree of ionization

References

1. Robert J. Donohue and Richard F. Majkowski, J. Appl. Phys. $\underline{33}$, 3, 1962.

2. H. R. Griem, Plasma Spectroscopy, McGraw-Hill Book Company, New York, 1964.

3. H. R. Griem, Phys. Rev., $\underline{128}$, 515 (1962).

APPENDIX B

ABSORPTION OF RADIATION IN RADIATING AND NONRADIATING MEDIA

INTRODUCTION

The intensity of a spectral line can yield much information concerning the radiating particles and their environment if the radiation is not absorbed when traveling between the radiating particles and the detector. The atom number densities and excitation temperature can be obtained from absolute and relative intensity measurements and an analysis of the line shape will determine the perturbing mechanism which could yield electron densities or atom temperatures. However, if the radiation is absorbed this information will be masked by the effect of the absorption. Consequently an estimate of the absorption must be made for each line before its intensity or intensity profile can be analyzed.

In order to establish a basis for these corrections a description of the absorption is first given for a radiating gas which obeys Kirchoff's Law and which has a constant temperature and number density throughout its length. A factor δ is then developed which allows absorbed intensities to be reduced to their nonabsorbed values so that the foregoing analysis can be made. The limitations on the use of this factor are defined and the results of a more general treatment of the absorption of spectral lines are quoted for lines which have a Lorentz or Doppler profile.

Finally, the intensity equations derived for a radiating gas are shown to have the same form as the absorption profile of a continuous light source which is absorbed by a neutral gas. The equations are applied to cesium absorption data[1] for comparison.

ABSORPTION OF EMITTED RADIATION IN PLASMA

General Radiation Equation

The intensity of radiation from radiating atoms can be derived from the general equation for radiation transfer. In plasmas, where the scattering of radiation is negligible, the change in intensity of radiation per unit volume, solid angle and frequency interval is the difference between the emission and absorption.

Namely, in the direction x,

$$\frac{d}{dx} I_\nu(\Theta, x) = \epsilon_\nu(x) - k'_\nu(x) I_\nu(\Theta, x) \tag{1}$$

where $\epsilon_\nu(x)$ is the emission per unit volume. $I_\nu(\Theta, x)$ is the intensity in the region between x and x + dx at an angle between Θ and $\Theta + d\Theta$, and $k'_\nu(x)$ is the effective absorption coefficient.

In collision dominated plasmas the effective absorption coefficient and the emission are related by Kirchoff's Law,

62

i.e. $\qquad \epsilon_\nu(x) = k'_\nu(x) B_\nu(T)$ $\qquad\qquad\qquad\qquad$ (2)

where $\qquad B_\nu(T) = \dfrac{2h\nu^3}{c^2} \cdot \dfrac{1}{e^{h\nu/kT}-1} \dfrac{ergs}{cm^2\ str.}$ $\qquad\qquad$ (2a)

The differential equation for radiation transfer, Eq. 1, can be integrated[2] to give

$$I_\nu(\Theta,b) = \int_a^b \epsilon_\nu(x)\, e^{-\tau(\nu,x)}\, dx + I_\nu(\Theta,a)\, e^{-\tau(\nu,a)} \qquad\qquad (3)$$

where a is the point of the plasma furthest from the line of sight and b is the near point: e.g., a is the point at which the radiation $I_\nu(\Theta,a)$ enters the plasma volume and b is the point at which it emerges from the plasma in the direction of observation (see Fig. 1).

Here $I_\nu(\Theta,b)$ is the energy/cm^2-sec-str per frequency interval (intensity/str- $\Delta\nu$) emitted from the end of the plasma volume of length (b - a). $I_\nu(\Theta,a)$ is the intensity/str-$\Delta\nu$ incident on the plasma boundary at point a and $\tau(\nu,x) = \int_x^b k'_\nu(x)dx$.
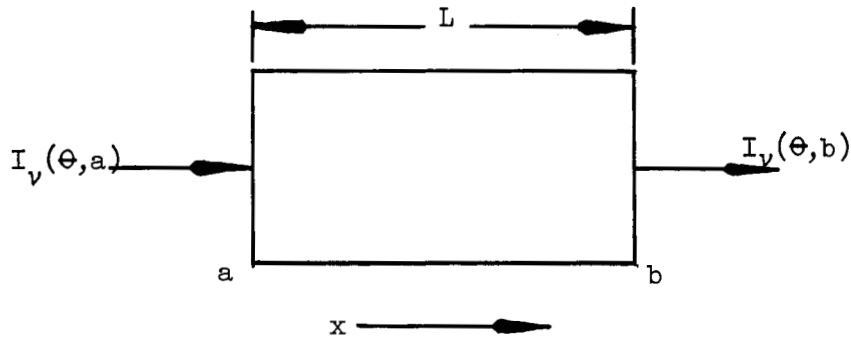

Figure 1

$I_\nu(\Theta,x)$ will be considered isotropic and $I_\nu(\Theta,a)$ shall be taken to be zero, i.e. the radiation source is within the boundary a - b. Then Eq. 3 becomes:

$$I_\nu(b) = \int_a^b \epsilon_\nu(x)\, e^{-\tau(\nu,x)}\, dx \qquad\qquad (4)$$

If $k'_\nu(x)$ and $\epsilon_\nu(x)$ are independent of x, $\tau(\nu,x) = k'_\nu(b-x)$, and Eq. 4 becomes:

$$I_\nu(b) = \epsilon_\nu\, e^{-k'_\nu b} \int_a^b e^{k'_\nu x}\, dx$$

From which,

$$I_\nu = B_\nu(T)\left[1 - e^{-k'_\nu L}\right] \tag{5}$$

where $L = b - a$.

This expression will now be used to develop the equations for the spectral profiles for optically thin lines, lines which are slightly absorbed, and optically thick lines.

Optically Thin Plasma

While most laboratory plasmas are not optically thin, the expression for optically thin lines is the only one that can be developed in terms of the atomic parameters of the radiating system. The absorbed lines can then be treated as having "perturbations" in their profiles caused by absorption.

The exponential in Eq. 5 can be expanded in a series:

Viz. $$I_\nu = B_\nu(T)\left\{1 - \left[1 - k'_\nu L + \frac{(k'_\nu L)^2}{2!} - \frac{(k'_\nu L)^3}{3!} + ...\right]\right\} \tag{6}$$

If $k'_\nu L$ is so small that the terms of higher order than the first order can be neglected, the radiating system (plasma) is termed optically thin.

Then Eq. 6 can be written as:

$$I_\nu^o = B_\nu(T)\, k'_\nu L \tag{6a}$$

The superscript o is to designate the optically thin intensity.

From the theory of absorption[3]

$$k'_\nu = \alpha_\nu\left[1 - e^{h\nu/kT}\right] \tag{7a}$$

where $\nu = (E_m - E_n)/h$ and E_m is the energy of the upper state and E_n is the energy of the lower state involved in the radiative transition.

Also,

$$\alpha_\nu = \frac{\pi e^2}{mc}\, N_n\, f_{nm}\left[\text{Normalized Line Profile}\right] \tag{7b}$$

Here N_n is the number density of particles in the absorbing (lower) state and f_{nm} is the absorption oscillator strength.

The normalized line profile is Lorentzian if the broadening mechanisms are natural, pressure, resonance or Stark broadening. This shape will be used exclusively in the development of the intensity equations because the Stark broadening is the dominant broadening mechanism for the lines of interest in the Cs rf plasma.

64

The normalized Lorentz profile, $\mathcal{L}$, has the following frequency and wavelength dependent form:

Frequency dependence:
$$\mathcal{L} = \frac{\Gamma}{4\pi^2 (\Delta \nu)^2 + (\frac{\Gamma}{2})^2} \quad , \tag{8a}$$

where $\frac{\Gamma}{2\pi} = \gamma$ is the full width at one half the maximum intensity and $\Delta \nu = \nu - \nu_o$. The frequency dependent form can also be written as

$$\mathcal{L} = \frac{2}{\pi \gamma} \frac{1}{1 + 4(\frac{\Delta \nu}{\gamma})^2} \tag{8b}$$

Wavelength dependence:
$$\mathcal{L} = \frac{\lambda'}{4\pi^2 (\Delta \lambda)^2 + (\frac{\lambda'}{2})^2} \tag{8c}$$

where $\frac{\lambda'}{2\pi} = w$, the full width at one half the maximum intensity and $\Delta \lambda = \lambda - \lambda_o$.

Similarly the wavelength dependent form can also be written as

$$\mathcal{L} = \frac{2}{\pi w} \frac{1}{1 + 4(\frac{\Delta \lambda}{w})^2} \tag{8d}$$

Using Eqs. 2a, 7a, 7b, and 8a, Eq. 6a can be written as

$$I_\nu^o = \frac{2\pi e^2 h}{mc^3} \nu_{mn}^3 f_{nm} N_m \frac{g_n}{g_m} L \left[\frac{\Gamma}{4\pi^2 (\Delta \nu)^2 + (\frac{\Gamma}{2})^2} \right] \frac{erg}{cm^2\text{-sec-str.}}$$

In this expression N_n was replaced with $N_n = N_m \frac{g_n}{g_m} e^{-h\nu/kT}$ where g_n and g_m are the statistical weights of the lower and upper states respectively.

Also, the total intensity

$$I^o = \int_{line} I_\nu d_\nu = \frac{2\pi e^2 h}{mc^3} \nu_{mn}^3 f_{nm} N_m \frac{g_n}{g_m} L \frac{ergs}{cm^2\text{-sec-str}} \tag{9b}$$

Eq. 9b can also be written as:

$$I^o = \frac{A_{mn}}{4\pi} N_m h \nu_{mn} L \qquad ergs/cm^2\text{-sec-str} \tag{9c}$$

where $A_{mn} = \frac{8\pi^2 e^2 h \nu_{mn}^2}{mc^3} f_{mn} \frac{g_n}{g_m}$, the transition probability.

Finally, rewriting Eq. 6a:

$$I_\nu = I^o \left[\frac{\Gamma}{4\pi^2(\Delta\nu)^2 + (\frac{\Gamma}{2})^2} \right] \tag{9d}$$

Slightly Optically Thick Plasma

The general expressions for the line profiles from a radiating system are now amended for a system with an absorption of sufficient magnitude that the second order term in Eq. 6 must be used. An expression for the profile for these "second order absorbed" or slightly optically thick lines is written in terms of the optically thin total intensity, I^o. From this expression an equation which relates the observed total intensity and full width at one-half maximum intensity (hereafter simply called the width) to those quantities for the optically thin case is developed. In performing this derivation the parameter δ is introduced. δ is defined in terms of the atomic constants, absorber number density and width of the optically thin profile. This factor is most useful in defining the regions of application of the various absorption corrections. Plots of the ratios of observed to optically thin width and intensity as a function of the absorption are presented to illustrate the usefulness of these corrections.

Rewriting Eq. 6 to include the second order term yields:

$$I_\nu = B_\nu(T) \, k'_\nu L \left[1 - \frac{k'_\nu L}{2} \right]$$

or

$$I_\nu = I^o_\nu \left[1 - \frac{k'_\nu L}{2} \right] \tag{10}$$

One can call this expression the intensity for a slightly optically thick plasma.

Total Intensity Correction: The total intensity is:

$$I = \int_{line} I_\nu d_\nu = I^o - \frac{L}{2} \int_{line} I^o_\nu k'_\nu \, d\nu \tag{10a}$$

For isolated lines the integral on the right can be written as:

$$\int_{line} I^o_\nu k'_\nu \, d_\nu = \int_{-\infty}^{\infty} I^o_\nu k'_\nu \, d_\nu = \int_{-\infty}^{\infty} I^o_\nu \alpha_\nu (1 - e^{-h\nu/kT}) \, d\nu$$

Now, $e^{-h\nu/kT} \ll 1$ for $\lambda \leq 1.4$ μ's if the plasma temperature is less than $5000\,°K$. Under these conditions, $k'(\nu) = \alpha(\nu)$ and with the aid of Eqs. 7b, 8a and 9d the integral becomes:

$$\int_{-\infty}^{\infty} I^o_\nu \alpha_\nu \, d\nu = I^o \frac{\pi e^2}{mc} N_n f_{nm} \int_{-\infty}^{\infty} \left[\frac{\Gamma}{4\pi^2(\Delta\nu)^2 + (\frac{\Gamma}{2})^2} \right]^2 d\nu \tag{11}$$

66

Since

$$\int_{-\infty}^{\infty}\left[\frac{\Gamma}{4\pi^2(\Delta\nu)^2 + (\frac{\Gamma}{2})^2}\right]^2 d\nu = \frac{2}{\Gamma} = \frac{\gamma}{\pi},$$

the expression for the total line intensity, Eq. 10a, becomes,

$$I = I^0\left[1 - \frac{L}{2}(\frac{e^2}{mc})\frac{N_n f_{nm}}{\gamma}\right] \tag{12}$$

And,
$$I = I^0 (1 - \delta) \tag{13}$$

or
$$\frac{I}{I^0} = (1 - \delta) \tag{13a}$$

where
$$\delta = \frac{L}{2}\frac{e^2}{mc}\frac{N_n f_{nm}}{\gamma} \tag{14a}$$

or, if the profile is plotted in terms of λ,

$$\delta = \frac{L}{2}\frac{e^2\lambda_o^2}{mc^2}\frac{N_n f_{nm}}{w} \tag{14b}$$

Therefore,

$$I^0 = \frac{I}{1-\delta} = I\left[1 + \delta + \delta^2 + \dots\right] \tag{15}$$

or
$$I^0 = I (1 + \delta) \tag{15a}$$

or
$$\frac{I}{I^0} = \frac{1}{1 + \delta} \tag{15b}$$

I is the observed intensity (data) and I^0 (the corresponding thin line intensity which is to be used in the plasma parameter computation) is the desired quantity.

Figure 2 is a plot of I/I^0 determined from the complete radiation treatment (see below) along with the factors $(1 - \delta)$ and $\frac{1}{1 + \delta}$ as a function of the absorption at $\Delta\lambda = 0$. Notice that the factor $1/(1 + \delta)$ fits the true ratio over a much larger region of absorption than does the factor $(1 - \delta)$ which required one less approximation: (see Eqs. 15 and 15a). The factor $1/(1 + \delta)$ fits the true ratio to within a few percent up to a value of $\alpha_{\lambda_o} L = 4$. The plot shows how the observed intensity diminishes with respect to the optically thin intensity as the absorption increases. Thus Eq. 15b may be used to describe a slightly optically thick plasma for $0 < \alpha_{\lambda_o} L < 4$.

67

Width Correction: Equation 10 (with $k'_\lambda = \alpha_\lambda$) can be rewritten to show the line profile in terms of λ.

$$\text{Viz.} \quad I_\lambda = I^\circ \frac{\lambda'}{4\pi^2(\Delta\lambda)^2 + (\frac{\lambda'}{2})^2}\left[1 - \frac{L}{2}\frac{\pi e^2}{mc^2}\lambda_0^2 \, N_n \, f_{nm} \frac{\lambda'}{4\pi^2(\Delta\lambda)^2 + (\frac{\lambda'}{2})^2}\right] \tag{16}$$

Rewriting this equation in terms of the line profile Eq. 8d and the factor δ gives:

$$I_\lambda = I^\circ \frac{2}{w\pi} \frac{1}{1 + 4(\frac{\Delta\lambda}{w})^2}\left[1 - 2\delta \frac{1}{1 + 4(\frac{\Delta\lambda}{w})^2}\right] \tag{17}$$

The maximum intensity is at $\Delta\lambda = 0$ so that

$$I_{\lambda_0} = I^\circ \frac{2}{w\pi}\left[1 - 2\delta\right] \tag{18}$$

The ratio of this intensity to the intensity at one-half maximum is 2.

$$\frac{I_{\lambda_0}}{I_{\lambda_0 \pm \Delta\lambda_{1/2}}} = 2 \tag{19}$$

where $\Delta\lambda_{1/2}$ is the half width at one-half the intensity of the slightly absorbed line.

Substitution of Eqs. 17 and 18 into Eq. 19 gives:

$$2 = \frac{\left[1 - 2\delta\right]}{\frac{1}{1 + 4(\frac{\Delta\lambda_{1/2}}{w})^2}\left[1 - \frac{2\delta}{1 + 4(\frac{\Delta\lambda_{1/2}}{w})^2}\right]}$$

Let

$$1 + 4\left(\frac{\Delta\lambda_{1/2}}{w}\right) = A$$

Then,

$$(1 - 2\delta) A - 2A + 4\delta = 0$$

The only physically possible solution for A is the positive root where the assumption $4\delta \gg 8\delta^2$ is made, so that

$$A = 2 \frac{1 - \delta}{1 - 2\delta} = 2(1 - \delta)(1 + 2\delta + 4\delta^2 + \ldots)$$

68

If the previous assumption holds:

$$A = 2(1 + \delta)$$

and

$$\left(\frac{2\Delta_{1/2}}{w}\right)^2 = 1 + 2\delta.$$

Therefore

$$2(\Delta\lambda_{1/2}) \cong w(1 + \delta) = w' \tag{20}$$

or

$$w'/w = 1 + \delta \tag{20a}$$

where $2\Delta\lambda_{1/2}$ is the full width, w'.

Again, w' is the observed value and w is the optically thin width, so that

$$w = w'/(1 + \delta) \tag{21}$$

Figure 3 is a plot of the ratio of w' to w determined from the general theory (see below) along with the factor $(1 + \delta)$ as a function of the absorption at $\Delta\lambda = 0$. The factor $(1 + \delta)$ gives a reasonable fit to the ratio for values of $\alpha\lambda_0 L$ up to 1.0 and gives a fit to within 20% for values of $\alpha\lambda_0 L$ up to 15. Actually the factor $1/(1 - \delta)$ gives a better fit for absorption values up to 1.0 but then rapidly diverges from the actual shape of the ratio.

Optically Thick Plasma

In this section the results from the computation of Eq. 5 for the Lorentz profile will be quoted in terms of the absorption at the line peak ($\Delta\lambda = 0$). These computations were made with no assumptions concerning the magnitude of the absorption but it is still considered constant throughout the radiating system. Also, the absorption profile for the Doppler and combined Doppler and Lorentz broadened lines is defined. The steps required to obtain the ratio of observed to optically thin intensities is outlined for each of these two conditions.

Lorentz Profile: If the absorption is large such that no approximation can be made to Eq. 5, the plasma is said to be optically thick.

Eq. 5 can be rewritten as:

$$I_\lambda = B_\lambda(T)\left[1 - e^{-\alpha_\lambda L}\right] \tag{22}$$

where $k'_\lambda = \alpha_\lambda$ as before.

Now in order to derive an expression for line profile we first recall Eqs. 7 and 8d which give the relation:

$$\alpha_\lambda = \frac{\pi e^2}{mc^2}\lambda_0^2 N_n f_{nm} \frac{2}{\pi w} \frac{1}{1 + 4\left(\frac{\Delta\lambda}{w}\right)^2} \tag{22a}$$

69

and
$$\alpha_\lambda = \alpha_{\lambda_\sigma} \frac{1}{1 + 4\ F^2} \qquad (23a)$$

where $F = \Delta\lambda/w$ and α_{λ_0} is the absorption at the line center ($\Delta\lambda = 0$)

Also, for reference,

$$\alpha_{\lambda_g} = 4\delta \qquad (23b)$$

where, hereafter α_{λ_σ} is replaced with α_0.

Now if the spectral range of $\frac{1}{1 + 4\ F^2}$ is small, the variation of $B_\lambda(T)$ with λ over this range can be neglected and $B_\lambda(T)$ held constant; the line profile is then given by

$$I_\lambda = B_\lambda(T) \left\{ 1 - \exp\left[-\alpha_0 L \frac{1}{1 + 4\ F^2} \right] \right\}. \qquad (24)$$

And the total intensity is

$$\int_{line} I_\lambda\, d\lambda = B_{\lambda_0}(T) \int\int_{-\infty}^{\infty} \left[1 - \exp(-\alpha_0 L \frac{1}{1 + 4\ F^2} \right] d\lambda \qquad (24a)$$

But the intensity of optically thin radiation is:

$$\int_{line} I_\lambda\, d\lambda = I^0 = B_{\lambda_0}(T)\ \alpha_0 L\ \frac{\pi w}{2} \qquad (25)$$

The ratio of the intensity of the optically thick to optically thin line radiation is therefore,

$$\frac{I}{I^0} = \frac{\int_{-\infty}^{\infty} \left\{ 1 - \exp\left[-\alpha_0 L\ (\frac{1}{1 + 4\ F^2} \right] \right\}\, d\lambda}{\alpha_0 L\ \frac{\pi w}{2}} \qquad (26)$$

Landenberg and Reich[3] show that this integral could be calculated with the aid of Bessel functions. Their result is:

$$\int_{-\infty}^{\infty} \left\{ 1 - \exp\left[-\alpha_0 L(\frac{1}{1 + 4\ F^2}) \right] \right\} d\lambda = \pi w\ f(\alpha_0 L/2) \qquad (27)$$

A plot of $f(\alpha_0 L/2)$ vs $(\alpha_0 L/2)$ is tabulated by Penner.[4]

Finally,
$$\frac{I}{I^0} = \frac{f(\alpha_0 L/2)}{(\alpha_0 L/2)} \qquad (28)$$

This ratio is plotted in Fig. 2 along with the values of $(1 - \delta)$ and $1/(1 + \delta)$ for values of $\alpha_0 L$ to 20.

For large values of $\alpha_o L$, say $\alpha_o L \geqslant 10$, the function $f\left(\frac{\alpha_o L}{2}\right) \longrightarrow \sqrt{\frac{\alpha_o L}{\pi}}$ so that

$$\frac{I}{I^o} = \left(\frac{\alpha_o L}{\pi}\right)^{1/2} \left(\frac{1}{\alpha_o L/2}\right)$$

and

$$\frac{I}{I^o} = \frac{2}{\sqrt{\pi \alpha_o L}} \quad \text{for } \alpha_o L \geqslant 10 \tag{29}$$

The width of the absorption profile w' for large absorption can be obtained simply by setting the profile equal to 1/2 and solving for $2 \Delta\lambda$.

i.e.
$$1 - \exp\left\{-\alpha_o L \bigg/ \left[1 + 4(\frac{\Delta\lambda}{w})^2\right]\right\} = 1/2$$

From which $w' = 2\Delta\lambda = w\left[\frac{\alpha_o L}{\ln 2} - 1\right]^{1/2}$

or
$$w' = w\left[1.45\,\alpha_o L - 1\right]^{1/2} \tag{29a}$$

A comparison of the ratio w'/w from this expression with the ratio obtained from plots of Eq. 5 indicate that Eq. 29a is valid for

$$\alpha_o L \geqslant 8$$

This ratio of the full width of the profile of Eq. 5 to the optically thin width is plotted in Fig. 3 for values of $\alpha_o L$ to 16. For the cesium plasmas in our program, the width is generated primarily from Stark broadening effects.

Doppler Profile: When the absorption profile is governed by Doppler broadening, the absorption Eq. 7b is written:

$$\alpha_\lambda = \frac{\pi e^2}{mc^2} \lambda_o^2 N_n f_{nm} \left[\frac{1}{\sqrt{\pi}\,w_D} e^{-\left(\frac{\Delta\lambda}{w_D}\right)^2}\right] \tag{30}$$

where the term in the brackets is the normalized Doppler line profile and w_D is the half width at 1/e times the maximum intensity and is normally called the Doppler width.

Also,
$$w_D = \left[\frac{2\,k\,T}{M}\right]^{1/2} \frac{\lambda_o}{c} \text{ cm} \tag{31}$$

where M is the mass of the radiating particle, T its temperature and λ_o the wavelength at the line center.

Since the Doppler profile introduces a new normalization factor into the expression for α_λ, Eq. 30 will be rewritten in terms of a constant factor K.

Namely,

$$\alpha_\lambda = K \frac{1}{\sqrt{\pi}\, w_D}\, e^{-\left(\frac{\Delta\lambda}{w_D}\right)^2} \tag{32}$$

where

$$K = \frac{\pi e^2}{mc^2}\, 2\, N_n\, f_{nm}$$

Or, one could write

$$(\alpha_o)_{\text{Doppler}} = \frac{K}{\sqrt{\pi}\, w_D} \tag{33}$$

The total intensity of the Doppler broadened line can again be obtained by integrating Eq. 5 (and changing subscripts to λ).

Viz.

$$I = \int_{\text{line}} I_\lambda\, d\lambda = B_{\lambda_o}(T) \int_{-\infty}^{\infty} \left\{ 1 - \exp\left[- \frac{K\, L}{\sqrt{\pi}\, w_D}\, e^{-\left(\frac{\Delta\lambda}{w_D}\right)^2} \right] \right\} d\lambda$$

The ratio of I to I^o, the intensity of an optically thin Doppler line (I^o is independent of the broadening mechanism) has been determined.[4,5]

For $0.1 \leq \dfrac{K\, L}{\sqrt{\pi}\, w_D} \leq 30$,

$$\frac{I}{I^o} = \exp\left\{ - \frac{1}{2} \left[\frac{K\, L}{\sqrt{\pi}\, w_D} \right]^{1/2} \right\} \tag{34}$$

Values of $\dfrac{I}{I^o}$ for $\left[\dfrac{K\, L}{\sqrt{\pi}\, w_D} \right]^{1/2}$ outside of this range can be found in reference 4.

A comparison of Eq. 34 with Eq. 29 shows that Doppler broadening causes much greater absorption than Lorentz broadening. This is to be expected since Lorentz profiles have larger wings so that the radiation can effectively "leak out" through the wings of the lines where the absorption is much less than at the center.

Combined Doppler and Lorentz Broadening: The expression for the profile of a line which is both Doppler and Lorentz broadened is called the Voight formula, V.

And,

$$V = \frac{w/2\, w_D}{\pi^{3/2}} \left\{ \int_{-\infty}^{\infty} \frac{\exp\left[- \frac{(\lambda' - \lambda_o)^2}{w_D} \right]}{(\lambda - \lambda_o) - (\lambda' - \lambda_o)^2 + \left(\frac{w}{2}\right)^2}\, d\lambda' \right\} \tag{35}$$

where w_D is the Doppler width (1/2 width at 1/e peak intensity) and w is the Lorentz width (full width at 1/2 peak intensity).

This expression is placed into Eq. 7b to yield α_λ and α_λ into Eq. 5 (with the appropriate subscript change) to obtain the intensity per unit wavelength. This equation is integrated and compared with I^o for a large range of KL and for a

variety of $w/2w_D$ ratios by Penner.[4] The procedure which he outlines for obtaining I/I^O is the following:

First the intensity ratio (I/I^O) of absorbed to optically thin lines for a purely Doppler broadened line (characterized by w_D) is computed. Then the factor by which this ratio is increased by the Lorentz broadening (leakage through the wings) is determined. This factor is given in Fig. 4-6 in reference 4 in terms of $\frac{KL}{\sqrt{\pi}\, w_D}$

and $w/2w_D$. The effect of the Lorentz broadening is always to reduce the absorption due to Doppler broadening alone.

A Criterion on Equation 5 for Cesium Plasmas

The derivation of Eq. 5 requires that the emission and absorption coefficient are proportional (Eq. 2). This implies that the profile for the absorption and emission are identical - a large absorption means a large emission, etc. This means that the emission and absorption processes are independent of each other and that each photon absorbed is essentially lost, to the radiation beam. This is true if the rate of population of the excited state of an atom by collisions is substantially greater than the lifetime of the state. This requirement is most easily satisfied for _non_ resonance radiation. Consequently, a simple test of the criterion is to determine the ratio of collisional population of a resonance state and the lifetime of the state.

For hydrogenic atoms this ratio is:[6]

$$r = \frac{R_{coll.}}{R_{rad.}} \approx \frac{N_e}{2.3 \times 10^{16}} \left(\frac{E_H}{h\nu}\right)^3 \left(\frac{E_H}{kT}\right)^{1/2} \tag{36}$$

where E_H is the ionization potential of hydrogen (13.6 ev), and T is the kinetic temperature of the colliding particles.

And,

$$r = \frac{N_e}{2.5 \times 10^{12}} \left[h\nu(ev)\right]^{-3} \left[kT(ev)\right] \tag{37}$$

For cesium resonance radiation, $h\nu \sim .73$ and for our cesium rf experiments, $kT \sim .3$ ev.

Then,

$$r = \frac{N_e}{.5 \times 10^{12}}$$

If the collision population rate is ten times the radiation depopulation of the state we shall assume that Eq. 5 is valid.

If it is greater than 10, then

$$N_e \geqslant 5 \times 10^{12} \text{ cm}^{-3} \tag{38}$$

The majority of the rf experiments are made with Eq. 38 satisfied.

RESONANCE BROADENING

If the electron or ion density in a partially ionized radiating system is sufficiently low or if the system is not ionized and can only absorb radiation, the emission and absorption profiles can be governed either by Doppler or resonance broadening. The criteria for the exclusion of Stark broadening in the case of slightly ionized plasmas and pressure broadening in the case of the neutral gas must be checked for each element and line thereof. However very rough limits can be stated; namely $N_e \leq 10^{12}$ for the exclusion of Stark broadening $N_a \leq 10^{18}$ for the exclusion of pressure broadening where N_a is the number density of absorbers. In these last two sections only the case of the neutral gas will be treated so that only the pressure broadening criteria need be considered. A comparison of resonance and Doppler broadening will be made for a cesium absorption cell, which simply contains cesium atoms in their ground state.

The Doppler broadening profile is given by Eq. 30 and the width by Eq. 31.

Consequently for cesium,

$$w_D = 3.74 \ T^{1/2} \ \lambda_o \ \overset{o}{A} \tag{39}$$

For the cesium resonance line (8521 $\overset{o}{A}$)

$$w_D = 0.006 \ \overset{o}{A} \ \text{for} \ T = 130°C$$

$$w_D = 0.008 \ \overset{o}{A} \ \text{for} \ T = 330°C$$

Resonance broadening is caused by the coupling of "oscillators" which are normally the ground state atoms (i.e. atoms which absorb the resonance radiation) with their resonance frequency and the spread in frequencies can be described by a Lorentz distribution, Eq. 8d:

$$\mathscr{L} = \frac{2}{w\pi} \ \frac{1}{1 + 4 \ (\frac{\Delta\lambda}{w_R})^2}$$

where w_R is the __full__ width at $\mathscr{L} = 1/2$.

The best value of the width for resonance broadening is:[7]

$$w_R = \frac{2}{3\pi} \ \frac{e^2}{m} \ \frac{\lambda^3}{c^2} \ f_{nm} \ N_n \tag{40}$$

where f_{nm} is the absorption oscillator strength and N_n is the number density of absorbers (ground state).

Upon evaluation of the constants Eq. 40 becomes:

$$w_R = 0.6 \times 10^{-17} \ \lambda^3 \ f_{nm} \ N_n \ \overset{o}{A} \tag{41}$$

where λ is in μ's.

For the Cs resonance line, $f_{nm} = 0.814$

and $\lambda = 0.8521$ μ's.

Therefore,

$$w \simeq .3 \times 10^{-17} N_n \text{ Å}.$$

The profile of a spectral line (in absorption or emission) will be a combined Doppler and Lorentz profile. However, if the resonance width is much larger than the Doppler width, the Lorentz distribution will describe the line. If the criterion,

$$w \geq 10 \ w_D \text{ is used,}$$

then

$$N_n \geq 3.3 \times 10^{18} \ w_D \ (\text{Å}) \ \text{cm}^{-3} \tag{42}$$

The cesium vapor pressure is a function of cold spot temperature but an upper limit on temperature is determined by the vapor container. For a glass absorption cell the upper limit on temperature is about 350°C which limits the atoms to a Doppler width of $w_D \sim .08$ A. Therefore, from Eq. 42, criterion for resonance broadening domination in the vapor is

$$N_n \geq 2.64 \times 10^{16} \ \text{cm}^{-3} \tag{43}$$

The number density of cesium atoms is determined by its vapor pressure above a cold spot. The equation which relates the cold spot temperature (in °K) to the vapor pressure (in mm of Hg) is:

$$\log_{10} P = 6.949 - \frac{3833.682}{T}$$

and $N_a = \dfrac{.94 \times 10^{19} P}{T}$ where P is in mm of Hg and N_a is the number density.

For a cold spot temperature of 300°C, $N_a = 3.3 \times 10^{16}$ cm^{-3}. Consequently, the resonance width should predominate and the line shape should be Lorentzian for an unexcited cesium vapor above a cold spot of 300°C (1.7 mm Hg) or greater.

ABSORPTION OF RADIATION IN NON RADIATING MEDIA

The equation which governs the amount of radiation which travels through an absorbing media is given. This equation is shown to have an equivalent form as Eq. 5 and hence the theory developed in a previous section is applicable for a pure absorber. The equation is then used to describe the absorption shape of the Cs 8521 A line. Data obtained from an absorption experiment performed by Jensen[1] is quoted and the width of the predicted and measured shapes are compared.

If a beam of radiation passes through an absorbing media, and <u>if</u> the absorbed radiation is <u>not</u> re-radiated into the beam, the intensity diminishes exponentially, i.e.

$$I_\lambda (x) = I_\lambda(o) \; e^{-\alpha_\lambda x} \tag{44}$$

where α_λ $(= k_\lambda)$ is independent of x, the absorbing length, and $I_\lambda (o)$ is the incident radiation. Consequently, the amount of radiation absorbed in the distance x is:

$$I_\lambda (x)_{abs} = I_\lambda(o) \left[1 - e^{-\alpha(\lambda) x} \right] \tag{45}$$

Finally, if $I_\lambda (o)$ is constant over the wavelength range where α_λ is finite,

$$\frac{I_{absorbed}}{I_{incident}} = 1 - e^{-\alpha_\lambda L} \tag{46}$$

Resonance Absorption

If for an absorbing medium of length L the lines are resonance broadened we can write α_λ by combining Eqs. 40 and 22a,

Viz.

$$\alpha_\lambda = \frac{3\pi}{\lambda_o} \; \frac{1}{1 + 4 \, (\frac{\Delta\lambda}{w_R})^2} \tag{47}$$

For the cesium resonance line (Cs 8521 A):

$$\alpha_\lambda = \frac{1.1 \times 10^5}{1 + 4 \, (\frac{\Delta\lambda}{w_R})^2} \tag{47a}$$

where w_R is given by Eq. 41.

Therefore, the ratio of absorbed to incident radiation for Cs 8521 A is:

$$\frac{I_a}{I_i} = 1 - \exp\left\{ \frac{- 1.1 \times 10^5 \, L \, (cm)}{1 + 4 \, (\frac{\Delta\lambda}{w_R})^2} \right\} \tag{48}$$

Since this expression has the same shape as the optically thick radiation, where $\alpha(o) = 1.1 \times 10^5$ cm^{-1}, the width of this shape should be given by Eq. 29a of a previous section.

Or, w' at $\frac{I_a}{I_i} = 1/2$ is:

$$w' = w_R \left[1.45 \, \alpha(o) \, L - 1 \right]^{1/2}$$

For this case,
$$w' = w_R \left[1.6 \times 10^5 L - 1 \right]^{1/2} \qquad (49)$$

where $L \geq 6 \times 10^{-5}$ cm because of the criterion placed on the range of this expression.

Comparison with Data

An application for this simple theory can be found in the absorption data of Jensen.[1] He measured the absorption of the Cs 8521 Å line in a cesium cell with a .075 cm path length. The cell temperature was kept constant and the pressure was varied by changing the temperature of a cold spot outside the cell. With a cell temperature of 393°C (676°K) the following data were obtained:

Pressure of Cesium	Number Density of Ground State	Measured Width of Absorption Shape at 1/2 Maximum	w_R	w'
5 Torr	7×10^{16} cm-3	51.7 Å	.21 Å	70 Å
2.3	3.24×10^{16} cm^{-3}	20 Å	.097 Å	34 Å
1.4	1.96×10^{16} cm^{-3}	14 Å	.04 Å	14 Å
.7	$.98 \times 10^{16}$ cm^{-3}	8 Å	.02 Å	7 Å

The measured widths of the absorption shapes compare well with the values computed from Eq. 49 (w') for the low pressures of cesium but overestimate the width for the higher pressures. This effect may be accounted for by a reduction of the number density of cesium atoms through the conversion of excited Cs atoms to molecules. Equilibrium equations predict a small fraction ($\sim$ .001%) of molecules in the gas. However, the data obtained by Jensen shows a large amount of molecular absorption for the two higher pressures, indicating the existence of Cs_2 and the reduction of the cesium atom concentration which would decrease the width of the resonance line.

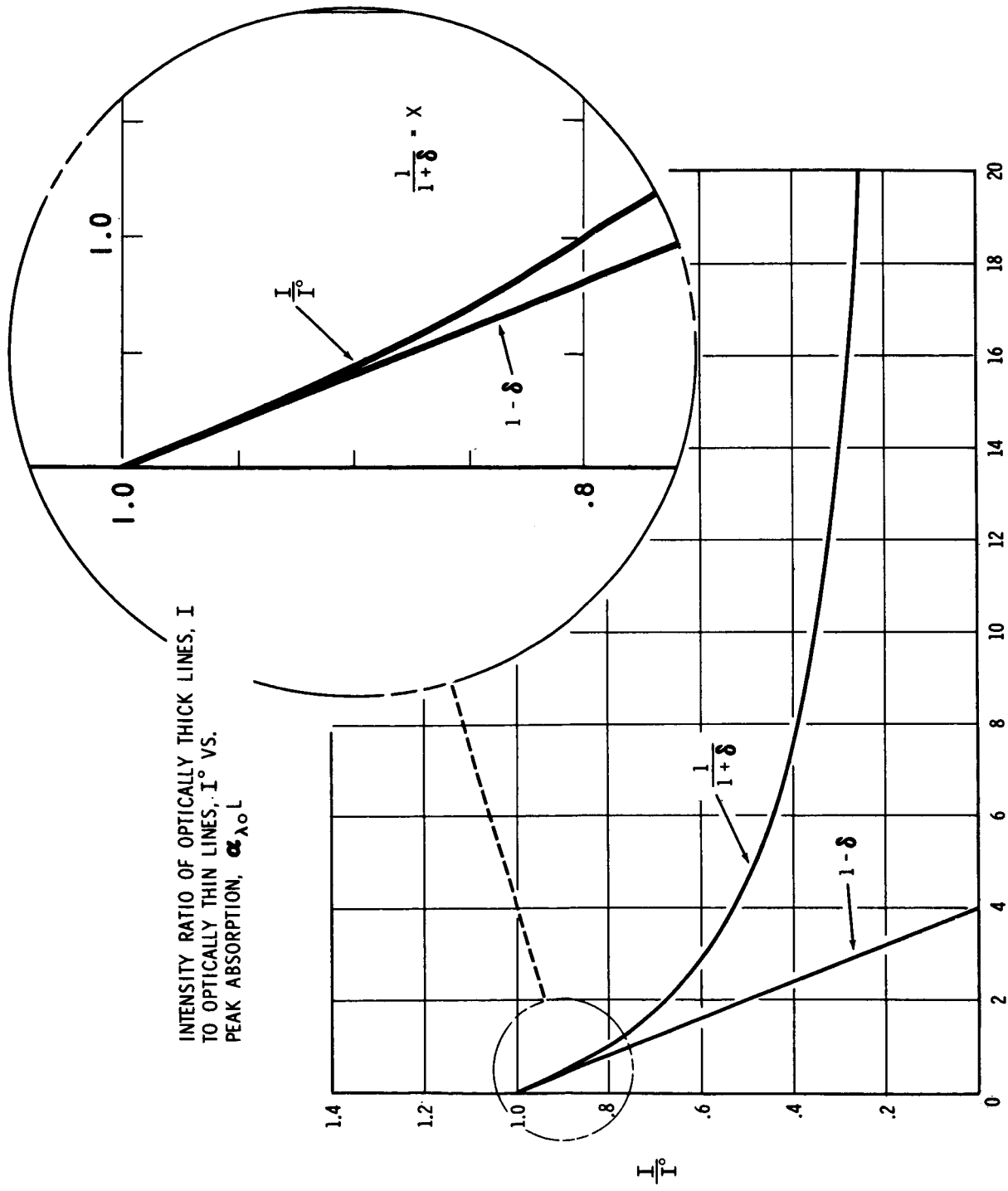The mechanism proposed for the conversion of Cs atoms to molecules is the following:

$$Cs^* + Cs^* \longrightarrow Cs_2^+ + e$$
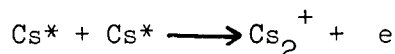
where the excitation energy of the cesium atom (Cs $6^2P_{3/2}$) is 1.45 ev. The energy required to form a cesium molecular ion is 2.835 ev and sufficient energy is provided by the two excited atoms to make this transformation. Upon recombination of an electron and a cesium molecular ion a neutral cesium molecule is formed which removes two neutral atoms from the gas and, of course, reduces the resonance absorption.

REFERENCES

1. A. O. Jensen, EOS Report 3130 Final, Oct. 30, 1963, Electro-Optical Systems, Pasadena, California.
2. A. Chandrasekhar, Radiative Transfer, Oxford at the Clarendon Press, 1950.
3. R. Ladenberg and F. Reich, Annalen der Physik and Chemie, 42, 181, 1913.
4. S. S. Penner, Quantitative Molecular Spectroscopy and Gas Emissivities, Addison - Wesley Press, Reading, Mass. (1959).
5. R. Cowan and G. Dieke, Rev. Med. Phys. 20, 418 (1948).
6. H. R. Griem, Plasma Spectroscopy, McGraw-Hill Book Company, New York, 1964.
7. R. G. Breene, "The Shift and Shape of Spectral Lines", Pergamon Press, New York (1961).

INTENSITY RATIO OF OPTICALLY THICK LINES, I
TO OPTICALLY THIN LINES, I^o VS.
PEAK ABSORPTION, $\alpha_{\lambda o} L$

$\alpha_{\lambda o} L$

FIGURE 2

79

WIDTH RATIO OF OPTICALLY THICK LINES, ω' TO OPTICALLY THIN LINES, ω VS. THE PEAK ABSORPTION, $\alpha_{\lambda o}L$

$\delta = \alpha_{\lambda o}L/4$

$\dfrac{\omega'}{\omega} = 1 + \delta$

$\dfrac{1}{1-\delta}$
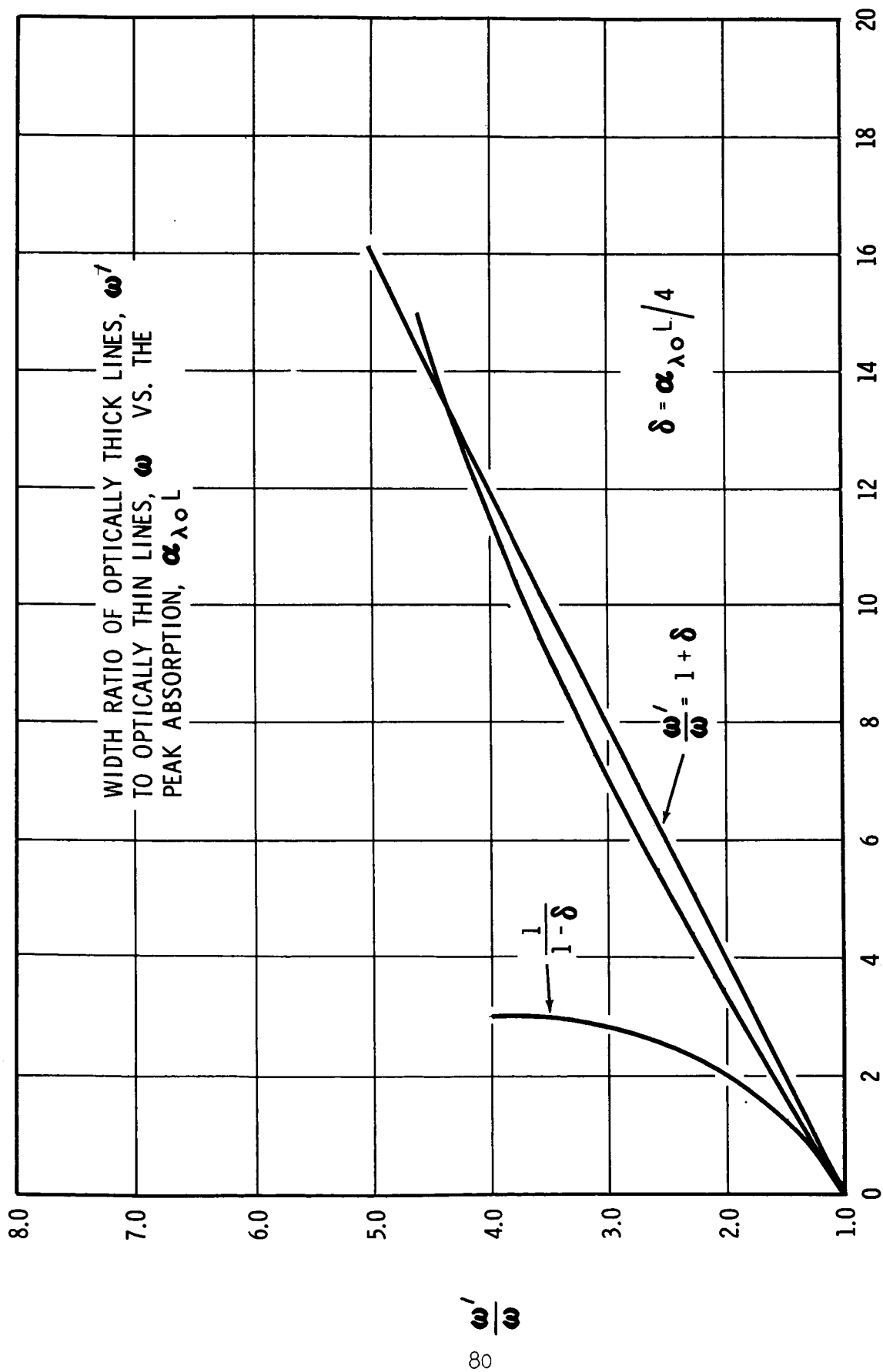
$\alpha_{\lambda o}L$

$\dfrac{\omega'}{\omega}$

FIGURE 3

80

DISTRIBUTION LIST

General Motors Research Laboratories
Contract NAS3-6470

Aerojet-General Nucleonics
San Ramon, California
Attention: K. Johnson

Aerospace Corporation
El Segundo, California
Attention: Librarian

Air Force Cambridge Research Center
(CRZAP)
L. G. Hanscom Field
Bedford, Massachusetts

Air Force Weapons Laboratory
WLDN-4/Lt. Brooks
Kirtland AFB, New Mexico   87117

Air Force Systems Command
Aeronautical Systems Division
Flight Accessories Laboratory
Wright-Patterson AFB, Ohio
Attention: ASRMFP-2/E, A. Wallis

Allison Division
General Motors Corporation
Indianapolis, 6, Indiana
Attention: J. D. Dunlop, II

Argonne National Laboratory
9700 South Cass Avenue
Argonne, Illinois
Attention: Aaron J. Ulrich

Atomics International
P. O. Box 309
Canoga Park, California
Attention: Robert C. Allen

Battelle Memorial Institute
505 King Avenue
Columbus 1, Ohio
Attention: David Dingee

The Bendix Corporation
Red Bank Division
Northwestern Highway
Detroit 35, Michigan
Attention: W. M. Spurgeon

Brookhaven National Laboratory
Upton, Long Island, New York
Attention: Dr. O. E. Dwyer

Bureau of Ships
Department of the Navy
Washington 25, D. C.
Attention: B. B. Rosenbaum

Consolidated Controls Corporation
Bethel, Connecticut
Attention: David Mende

Douglas Aircraft Company
Missile and Space Engineering
Nuclear Research (AZ-260)
3000 Ocean Park
Santa Monica, California
Attention: A. Del Grosso

Electro-Optical Systems, Inc.
300 North Halstead Avenue
Pasadena, California
Attention: A. Jensen

Ford Instrument Company
32-36 47th Avenue
Long Island City, New York
Attention: A. Medica

General Atomic
P. O. Box 608
San Diego 12, California
Attention: R. W. Pidd
          J. W. Holland
          L. Yang
          A. Weinberg

General Electric Company
Missile and Space Vehicle Department
P. O. Box 8555
Philadelphia 1, Pennsylvania
Attention: Library

General Electric Company
Knolls Atomic Power Laboratory
Schenectady, New York
Attention: R. Ehrlich

General Electric Company
Power Tube Division
1 River Road
Schenectady 5, New York
Attention: D. L. Schaefer

General Electric Company
Nuclear Materials & Propulsion Operation
P. O. Box 15132
Cincinnati 15, Ohio
Attention: J. A. McGurty

General Electric Company
Research Laboratory
Schenectady, New York
Attention: Volney C. Wilson
            John Houston

General Electric Company
Special Purpose Nuclear System Operations
Vallecitos Atomic Laboratory
P. O. Box 846
Pleasanton, California
Attention: E. Blue

Hughes Research Laboratories
3011 Malibu Canyon Road
Malibu, California
Attention: R. C. Knechtli

Institute for Defense Analyses
1666 Connecticut Avenue, N.W.
Washington 9, D. C.
Attention: R. C. Hamilton

Jet Propulsion Laboratory
California Institute of Technology
4800 Oak Grove Drive
Pasadena, California
Attention: Scott Luebbers
            Peter Rouklove

Los Alamos Scientific Laboratory
P. O. Box 1663
Los Alamos, New Mexico
Attention: G. M. Grover
            W. Reichelt

National Aeronautics & Space Administration
Scientific & Technical Information Facility
P. O. Box 5700
Bethesda 14, Maryland
Attention: NASA Representative

Marquardt Corporation
Astro Division
16555 Saticoy Street
Van Nuys, California
Attention: A. N. Thomas

Martin-Nuclear Division of Martin-
                Marietta Corporation
P. O. Box 5042
Middle River 3, Maryland
Attention: J. Psarouthakis

Massachusetts Institute of Technology
Cambridge, Massachusetts
Attention: Robert E. Stickney
            E. P. Gyftopoulos

National Aeronautics & Space Admin.
Manned Spacecraft Center
Houston, Texas   77001
Attention: B. Bragg

National Aeronautics & Space Admin.
1512 H Street, N. W.
Washington 25, D. C.
Attention: H. Harrison
            Arvin Smith

National Aeronautics & Space Admin.
Lewis Research Center
21000 Brookpark Road
Cleveland, Ohio   44135
Attention: Roland Breitwieser MS 302-1
            Robert Migra MS 49-2
            Bernard Lubarsky MS 500-201
(3 copies) Harold Nastelin MS 500-309
            James Ward MS 500-201
            Herman Schwartz MS 500-309
            Frank Rzasa MS 500-309
            Roger Mather MS 500-309
            Vince Hlavin MS 3-14
            John Weber   MS 3-19

National Aeronautics & Space Admin.
Marshall Space Flight Center
Huntsville, Alabama   35812
Attention: Library

National Aeronautics & Space Admin.
Electronics Research Center
Boston, Massachusetts
Attention: Francis Schwarz

National Aeronautics & Space Admin.
Goddard Space Flight Center
Greenbelt, Maryland   20771
Attention: Joseph Epstein

National Bureau of Standards
Washington, D. C.
Attention: Library

Oak Ridge National Laboratory
Oak Ridge, Tennessee
Attention: Library

Office of Naval Research
Power Branch
Department of the Navy
Washington 25, D. C.
Attention: Commander W. Diehl

Pratt and Whitney Aircraft Corporation
East Hartford 8, Connecticut
Attention: William Lueckel
            Franz Harter

Radio Corporation of America
Electron Tube Division
Lancaster Pennsylvania
Attention: Fred Block

Radio Corporation of America
David Sarnoff Research Center
Princeton, New Jersey
Attention: Karl G. Hernqvist
            Paul Rappaport

The Rand Corporation
1700 Main Street
Santa Monica, California
Attention: Librarian

Republic Aviation Corporation
Farmingdale, Long Island, New York
Attention: Alfred Schock

Space Technology Laboratories
Los Angeles, 45, California
Attention: Librarian

Texas Instruments, Inc.
P. O. Box 5474
Dallas 22, Texas
Attention: R. A. Chapman

Thermo-Electron Engineering Corp.
85 First Avenue
Waltham 54, Massachusetts
Attention: George Hatsopoulos
            S. Kitrilakis

Thompson Ramo Wooldridge, Inc.
7209 Platt Avenue
Cleveland 4, Ohio
Attention: W. J. Leovic

United Aircraft Corporation
Research Laboratories
East Hartford, Connecticut
Attention:R.H. Bullis
          A.F. Haught

University of Arizona
Tucson, Arizona
Attention: Monte Davis

U. S. Army Signal R & D Laboratory
Fort Monmouth, New Jersey
Attention: Emil Kittil

U. S. Atomic Energy Commission
Division of Reactor Development
Washington 25, D. C.
Attention: Direct Conversion Branch

U. S. Naval Research Laboratory
Washington 25, D. C.
Attention: George Haas
            Library

Varian Associates
611 Hansen Way
Palo Alto, California
Attention: Ira Weissman

Westinghouse Electric Corporation
Research Laboratories
Pittsburgh Pennsylvania
Attention: R. J. Zollweg

Beckman Instruments, Inc.
Special Products Division
2500 Harbor Boulevard
Fullerton, California   92632
Attn: A. P. Winter